NUREG/CR-5080

A Study of New England Seismicity With Emphasis on Massachusetts and New Hampshire

Final Report Covering the
Period 1976-1985

Prepared by M. N. Toksoz, K. Kadinsky-Cade

Massachusetts Institute of Technology

Prepared for
U.S. Nuclear Regulatory
Commission

NOTICE

This report was prepared as an account of work sponsored by an agency of the United States Government. Neither the United States Government nor any agency thereof, or any of their employees, makes any warranty, expressed or implied, or assumes any legal liability of responsibility for any third party's use, or the results of such use, of any information, apparatus, product or process disclosed in this report, or represents that its use by such third party would not infringe privately owned rights.

NOTICE

Availability of Reference Materials Cited in NRC Publications

Most documents cited in NRC publications will be available from one of the following sources:

1. The NRC Public Document Room, 1717 H Street, N.W.
   Washington, DC 20555
2. The Superintendent of Documents, U.S. Government Printing Office, Post Office Box 37082,
   Washington, DC 20013-7082
3. The National Technical Information Service, Springfield, VA 22161

Although the listing that follows represents the majority of documents cited in NRC publications, it is not intended to be exhaustive.

Referenced documents available for inspection and copying for a fee from the NRC Public Document Room include NRC correspondence and internal NRC memoranda; NRC Office of Inspection and Enforcement bulletins, circulars, information notices, inspection and investigation notices; Licensee Event Reports; vendor reports and correspondence; Commission papers; and applicant and licensee documents and correspondence.

The following documents in the NUREG series are available for purchase from the GPO Sales Program: formal NRC staff and contractor reports, NRC sponsored conference proceedings, and NRC booklets and brochures. Also available are Regulatory Guides, NRC regulations in the *Code of Federal Regulations*, and *Nuclear Regulatory Commission Issuances*.

Documents available from the National Technical Information Service include NUREG series reports and technical reports prepared by other federal agencies and reports prepared by the Atomic Energy Commission, forerunner agency to the Nuclear Regulatory Commission.

Documents available from public and special technical libraries include all open literature items, such as books, journal and periodical articles, and transactions. *Federal Register* notices, federal and state legislation, and congressional reports can usually be obtained from these libraries.

Documents such as theses, dissertations, foreign reports and translations, and non-NRC conference proceedings are available for purchase from the organization sponsoring the publication cited.

Single copies of NRC draft reports are available free, to the extent of supply, upon written request to the Division of Information Support Services, Distribution Section, U.S. Nuclear Regulatory Commission, Washington, DC 20555.

Copies of industry codes and standards used in a substantive manner in the NRC regulatory process are maintained at the NRC Library, 7920 Norfolk Avenue, Bethesda, Maryland, and are available there for reference use by the public. Codes and standards are usually copyrighted and may be purchased from the originating organization or, if they are American National Standards, from the American National Standards Institute, 1430 Broadway, New York, NY 10018.

NUREG/CR-5080

A Study of New England Seismicity With Emphasis on Massachusetts and New Hampshire

Final Report Covering the
Period 1976-1985

Manuscript Completed: December 1987
Date Published: January 1988

Prepared by
M. N. Toksoz, K. Kadinsky-Cade

Earth Resources Laboratory
Department of Earth, Atmospheric and Planetary Sciences
Massachusetts Institute of Technology
Cambridge, MA 02139

Prepared for
Division of Engineering
Office of Nuclear Regulatory Research
U.S. Nuclear Regulatory Commission
Washington, DC 20555
NRC FIN A4058
Under Contract No. NRC-04-76-209

ABSTRACT

The operation of M.I.T.'s regional seismic network in Massachusetts and New Hampshire is reviewed for the period April 1976 to March 1985. This includes a description of the configuration of permanent and field seismic monitoring stations. Among these is the Wallace Geophysical Observatory in Westford, Massachussetts, which houses several different types of geophysical instrumentation. Seven or eight additional field sites have been maintained throughout the 1976-1985 time period. We review the network's operating procedures, characteristics of the real-time digital data acquisition system that was developed in 1980, initial experiments with portable digital seismographs, and data exchange with surrounding regional seismic networks.

In addition to seismic monitoring operations in New England, several studies have been completed during the time period covered by this report which make use of data gathered by this and surrounding networks. (1) Several independent determinations of crust and upper mantle velocity structure in New England, based on teleseismic P-wave arrival times recorded by the network, on P- and S- travel times recorded by network stations from earthquakes and quarry blasts in New England, and on surface wave attenuation and dispersion across the area, all suggest that there is a significant difference in velocity structure between the Precambrian Grenville region and the Appalachian structures to the east. (2) Statistical determinations of earthquake hazard made during this time period include recurrence time estimates for earthquakes in the Boston-New Hampshire seismic zone, and in the Charlevoix and Western Quebec seismic zones of neighboring Southeastern Canada. The current regions of highest seismic activity appear to mirror those found in the historical record. Southern New England has undergone apparent temporal fluctuations in the rate of earthquake occurence from 1725 until present. (3) A number of fault plane solutions have been determined for small and moderate size earthquakes in New England. These include nine events located in New York and in the New England States (small earthquakes, for which mechanisms are based on P-wave first motions) and the Gaza, New Hampshire (m_b=4.6) and Miramichi, New Brunswick (m_b=5.0) earthquakes of 1982. Combining these data with other available stress measurements in the northeast suggests that stresses vary across the Appalachian - Grenville province boundary. Detailed studies of the rupture processes for the two larger events are included in this report. In the New Brunswick case regional network data are supplemented by an inversion of teleseismic body and surface waveforms. In the New Hampshire case the regional and teleseismic records are compared with strong motion accelerograms

from local dams. (4) Seismic attenuation measurements are described for New England. Based on the time domain decay of seismic coda wave amplitudes, they suggest that scattering is primarily responsible for the attenuation of high frequency (0.75-10 Hz) seismic waves in the crust.

Contents

List of Tables

List of Figures

1 Executive Summary

This is the final report for U.S. Nuclear Regulatory Commission contract No. NRC-04-76-209 with the Massachusetts Institute of Technology (M.I.T.) entitled " A Study of New England Seismicity with Emphasis on Massachusetts and New Hampshire". The contract period was from January 1, 1976 to March 31, 1985. During that time network daily activities progressed from determining phase arrival times on analog records from a handful of field stations to operation of an efficient real-time data acquisition system with advanced seismic data analysis capabilities. Quarterly Progress Reports have provided continuous reporting of seismic activity in our area for monitoring purposes. Phase data from the M.I.T. network have regularly been included in the Northeastern U.S. Seismic Network (N.E.U.S.S.N) bulletins.

This report summarizes daily operations for the time period of the above contract, and then describes some of the scientific results obtained from data provided by this and surrounding regional seismic networks. The scientific results can be divided into several categories or topics: velocity structure models, earthquake hazard studies, and the determination of earthquake mechanisms and focal depths, crustal stresses and seismic wave attenuation. Key components in our ability to complete these studies have been the reasonably close station spacing (about 50 km) in the northeastern U.S. and the continuous operation of the networks over a period of several years.

The M.I.T. seismic network has served as an invaluable instruction tool, providing students at various levels with data acquisition and waveform analysis skills. Many undergraduate students have helped us develop software or analyze records through the Undergraduate Research Opportunities Program at M.I.T., which is designed to introduce students to a real research environment. Several graduate students have used network data for research projects, and most notably, two PhD's have been awarded based on the analysis of regional seismic network data from M.I.T. and surrounding networks. A list of publications related to this contract is provided in Appendix A.

2 Network Operation

The M.I.T. regional short period seismic network went into operation in February, 1976. At that time it consisted of two permanent stations and six temporary field stations. The permanent stations were HRV (Harvard, Mass., Agassiz Geophysical Observatory) and WFM (Westford, Mass., George R. Wallace Geophysical Observatory). In addition to the short period (1.0 Hz) seismometers (Geotech S-13 three component instruments at HRV, Mark Products L-4C and L-4-3D three component instruments at WFM), these permanent stations housed long period seismometers, tiltmeters, a gravity meter and temperature/pressure sensors. The station at HRV was closed down in January, 1981, and all permanent station equipment combined at WFM. Initial field stations were GLO, ONH, PNH, WNH, DNH and DUX. All station locations and elevations are listed in Table 1. The only field station with three short period components is ONH (L-4C and L-4-3D's). Other field stations have L-4C vertical component seismometers. Two other field stations were added later: COD (a borehole seismometer located in an 85 m deep well to reduce noise levels) and NMA, on the island of Nantucket. COD was added in April, 1978, and NMA in September, 1980. NMA was shut down in October, 1984, due to noise problems. It was replaced in 1985 by UXB, which became operational shortly after the time period of this report. All stations are plotted in Figure 1. They have performed very reliably throughout the contract period, with the required $< 5\%$ downtime.

Station	Latitude (N)	Longitude (W)	Elevation (meters)
HRV- Harvard, MA	42.5064	71.5583	180.0
WFM- Westford, MA	42.6106	71.4906	87.5
GLO- Gloucester, MA	42.9403	70.7272	15.2
ONH- Oak Hill, NH	42.2792	71.5056	280.0
PNH- Pitcher Mntn., NH	43.0942	72.1358	659.0
WNH- Whiteface, NH	43.8683	71.3997	220.0
DNH- Durham, NH	43.1225	70.8948	24.0
DUX- Duxbury, MA	42.0686	70.7678	27.4
COD- Cape Cod, MA	41.6856	70.1350	-85.0
NMA- Nantucket, MA	41.2947	70.0261	3.1
UXB- Uxbridge, MA	42.0614	71.6773	137.0

Table 1: Station Locations

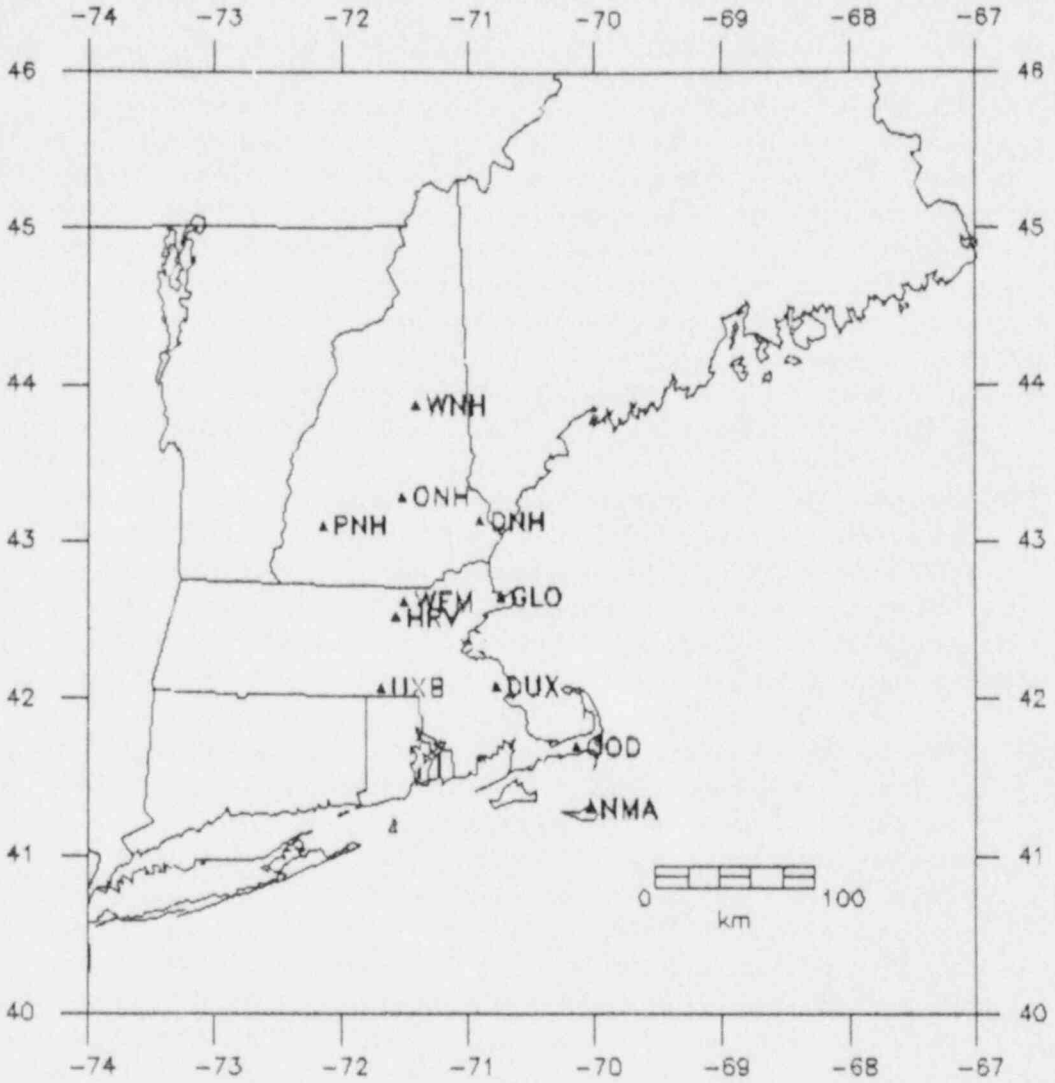

Figure 1: M.I.T. Seismic Stations

Data from the permanent and temporary field stations are telemetered over phone lines to recording instruments located on the M.I.T. campus in Cambridge, Mass. ,Signals are low-pass filtered before and after phone line transmission to minimize noise interference. Filter cutoff frequencies are 10 Hz and 30 Hz before transmission for long and short period signals respectively, and 1 Hz and 10 Hz after transmission for long and short period signals respectively. Upon arrival at the central recording station, the analog signals are first demodulated, then sent (1) to a rack of helicorders for visual examination, and (2) to an HP/1000 for digitizing and further analysis. A summary of the location procedure used by the M.I.T. network has been prepared by Michael Guenette, and is shown in Figure 2 and Figure 3. The main features of this flowchart will be outlined briefly. Continuous helicorder (and develocorder, originally) records are scanned daily. They have been maintained even since the HP/1000 computer was installed, both as a cross-check and to monitor possible problems occurring at the individual stations. M.I.T.'s real-time digital seismic event detection and recording system has been operational on the HP/1000 since 1980. Analog short period signals from all stations and long period signals from WFM are passed through an A/D converter, digitized at rates of 100 Hz (25 Hz before 1983) and 1 Hz respectively, then checked automatically for event detections. Accurate time information is provided by a Kinemetrics model 468-DC satellite clock, which receives GOES signals.

Details of the event detection and analysis system are described in *Michael et al. (1982)*. It is named $ASAP^2$ (As soon as possible Seismic Analysis Package), and has been very successful in the New England environment, which is characterized by a relatively low level of seismic activity and by variable weather and cultural noise levels. The event detection algorithm is based on a metric computed from the Walsh transform of the data (*Goforth and Herrin, 1981*). This allows detection of both frequency and amplitude shifts in the signals. Detection at several predetermined stations within a short time interval is required in order for an event to be saved: this reduces the number of false triggers due to electronic noise. Seismic events are archived on magnetic tape.

A method of distinguishing quarry blasts from earthquakes by overlaying digital plots of unknown events on known quarry blast records has become common procedure. This saves a lot of time during summer months when several quarry blasts are recorded daily from Massachusetts and New Hampshire quarries. When a full location procedure is required, arrival times are picked interactively using a cursor, and automatically stored in a location file. Arrival times from surrounding networks are incorporated into that file whenever possible. Earthquakes were initially located using HYPO71 (*Lee and Lahr,*

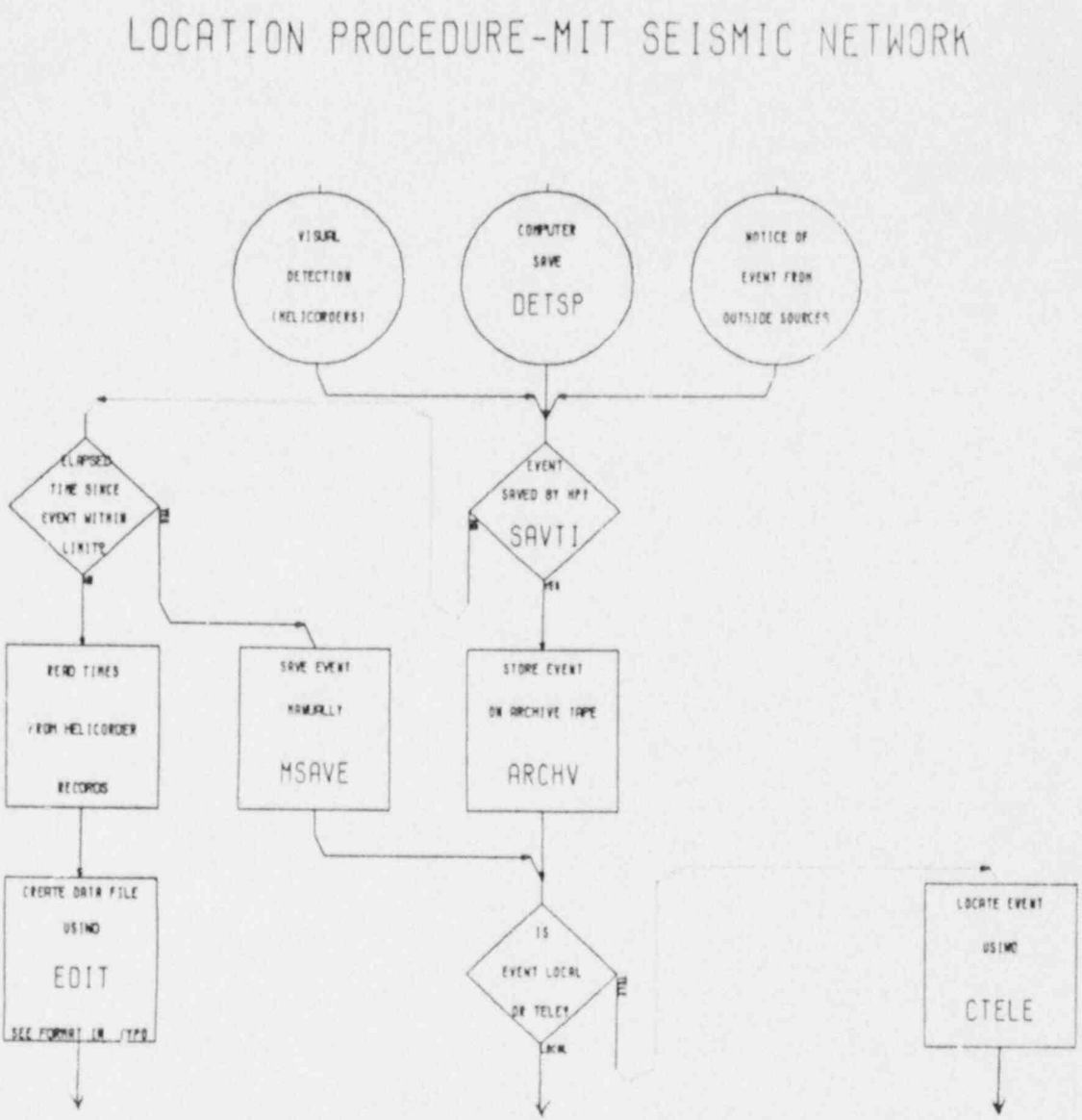

Figure 2: Location Procedure- first part

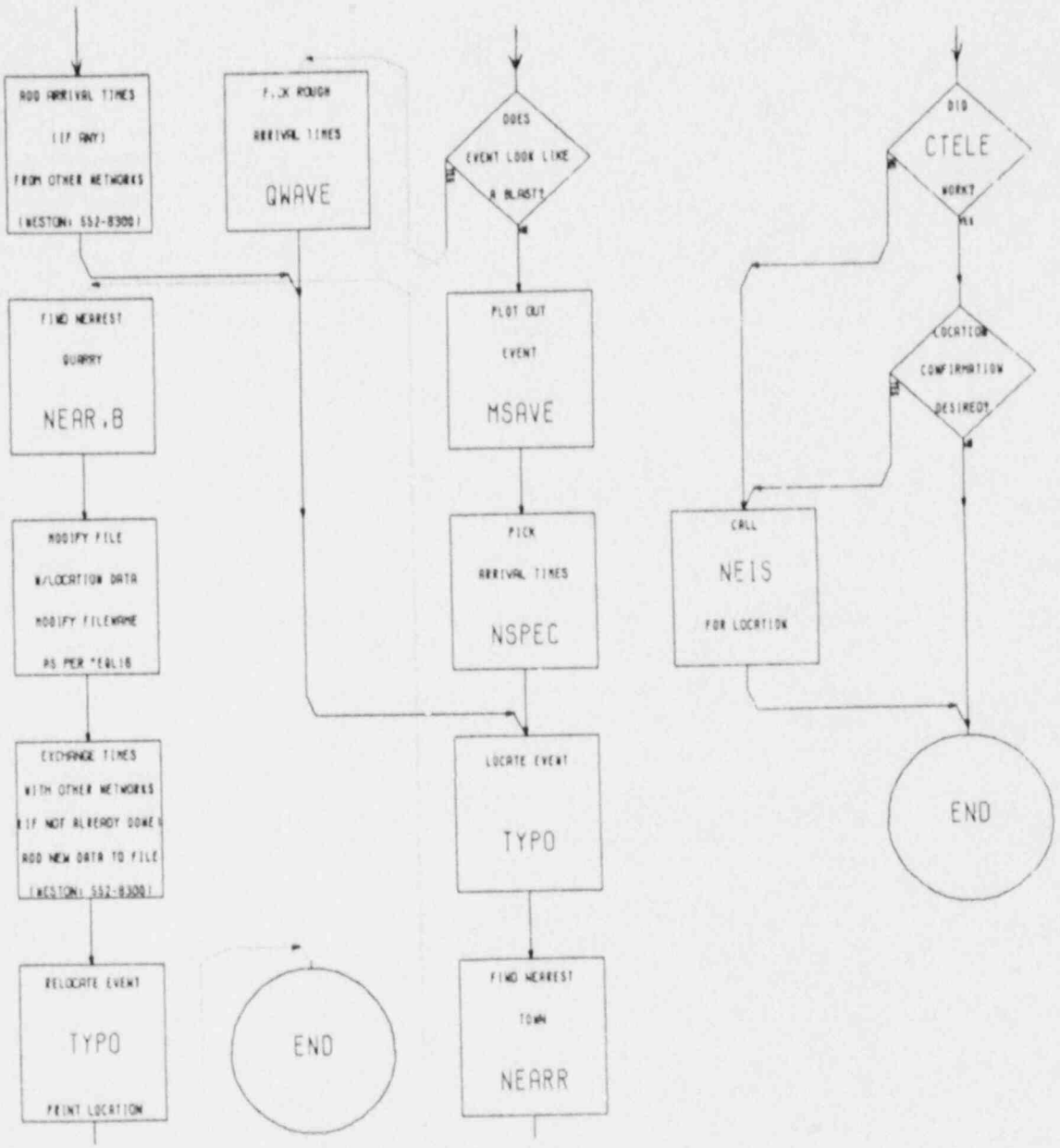

Figure 3: Location Procedure- second part

1975). However, when HYPOINVERSE (*Klein, 1978*) became available, it was adapted to suit the needs of the M.I.T. network. It has become the standard location program. Teleseismic locations using network stations alone are not always reliable, and are usually cross-checked against National Earthquake Information Service (NEIS) locations.

As part of an effort to determine the nearest town or quarry to an event, a method of spatially sorting catalogued earthquake data has been developed. This computer algorithm permits a rapid determination of whether each event is located within a region with an irregularly shaped boundary. This region can be a particular seismic zone of interest, or for example a particular New England state. This method, called the "Winding-Number Algorithm", is described in *Godkin and Pulli (1984)*.

Local earthquake magnitudes are determined from empirical coda length (signal duration) measurements. The relation used for this purpose was developed at M.I.T. by *Chaplin et al. (1980)*. In that study a linear relation was found to exist between the coda length of the recorded signals and Nuttli's local Mn magnitude, with a negligeable dependence on distance from the source. The relation is given by $Mn = 2.21 * log_{10}T - 1.70$, where T is the signal duration in seconds. Results of this study were based on 196 coda length measurements from 45 local events. Mn measurements had been determined by Weston Observatory (*Chiburis et al., 1976-1979*) using the method of *Nuttli (1973)*. Advantages of the coda length magnitude method are that it does not depend on on source spectrum or radiation pattern, or on an accurate calibration of the seismic stations.

A map showing local earthquakes recorded during the time period of this contract is shown in Figure **4**. Typical short period recordings of local and teleseismic earthquakes by the network are published in *Michael et al. (1982)* and in the network's Quarterly Bulletins. Instrument calibrations are performed by inputting a current step into the seismometer calibration coils. Several step responses can be stacked and averaged for noise cancellation. Typical acceleration, velocity and displacement response curves are shown in Figure 5. The curves shown in Figure 5 were obtained for the station DNH. The step response shown in the upper right curve (0-10 second x-axis) is in units of 5 millivolts. Earthquake spectra can be corrected for instrument response using these curves and knowing the value of current applied to the calibration coil, the calibration coil motor constant and the seismometer mass. These last two values are provided by the seismometer manufacturer, and have not been redetermined at M.I.T.

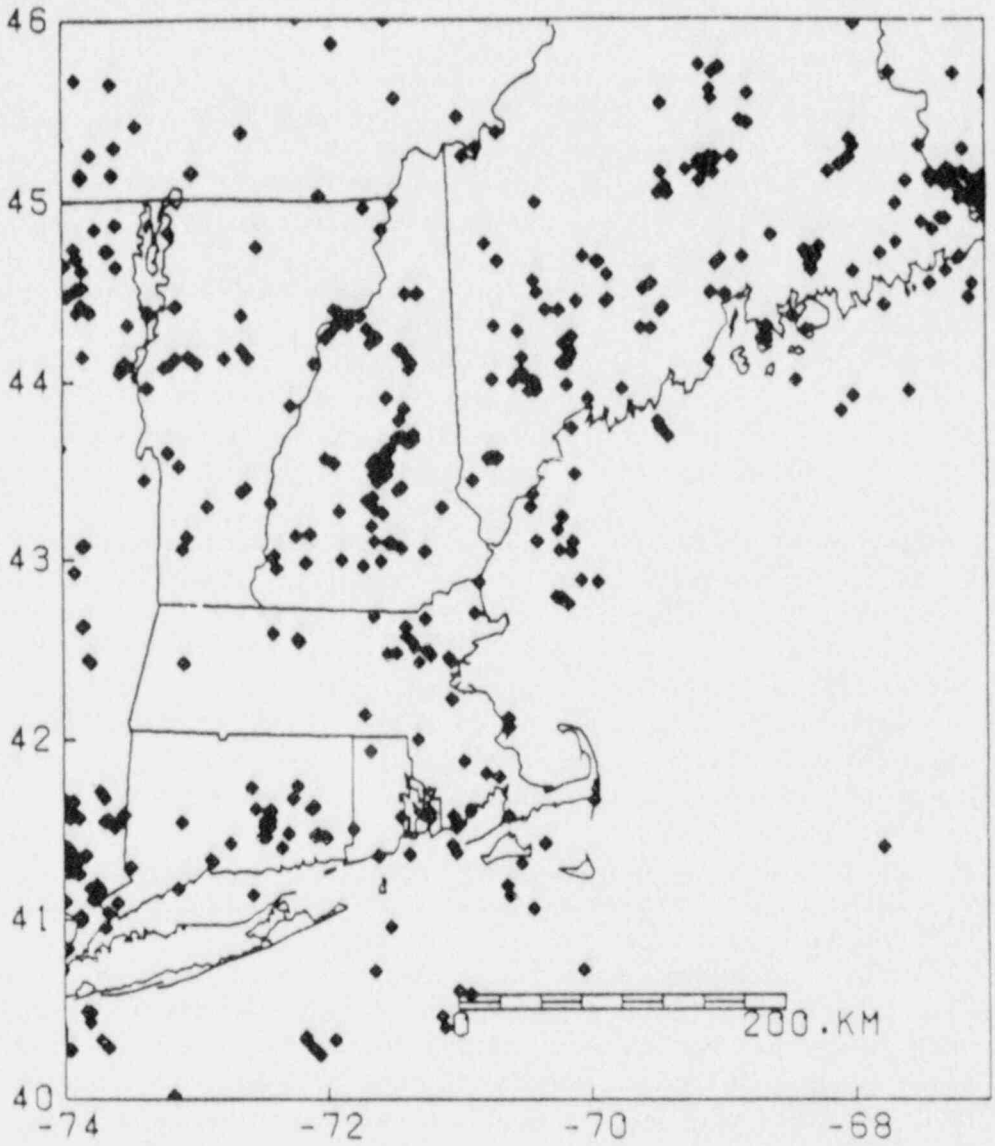

Figure 4: Epicenters, October 1975 - September 1985

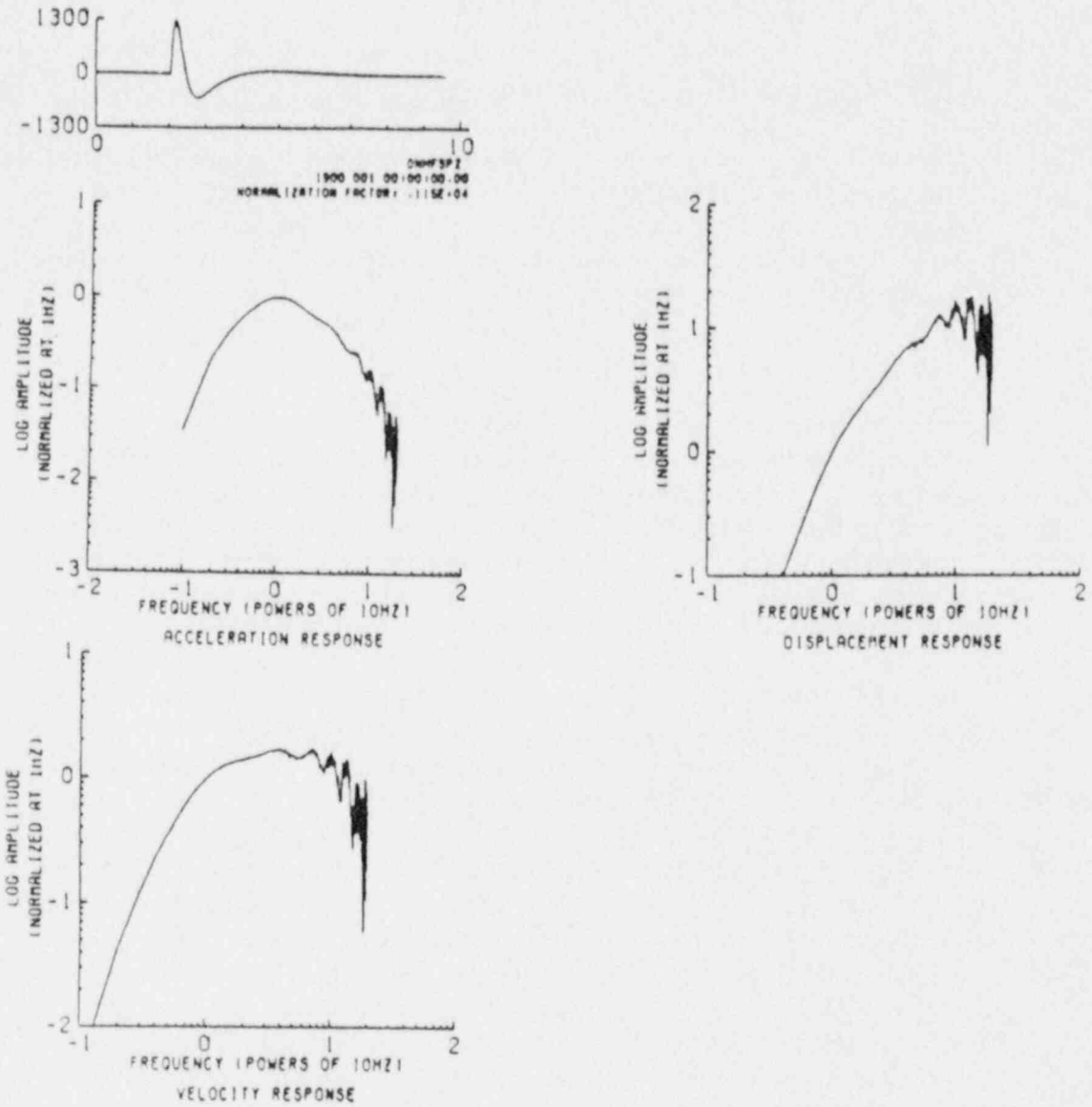

Figure 5: Response Curves for M.I.T. Seismic Network Stations

3 Crust and Upper Mantle Velocity Structure

Several independent determinations of crust and upper mantle velocity structure under New England have been made using regional seismic network data during the 1976-1985 time period. These results have been compared with published gravity and magnetic data and known geology to constrain structural interpretations in the Northeastern U.S.

3.1 Regional travel times

Average crustal models for the northeastern U.S. have been derived from P- and S- travel times recorded from local and regional earthquakes by the Northeastern U.S. Seismic Network (*Taylor, 1980; Taylor et al., 1980*). Based on 1545 P-wave and 546 S-wave readings from 170 regional events (epicentral distance up to 600 km), separate velocity structures are found for the Appalachian and Grenville Provinces. The Appalachian province is characterized by a two-layer crust: an upper layer approximately 15 km thick with $V_P = 6.1 km/sec$ and $V_S = 3.6 km/sec$, and a lower layer approximately 25 km thick with $V_P = 7.0 km/sec$ and $V_S = 4.1 km/sec$. The Pn velocity in this province is 8.1 km/sec. In contrast the Grenville province is characterized by a more homogeneous crust with nearly constant P and S velocities of 6.6 and 3.7 km/sec. The crustal thickness and Pn velocity in the Grenville province are 37 km and 8.0 km/sec respectively. An inversion of Pn time terms for crustal thickness throughout the Northeast suggests that crustal thicknesses are relatively high (or crustal velocities relatively low) along a northeast-trending belt running from eastern New York through central New Hampshire and into Maine (*Taylor, 1980*). This result is illustrated in Figure 6. The difference between the Appalachian and Grenville provinces was attributed in *Taylor (1980)* and *Taylor et al. (1980)* to the tectonic history of the area. The Appalachian province would have been affected by repeated orogenies, with possible presence of oceanic material in the crust due to the repeated opening and closing of the Atlantic. The Grenville structure could be attributed to crustal reactivation/thickening and subsequent erosion (e.g., *Dewey and Burke, 1973; Putnam and Sullivan, 1979*).

A more site specific crustal model has been determined for central New England by *Curtin et al. (1983)*. They used 889 P-wave and 468 S-wave arrival times from quarry blasts and shallow earthquakes recorded by regional seismic network stations throughout New England. Velocity models resulting from this study are (thickness in km, velocity in km/sec): 8.8, 6.00; 11.3, 6.35;

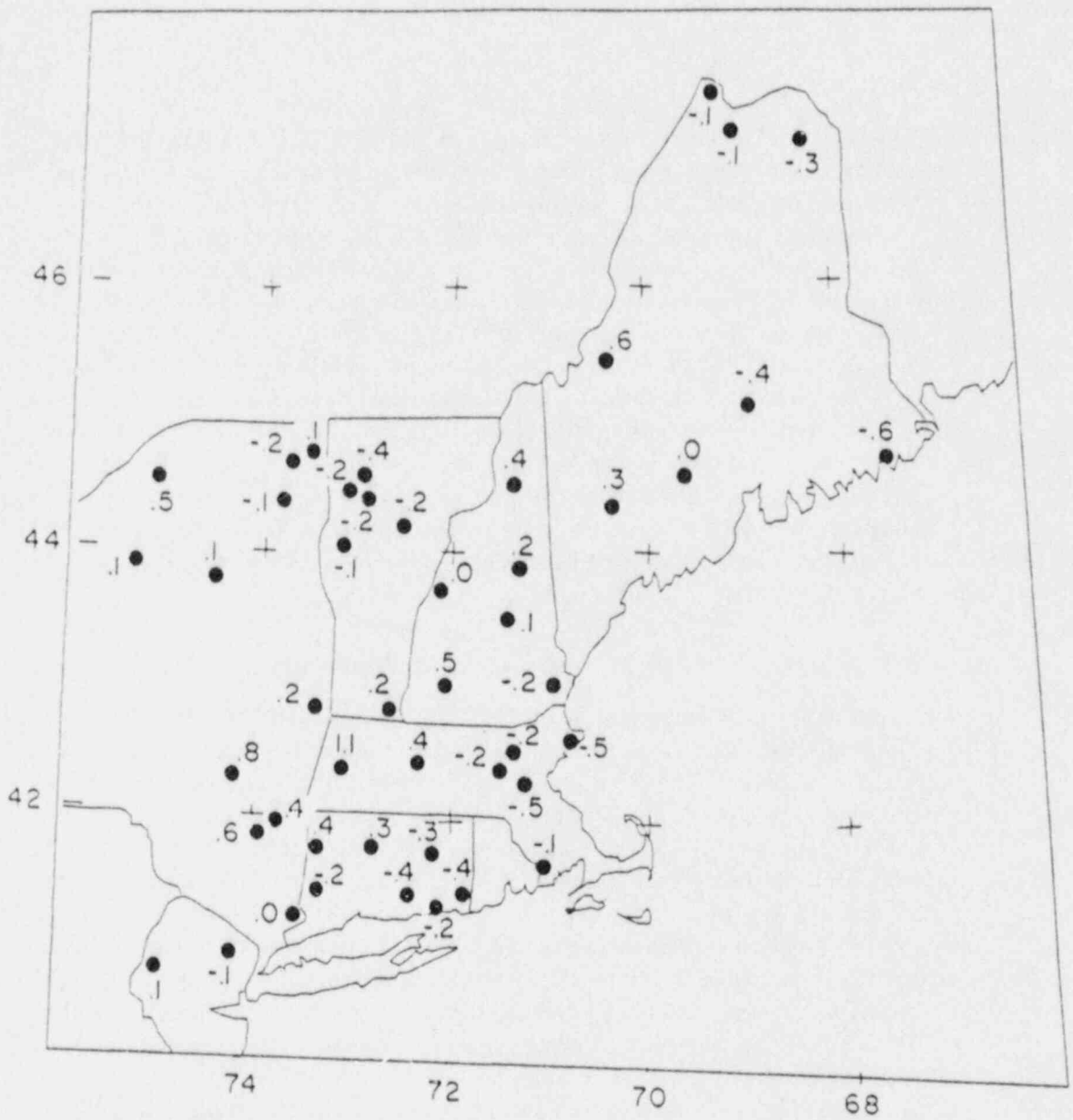

Figure 6: Relative station Pn time terms, in seconds. From Taylor (1980)

19.8, 6.95; halfspace, 8.18 for P-waves, and 11.3, 3.51; 7.2, 3.86; 19.9, 4.04; halfspace, 4.67 for S-waves. Station elevations and hypocentral depths have not been taken into account in this analysis.

Finally, a set of 906 P-wave and 502 S-wave travel times was used to generate a crustal velocity model for New England which is characterized by a layer with a linear velocity increase with depth overlying a higher speed half space. The resulting P-wave model is $V_P(z) = 5.81 + 0.0430z$ km/sec, and the S-wave model is $V_S(z) = 3.45 + 0.0193z$ km/sec. This study, by Carl Godkin, is included in Appendix B. Velocity models described above are plotted as figures in that paper. From these studies alone we cannot differentiate between these models (linear velocity increase versus flat layers). Possible ways to examine this problem are waveform modeling at regional distances or an examination of amplitude falloff with distance for regional phases. These studies will be undertaken in the future using controlled experiments such as recording quarry blasts at predetermined distances.

3.2 Surface Wave Dispersion and Attenuation

Interstation phase and group velocities have been calculated from long period (15-50 sec) surface waves recorded at stations in the Northeastern U.S. and Southern Canada. The calculations make use of a Wiener filtering technique which is described in *Taylor (1980)* and in *Taylor and Toksoz (1982)*. By constructing a filter that can estimate a signal recorded at a more distant station based on a signal recorded at a nearer station to the source (stations located along a great circle path from the source) it is possible to derive a transfer function corresponding to the raypath between the two stations. The transfer function (Green's function) is then used to obtain group and phase velocities. Group velocities are calculated by narrow bandpass filtering of the Green's function. Interstation phase velocities are calculated directly from the phase spectrum of the Green's function.

Fundamental mode Rayleigh wave phase and group velocities have also been estimated from the frequency-wavenumber (f-k) power spectra of signals traversing six short period stations in Southeastern New England (*Taylor, 1980*). This stacking method significantly reduced the errors resulting from large wavelength to distance ratios in the two-station technique. Beamsteering is used to identify lateral refractions causing large apparent phase velocities.

Group and phase velocities calculated using both the two-station and f-k power spectra techniques have been inverted for crust and upper mantle structure using a maximum likelihood technique. Details can be found in *Taylor*

et al. (1980). Resulting structural models are consistent with those obtained by analysis of regional P and S travel times. They include the following features. For a path along the strike of the Appalachians (Newfoundland - Weston, MA - Ogdensburg, NJ) the average crust is 40 km thick. The S-wave velocity in the top 15 km is 3.6 km/sec; in the lower 25 km it is 3.9-4.1 km/sec. For another path within the Appalachians (Montreal or Ottawa - Weston, MA) the crust is 40-45 km thick. The S-wave velocity in the upper 20 km is 3.5-3.6 km/sec; in the lower crust it is 3.9-4.0 km/sec. In this case the lower crustal layer has a positive velocity gradient with depth. Finally, a path within the Grenville province (Montreal or Ottawa - Ogdensburg, NJ) has a thinner crust (35 km thick) than either Appalachian path. The S-wave velocities of the upper 15 km and lower 20 km of the crust are 3.5 and 3.8-3.9 km/sec respectively. Note that phase and group velocities have been inverted only for shear velocity structure, while density and P-wave velocity have been held fixed. However, inverting phase and group velocities simultaneously increased sensitivity to different types of structure as well as model resolution.

3.3 Teleseismic P-Wave Residuals

A three dimensional inversion of teleseismic P-wave arrival times recorded by the Northeastern Seismic Network has resulted in detailed velocity information down to depths of 500 km (*Taylor and Toksoz, 1979; Taylor, 1980; Taylor and Toksoz, 1980*). Fifty short period stations and 68 events have been used in this analysis. Epicentral distances range between 25° and 95°. From analysis of P-wave residuals it is possible to correlate structures down to 200 km with tectonic and geologic features at the surface. Grenville province upper mantle velocities are approximately 2% higher than those beneath the Appalachian province. The highest upper mantle velocities are located beneath the Adirondack dome. A relative low velocity anomaly dips to the northwest beneath Massachusetts, New Hampshire and central Maine. This anomaly is well constrained between 35 and 200 km depth, and shows a spatial correlation with the Bronson Hill - Boundary Mountains Anticlinorium in New Hampshire and Maine. There is some evidence that this anomaly continues to depths greater than 200 km. Crustal thicknesses resulting from this study are shown in Figure 7. Crustal velocities and thicknesses derived from the teleseismic P-wave inversion are relatively consistent with those obtained from the regional travel time analysis described in an earlier section. The Appalachian crust is slightly thicker than the crust in the Grenville province. Crustal thinning was observed in northwestern Vermont, southwestern Connecticut and possibly near

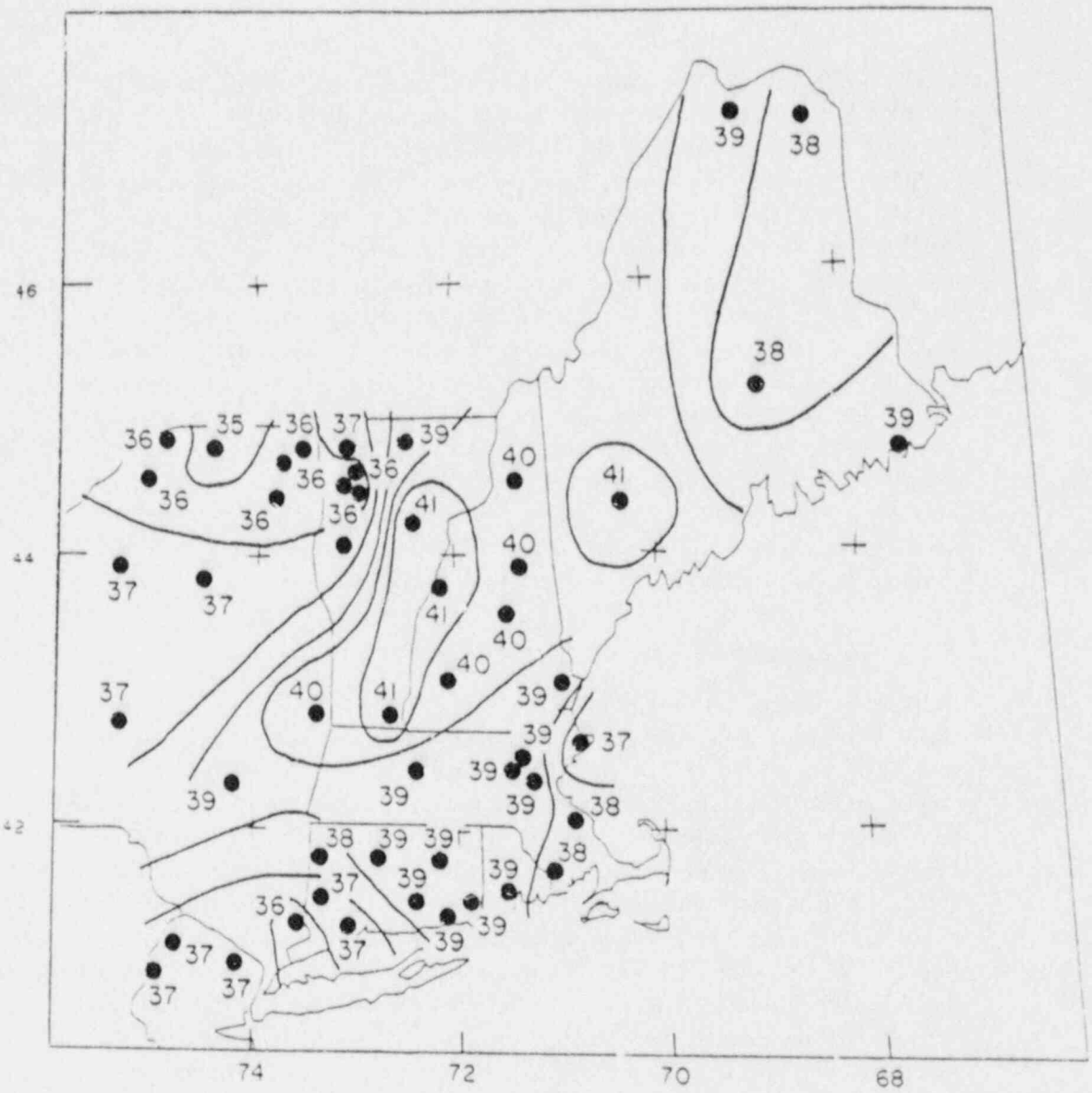

Figure 7: Crustal thickness variations (km) from Taylor (1980)

the coastline. Thick crust is associated with the Taconic thrusts in east-central New York and western Massachusetts.

4 Statistical Determinations of Earthquake Hazard

Based on available seismic data for the period 1725 through 1974, *Shakal and Toksoz (1977)* have calculated earthquake return periods and probabilities of occurrence for the densely populated region of Southern New England. They determine the seismic energy release in five year intervals based on intensities, and find that the earthquake activity level was higher in the time period 1725-1849 than during the next 125 years. This result is found to be statistically significant based either on assuming a Poisson process or by using a χ^2 contingency test. The earthquake occurrence probabilities and return periods are calculated based on an extreme value method which uses data on only the largest earthquake in each 5-year sampling interval. Using the 1725-1974 time period results in higher probabilities of occurrence and lower return periods than for the 1850-1974 period. As long a time period as possible is chosen as appropriate for hazard studies because there are indications in the data that the rate of earthquake activity started to go up again after 1940, i.e., that further fluctuations are likely. For the time period 1725-1974 the estimated return periods for earthquakes of intensity $\geq VI$ and $\geq VIII$ are found to be 25 and 130 years respectively. The probabilities of occurrence of an earthquake in those categories of intensity, during a period of 100 years, are 99% and 55% respectively.

Earthquake occurrence statistics in the Northeastern U.S. and Southeastern Canada have also been examined by *Pulli (1989)*, who compared historical (1534-1975) and instrumental (1975-1981) datasets in the Northeastern U.S. and Southeastern Canada. First he attempts to regionalize the distribution of earthquake activity. He employs two techniques: a frequency regionalization, based on a 2-D filter that computes a weighted sum of events around each point in an area, and an energy regionalization, in which total seismic energy release is calculated for a series of overlapping areas ("Moving Block" method of *Bath, 1982*). Both methods are applied to the historical and instrumental datasets, using linear relationships between log (energy) and mb magnitude, and between mb and epicentral intensity I (the latter based on instrumental data in New England). From both methods, the zones of highest earthquake activity in the historic dataset are the Charlevoix seismic zone, the Western Quebec seismic

zone, and the Boston - New Hampshire seismic zone (see Figure 8). The Southeastern New York - New Jersey border is unusually active as well. The instrumental dataset is very similar, except that the Boston - New Hampshire zone is less pronounced than in the historic dataset. It was not clear if this is an artifact of the population distribution or a real trend in the data (see Figure 9).

The Charlevoix, Western Quebec and Boston - New Hampshire seismic zones are then examined separately in terms of probabilities of occurrence and return times of earthquakes. This has been done for the historical dataset using four statistical methods (*Pulli, 1989*): (1) a least squares determination of a and b values in the expression Log[N(M)/yr] = a - b(M), where magnitude M is related to epicentral intensity I by M = A + B(I), (2) a maximum likelihood estimation of b, (3) a Gumbel Type I asymptotic distribution of extreme magnitude values (no upper or lower magnitude limits assumed), and (4) a Gumbel Type III distribution, with an upper magnitude limit of mb=8. The four methods give comparable results in most situations. In the case of the instrumental data set N(mb) can be determined directly. Probabilities of occurrence and return times are compared for historical data (based on method (1)) and instrumental data in Table 2. Differences between these results of method (3) and those of *Shakal and Toksoz (1975)* for the Boston - New Hampshire area (the latter obtained using the same method) can be explained by differences in epicentral intensity assigned to the largest earthquakes in the data set (1727 and 1755 earthquakes, intensities VII and VIII in Pulli's study, versus VIII and IX in the study by Shakal and Toksoz).

5 Earthquake Mechanisms and Focal Depths

Fault plane solutions for ten earthquakes in the Northeastern U.S. were determined during the time period covered by this report (*Pulli et al., 1980; Pulli and Toksoz, 1981; Pulli and Guenette, 1981a,b; Pulli and Godkin, 1981; Pulli, 1989*). These solutions are summarized by *Pulli, 1989* (see Figure 10 and Figure 11), who includes a discussion of crustal models used in the determination of the ten new solutions. In addition, previously known fault plane solutions for earthquakes and microearthquakes in the Northeastern U.S. have been summarized by *Pulli (1988)* (see Table 3).

In an attempt to constrain focal depths of crustal earthquakes in New England, several events have been selected to fit the criteria of occurring within 10 km of a station and having good azimuthal coverage (*Pulli, 1989*). Using the

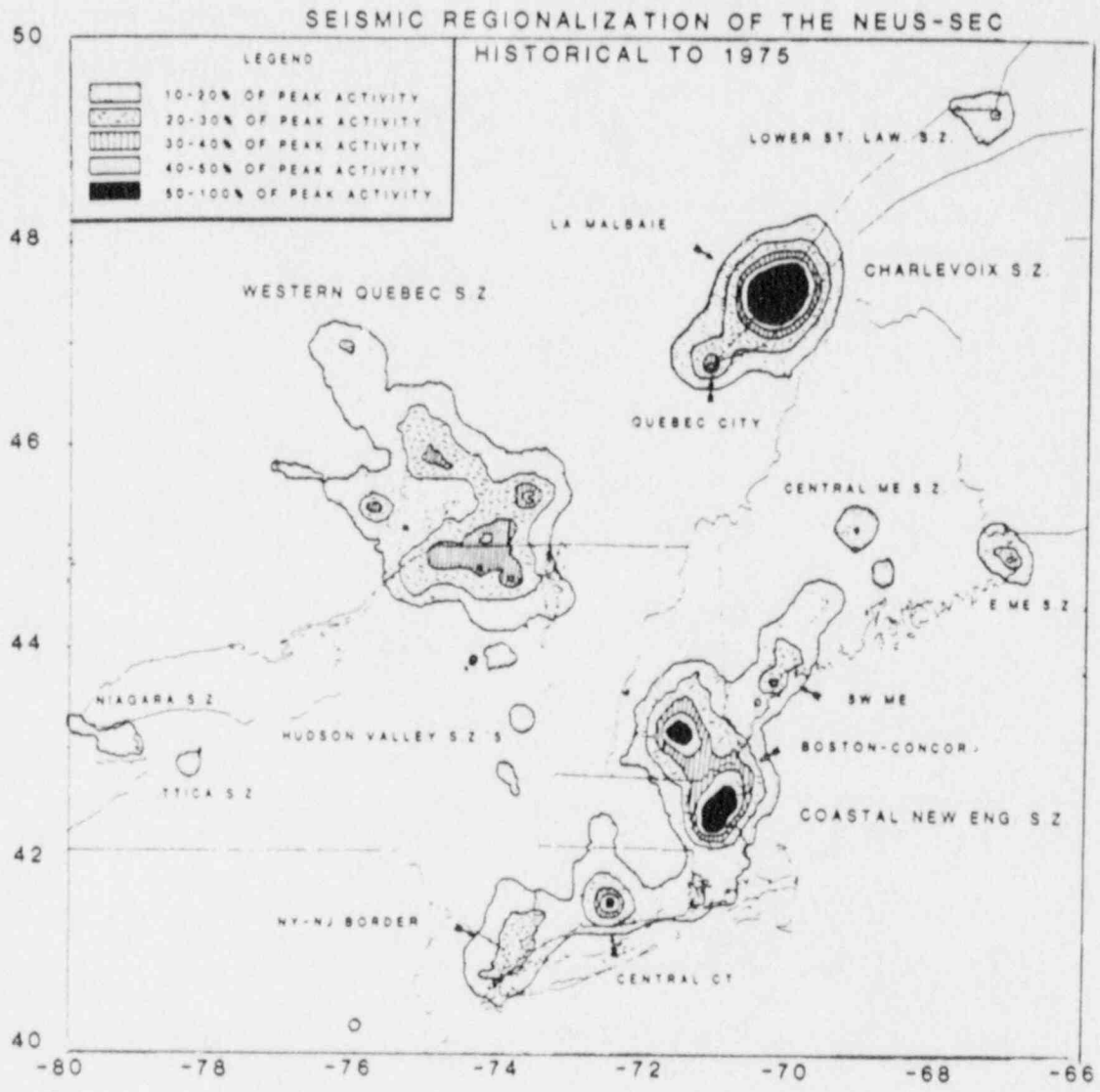

Figure 8: Frequency Regionalization: Historic Data, from Pulli, 1983

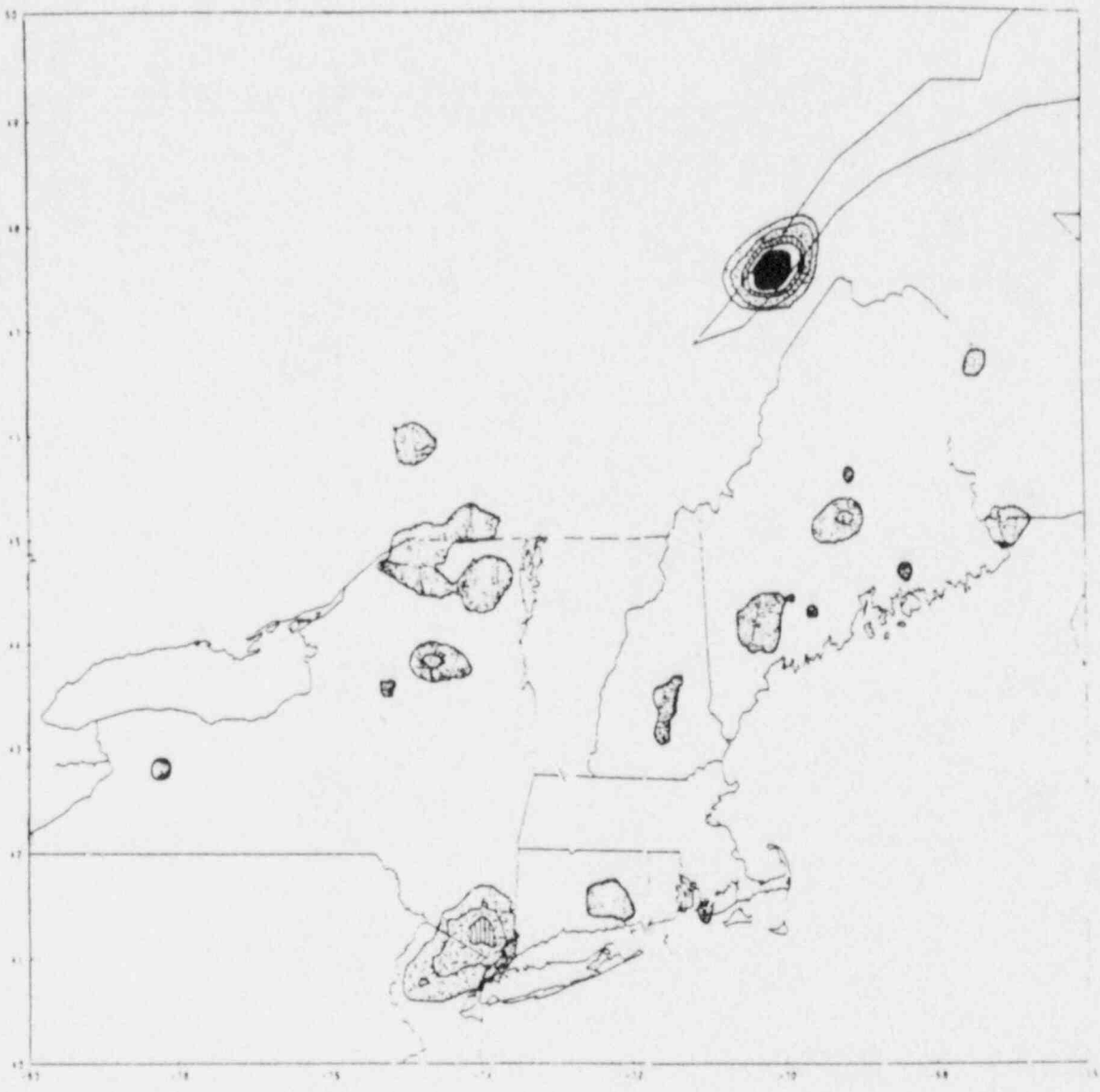

Figure 9: Frequency Regionalization: Instrumental Data, from Pulli, 1983

Western Quebec Seismic Zone

	Instrumental		Historical	
mb	Mean Return Time	P(1 event) in 100 yrs	Mean Return Time	P(1 event) in 100 yrs
5.0	29	97	24	99
5.5	79	72	67	78
6.0	217	37	188	41
6.5	595	15	526	17
7.0	1630	6	1480	7

Charlevoix Seismic Zone

	Instrumental		Historical	
mb	Mean Return Time	P(1 event) in 100 yrs	Mean Return Time	P(1 event) in 100 yrs
5.0	17	100	17	100
5.5	40	92	32	95
6.0	93	66	62	80
6.5	218	37	120	56
7.0	510	18	231	35

Boston - NH Seismic Zone

	Instrumental		Historical	
mb	Mean Return Time	P(1 event) in 200 yrs	Mean Return Time	P(1 event) in 200 yrs
5.0	101	86	60	96
5.5	262	53	157	72
6.0	679	26	408	39
6.5	1760	11	1060	17

Table 2: probabilities and Return Times, from Pulli, 1983

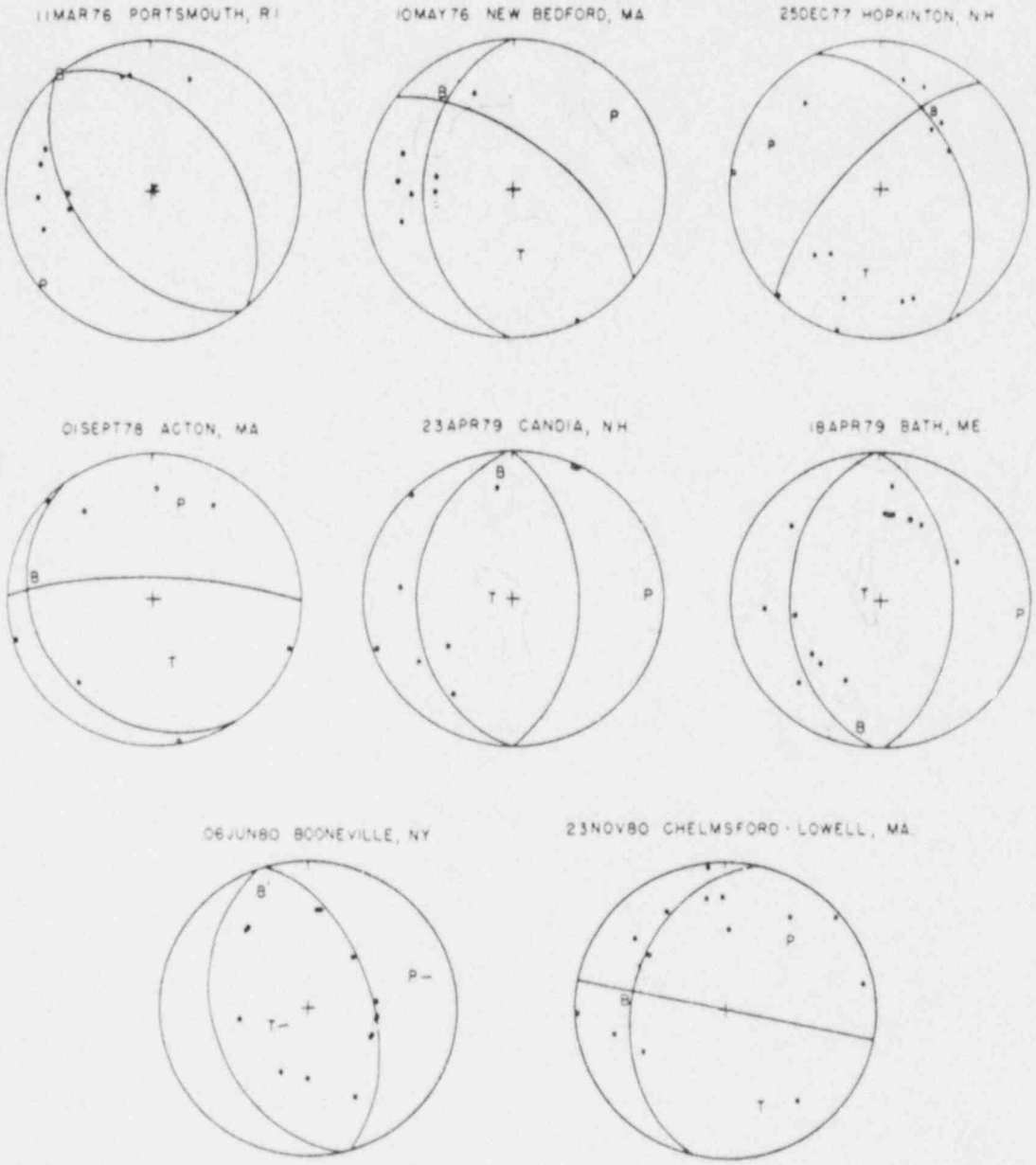

Figure 10: Fault Plane Solutions, from Pulli (1983).

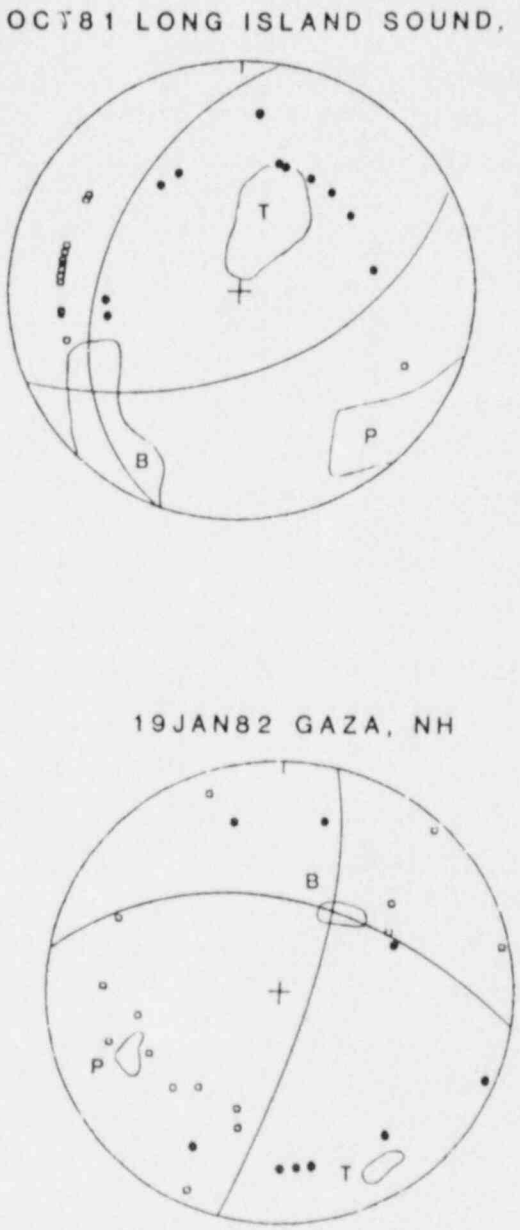

Figure 11: Fault Plane Solutions, continued, from Pulli (1983).

Fault Plane Solutions for NEUS-SEC Earthquakes
(Note: "C" in Column 2 Indicates Composite FPS)

						P-Axis		T-Axis			
MoDyYr	HrMn	Lat	Long	Dp	Mag	Tr	Pl	Tr	Pl	Area	Ref.
010166	1323	42.8	-78.2	2	4.6	62	1	331	28	Attica, NY	1
061367	1908	42.9	-78.2	3	4.4	74	11	336	53	Attica, NY	1
69	C	41.1	-74.6	2	2.5	235	65	130	10	Hopatcong, NJ	2
71	C	43.81	-74.45	3	3.2	251	18	70	73	Blue Mt Lake, NY	3
061573	0109	45.32	-70.91	6	4.8	47	32	187	51	ME-QUE Border	4
060974	0301	47.43	-70.36	19	-.3	256	7	351	37	La Malbaie, PQ	5
062074	1336	47.41	-70.18	17	1.7	219	58	353	24	La Malbaie, PQ	5
062374	0906	47.51	-70.22	15	0.5	317	1	217	83	La Malbaie, PQ	5
063074	1155	47.72	-69.84	15	2.0	94	5	310	83	La Malbaie, PQ	5
070274	0230	47.56	-70.23	4	0.3	100	3	191	25	La Malbaie, PQ	5
071374	1929	47.49	-69.97	13	0.6	110	17	246	67	La Malbaie, PQ	5
060774	1945	41.63	-73.94	1	3.3	225	10	45	70	Wap. Falls, NY	6
122174	1451	45.04	-74.03	3	2.9	249	6	140	83	Valleyfield, PQ	7
010475	2040	44.89	-74.55	0	2.8	259	16	56	72	Massena, NY	7
060975	1839	44.89	-73.57	13	4.2	253	8	75	84	Altona, NY	7
071275	1237	46.45	-76.21	17	4.2	210	15	5	50	Maniwaki, PQ	8
171975	2059	41.43	-73.79	3	2.3	135	30	333	58	Mahopac, NY	7
082275	1749	41.14	-73.95	3	2.3	276	18	96	72	Lake de For, NY	7
110375	2054	43.91	-74.64	4	3.9	250	7	65	85	Racquette, NY	7
031176	2107	41.56	-71.21	2	3.2	220	1	40	89	Portsmouth, RI	9
031176	2107	40.95	-74.35	1	2.6	118	38	303	52	Pomp Lake, NY	7
051076	0134	41.54	-71.01	0	2.7	55	15	175	45	New Bedford, MA	9
041376	1539	40.83	-74.05	3	3.0	260	32	133	45	Ridgefield, NJ	7
042476	1022	41.46	-72.49	0	2.2	205	5	30	65	E. Haddam, CT	10
042876	2132	44.58	-74.63	1	2.8	250	15	61	82	Potsdam, NY	7
082076	2208	41.13	-73.76	5	2.5	285	30	158	47	Mt. Pleasant, NY	7
092276	0904	41.29	-73.95	8	1.8	120	15	311	71	Indian Pt, NY	7
112276	0443	40.99	-73.86	5	1.9	294	25	37	64	Yonkers, NY	7
121776	1030	41.47	-72.07	0	2.2	90	45	295	40	Norwich, CT	10
031077	1622	41.18	-74.15	6	2.2	116	23	322	59	Sufferin, NY	7
09 77	C	41.31	-73.95	0	2.5	220	15	10	65	Annsville, NY	11
092877	1721	44.39	-73.89	3	3.1	64	36	180	34	Wilmington, NY	7
120477	2350	40.80	-74.77	1	2.3	311	7	80	77	Schooley Mt, NJ	7
122077	1744	41.78	-70.66	0	3.1	120	5	300	85	Wareham, MA	10
122577	1535	43.19	-71.65	0	3.2	285	15	180	35	Hopkinton, NH	9
010478	1928	44.04	-70.51	0	3.2	340	20	150	70	Otisfield, ME	10
021878	1448	46.35	-74.12	7	4.1	255	5	75	85	St. Donat, PQ	12
062178	1831	43.66	-71.38	0	1.8	100	5	10	25	Lake Winn, NH	10
073078	1054	45.64	-74.37	3	3.8	35	8	269	78	Lachutte, PQ	7
082178	0847	44.52	-74.51	1	1.9	53	28	279	62	Bay Pond, NY	7
090178	0333	42.48	-71.46	3	1.8	20	30	65	45	Acton, MA	8
102978	2359	43.94	-70.40	0	2.5	340	5	160	85	Crescent Lake, ME	10
041879	0234	43.95	-69.75	4	4.0	90	5	270	85	Bath, ME	9
042379	0005	43.04	-71.24	1	3.1	90	5	270	85	Candia, NH	9
081979	2249	47.67	-69.90	10	5.0	105	15	355	45	La Malbaie, PQ	13
01 80	C	41.31	-73.95	0	2.9	260	15	55	75	Annsville, NY	11
060680	1315	43.60	-75.10	2	3.5	85	5	265	85	Booneville, NY	9
112380	0039	42.63	-71.36	2	2.9	45	30	165	25	Lowell, MA	9
070481	2316	45.11	-74.61	16	3.3	45	20	150	45	Cornwall, ONT	14
070581	2147	45.11	-74.61	16	3.3	20	13	140	40	Cornwall, ONT	14
102181	1649	41.14	-72.57	5	3.4	135	15	20	70	Long Island, NY	15
010982	1253	46.98	-66.66	10	5.7	93	0	273	90	New Brunswick	16
011982	0014	43.52	-71.61	5	4.7	240	20	150	10	Gaza, NH	15

References: 1. Herrmann (1978); 2. Sbar et. al. (1970); 3. Sbar et al. (1972); 4. Herrmann (1979); 5. Leblanc and Buchbinder (1977); 6. Pomeroy et al. (1976); 7. Yang and Aggarwal (1981); 8. Horner et al. (1978); 9. Pulli and Toksoz (1981) and this work; 10. Graham and Chiburis (1980); 11. Seborowski et al. (1982); 12. Horner et al. (1979); 13. Hasegawa and Wetmiller (1980); 14. Schlessinger-Miller et al. (1981); 15. Pulli and Godkin (1981) and this work; 16. Nabelek et al. (1982).

Table 3: Summary of fault plane solution parameters, from Pulli (1983)

HYPOINVERSE program (*Klein, 1978*). RMS errors are calculated for various trial depths. The crustal velocity structure picked for each event is appropriate for source area. RMS errors are calculated for each depth in two cases: (1) freely varying latitude, longitude and origin time, and (2) latitude, longitude and origin time fixed at the values computed in the depth-free calculation. Results are shown in Figure 12 and Figure 13. Depths are clearly confined to the upper 10 km for the events shown. Reasonable perturbations of the top layer velocity and thickness did not have a significant effect on the resulting focal depths.

This result agrees with well constrained focal depths from earthquakes in other areas of the Northeastern U.S. and Southeastern Canada, as reviewed by *Pulli (1989)*: Attica, N.Y., 2-3 km (*Herrmann, 1978*); Cornwall, ONT, 16 km (*Schlesinger-Miller et al., 1981*); Blue Mountain Lake, N.Y., 0.5-3.5 km (*Sbar et al., 1972*); Racquette Lake, N.Y., 1-3 km (*Yang and Aggarwal, 1981*); Plattsburgh, N.Y., 0-20 km (*Yang and Aggarwal, 1981*); Maniwaki and St. Donat, PQ, 17 and 7 km respectively (*Horner et al., 1978, 1979*); La Malbaie, PQ, 0-20 km (*Lebanc et al., 1978; Leblanc and Buchbinder, 1977; Hasegawa and Wetmiller, 1980*); Miramichi, NB, 0-7 km (*Nabelek et. al., 1982; Wetmiller et al., 1984*); and southeastern NY - northern NJ, 0-10 km (*Aggarwal and Sykes, 1978*). Additionally, the mainshock and most of the aftershocks of the 10/7/1983 mbLg = 5.2 Goodnow, NY earthquake were located at depths of about 7-8.5 km (*Seeber and Armbruster, 1986*).

The occurrence of the Miramichi, New Brunswick (mb = 5.7) and Gaza, New Hampshire (mb=4.7) earthquakes in 1982 have resulted in two detailed source studies by our group. These are included as Appendices C and D of this report.

6 Crustal Stresses in the Northeastern U.S.

Fifty three earthquake fault plane solutions and 18 non-seismic stress measurements have been combined to examine crustal stresses in the Northeastern U.S. and Southeastern Canada (*Pulli, 1989*). Non-seismic stress measurements include hydrofracturing measurements in Quebec, New York and Pennsylvania (*Overby and Rough, 1968; Haimson, 1974; Haimson and Lee, 1979*), strain relief measurements in New England (*Hooker and Johnson, 1969*), fault slip measurements in New York and Massachusetts (*Woodworth, 1907; Oliver et al., 1970*), core offset measurements in Connecticut and Pennsylvania (*Block et al., 1979; Schafer, 1979*), and pop-ups in New York (*Cushing et al., 1910;*

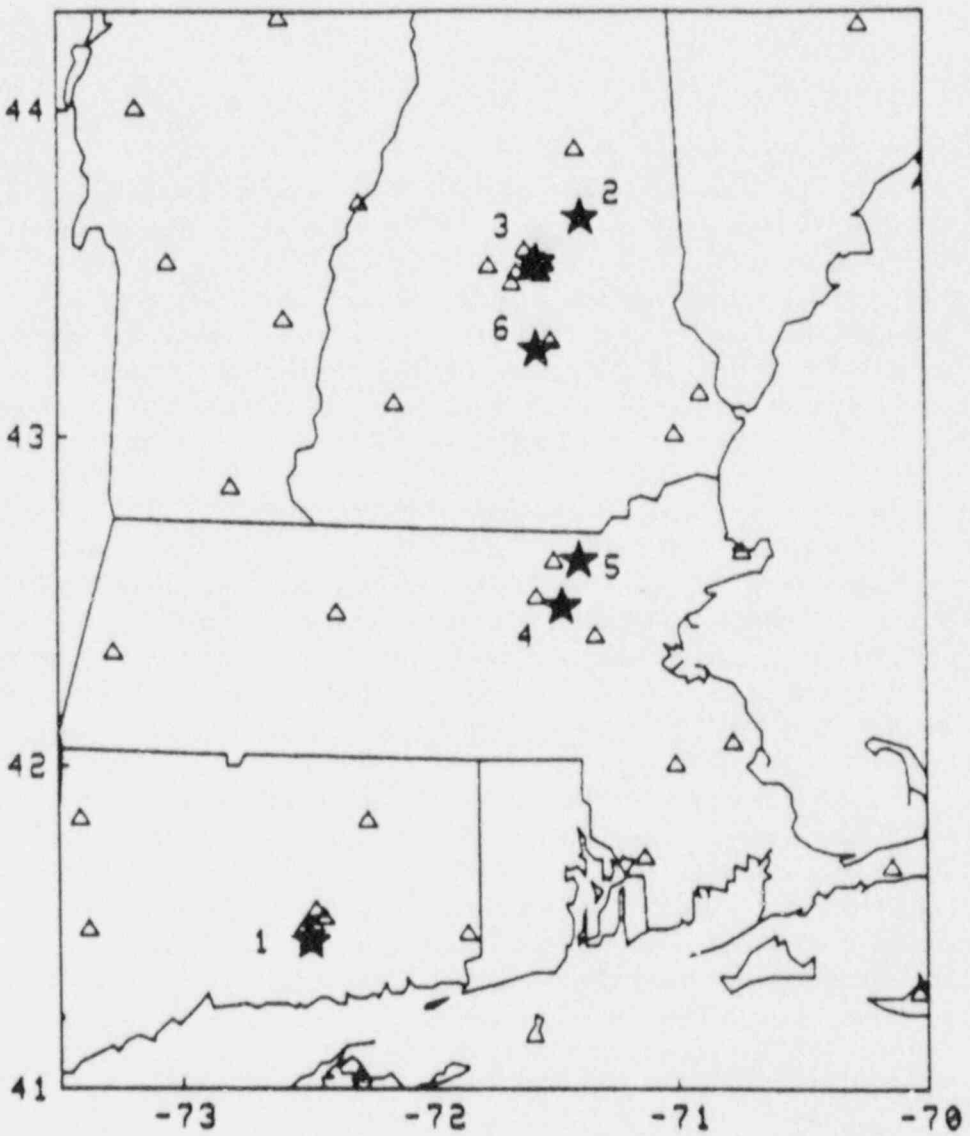

Figure 12: Events used in depth determination, from Pulli (1983)

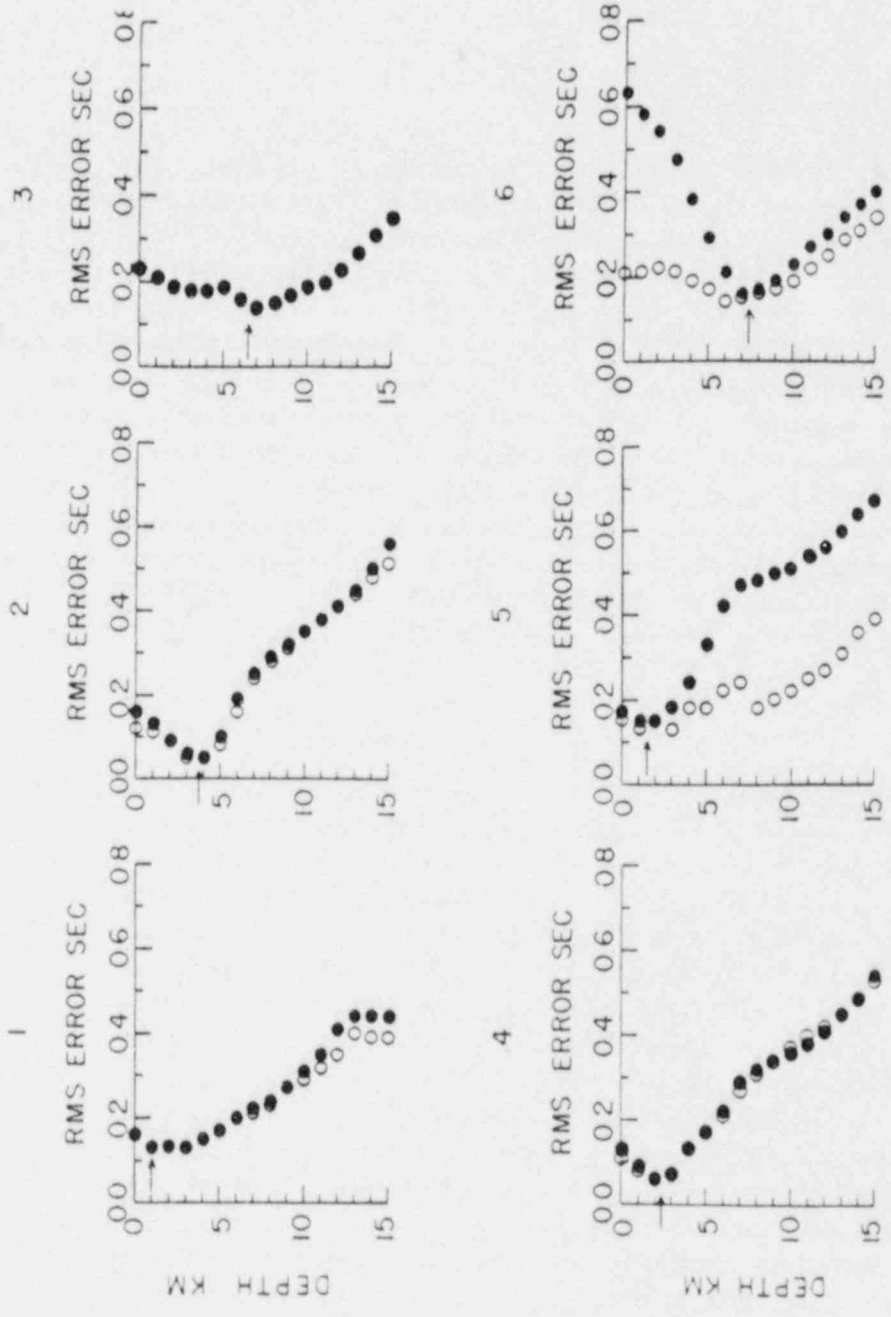

Figure 13: Determination of Focal Depths, from Pulli(1983)

Sbar and Sykes, 1978, 1977). The top sections of Figure 14 and Figure 15 show regional crustal stresses derived from a combination of these measurements. In the bottom section of these figures only earthquakes with $mb \geq 3.0$ have been considered, in an effort to reduce variability caused by measurements within the top few hundred meters. Figure 16 is a map of fault plane strikes in the area from Table 3. Based on Figures 14, 15 and 16, and on further tests by *Pulli (1983)* for uniform compressive stress fields within data subsets, it appears that the compressive stress field in the Precambrian Grenville province is uniform, horizontal and oriented ENE-WSW. In contrast, the stress field in the Appalachian province is non-uniform, although it may contain an underlying E-W regional trend. Somehow it appears that the Appalachians are modifying the regional tectonic stress field, perhaps due to topographic effects, or to residual stresses from past tectonic activity which did not affect the more stable Grenville province as much.

7 Seismic wave attenuation in New England

The attenuation of seismic coda waves was measured as a function of frequency using data from local earthquakes recorded digitally by the M.I.T. Seismic Network. Results of this study are described in *Pulli (1984)*. In the frequency band 0.75 to 10 Hz, Q_c was found to increase with frequency. At short lapse times within the train of coda waves ($t < 100sec$), Q_c increases from 400 at 3 Hz to 1300 at 10 Hz: $Q_c(f) = 140(f)^{0.95}$. This coda range results primarily from wavepaths in the upper crust. At longer lapse times ($t > 100sec$), Q_c increases from 660 at 1 Hz to 1500 at 10 Hz: $Q_c(f) = 660(f)^{0.40}$. This range corresponds to wavepaths primarily in the lower crust and upper mantle.

Pulli (1984) interpreted these results in terms of a scattering model from *Dainty (1981)*. According to this model, the coda Q can be divided into an anelastic or intrinsic Q_i component (frequency independent) and a scattering component: $1/Q_c(\omega) = 1/Q_i + v/\omega L$, where v is the seismic wave velocity (3.5 km/sec) and L is the mean free path. Two possible assumptions can be made. First, if Q_i is assumed to be infinite, i.e., only scattering occurs, L can be determined for short and long lapse times: 75 km for short lapse times; and a decrease from 400 km at 0.75 Hz to 90 km at 10 Hz. Second, if Q_i is assumed to be finite, fitting the above equation to the coda Q data leads to the following result: $Q_i = 1800$, L=80 km for short lapse times, L=400 km for long lapse times. Note that single scattering (the Born approximation) rather than multiple scattering has been applied, as justified in *Pulli (1984)*. A

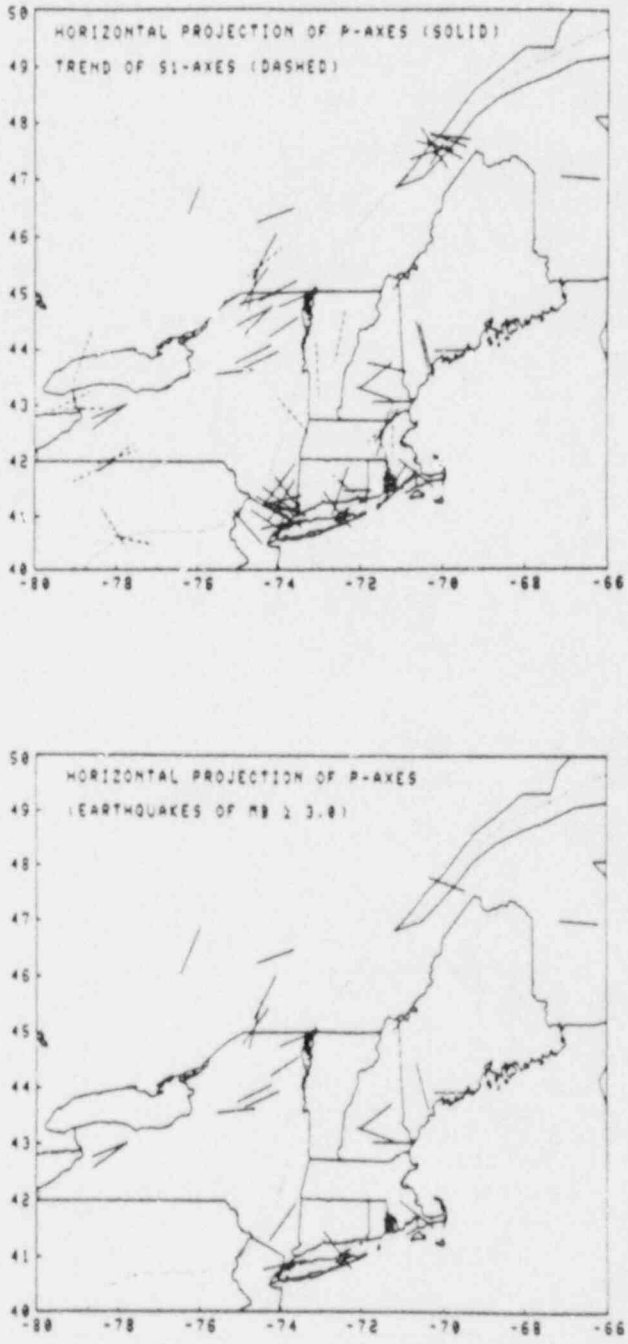

Figure 14: Maximum Horizontal Compressive Stress, from Pulli, 1983

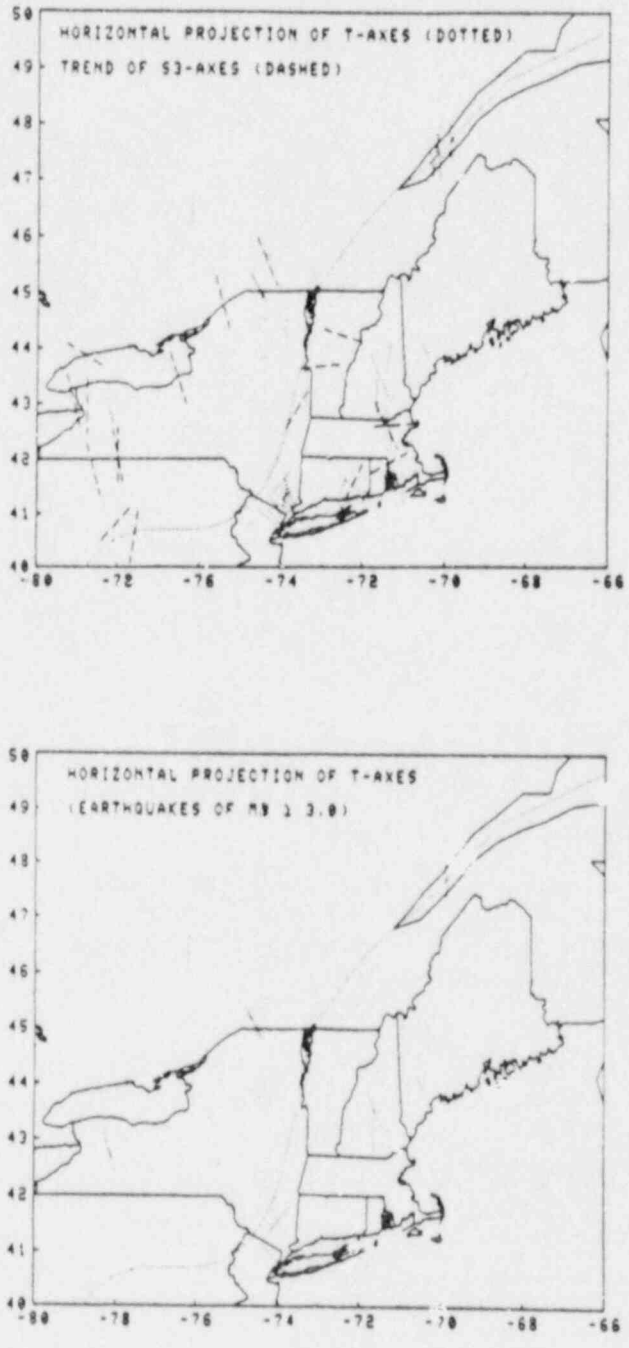

Figure 15: Minimum Horizontal Compressive Stress, from Pulli, 1983

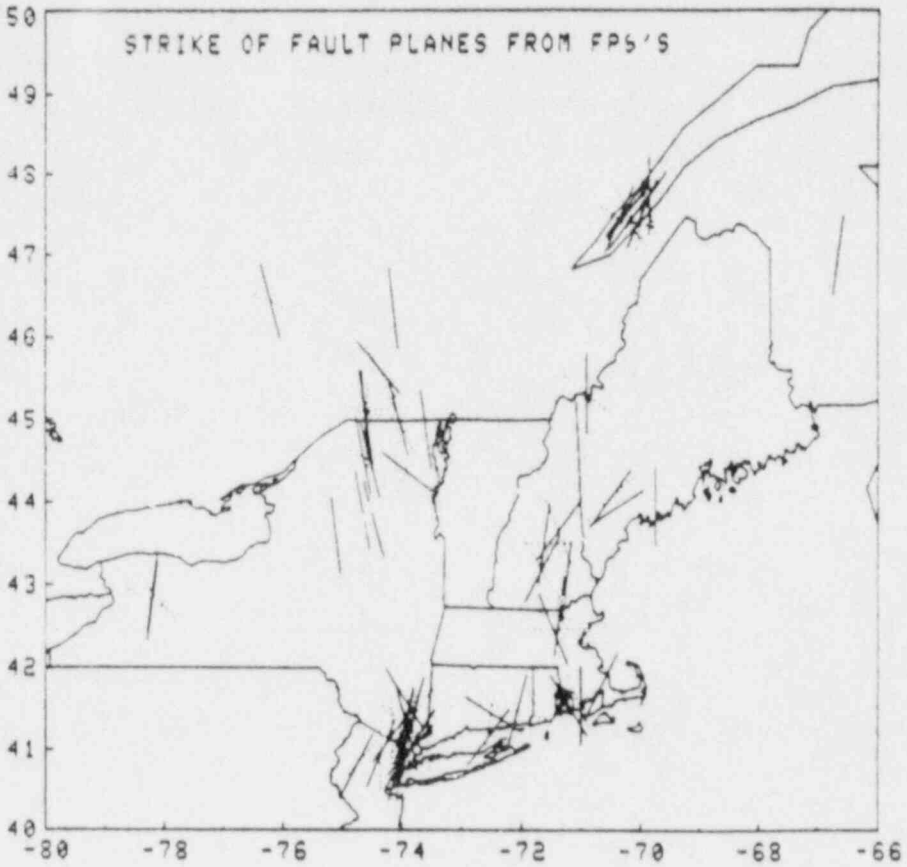

Figure 16: Strike of Fault Planes, from Pulli, 1983

comparison of results of this study with those of *Singh and Herrmann (1988)* in the Central and Western U.S. suggests that seismic attenuation in New England (proportional to Q_c^{-1}) is about twice as large as in the Central U.S., and about three times smaller than in the Western U.S. (*Pulli (1984)*.

References

[1] Aggarwal, Y.P and Sykes, L.R., Earthquakes, faults and nuclear power plants in Southern New York - Northern New Jersey, Science, 200,425-429, 1978.

[2] Bath, M., Seismic energy mapping applied to Turkey, Tectonophysics, 82, 69-87, 1982.

[3] Block, J.W., Clement, R.C., Lew, L.R. and de Boer, J., Recent thrust faulting in southeastern Connecticut, Geology, 7, 79-82, 1979.

[4] Chaplin, M.P., Taylor, S.R. and Toksoz, M.N., A coda-length magnitude scale for New England, Earthquake Notes, 51(4), 15-22, 1980.

[5] Chiburis, E.F., Ahner, R.O. and Graham, T., Northeastern U.S. Network Bulletin, Bulls. 1-11, 1976-1979.

[6] Curtin, P., Pulli, J. and Godkin, C., A new crustal model for central New England - implications for hypocentral calculations and fault plane solutions, Earthquake Notes, 54(3), Abstract, p.16, 1983.

[7] Cushing, H.P., Fairchild, H.L., Ruedemann, R., and Smith, C.H., Geology of the Thousand Island region, Bull. NY State Mus. Sci. Ser., 145, 1-185, 1910.

[8] Dainty, A., A scattering model to explain seismic Q observations in the lithosphere between 1 and 30 Hz, Geophys. Res. Letters, 11, 1126-1128, 1981.

[9] Dewey, J.F. and Burke, K.C.A., Tibetan, Variscan, and Precambrian basement reactivation: products of continental collision, J. Geol., 81, 683-692, 1973.

[10] Godkin, C.B. and Pulli, J.J., Application of the "Winding-Number Algorithm" to the spatial sorting of cataloged earthquake data, Bull. Seis. Soc. Am., 74, 1845-1849, 1984.

[11] Goforth, T. and E. Herrin, Automatic seismic detection algorithm based on the Walsh transform, Bull. Seis. Soc. Am., 71, 1351-1360, 1981.

[12] Graham, T. and Chiburis, E.F., Fault plane solutions and the state of stress in New England, Earthquake Notes, 51(2), 3-12, 1980.

[13] Haimson, B.C., A simple method for estimating in-situ stress at great depths, Field Testing and Instrumentation of Rock, Spec. Tech. Publ. 554, pp. 156-182, Amer. Soc. for Testing Materials, Philadelphia, PA, 1974.

[14] Haimson, B.C. and Lee, C.F., Stress measurements in underground nuclear slant design in Proceedings of 1979 Rapid Excavation and Tunneling Conference, Atlanta, GA, Soc. Mining Engrs. of AIME, Littleton, CO, 1979.

[15] Hasegawa, H.S. and Wetmiller, R.J., The Charlevoix earthquake of 19 August 1979 and its seismo-tectonic environment, Earthquake Notes, 51(4), 23-37, 1980.

[16] Herrmann, R.B., A seismological study of two Attica, New York earthquakes, Bull. Seis. Soc. Amer., 68, 641-651, 1978.

[17] Herrmann, R.B., Surface wave focal mechanisms for eastern United States earthquakes with tectonic implications, J. Geophys. Res., 84, 3543-3552, 1979.

[18] Hooker, V.E. and Johnson, C.F., Near surface horizontal stresses including the effects of rock anisotropy, U.S.B.M. Report 7224, 29 pp., 1969.

[19] Horner, R.B. Stevens, A.E., Hasegawa, H.S. and Leblanc, G., Focal parameters of the July 12, 1975 Maniwaki, Quebec, earthquake - an example of intraplate seismicity in eastern Canada, Bull. Seis. Soc. Amer., 68, 619-640, 1978.

[20] Horner, R.B., Wetmiller, R.J., and Hasegawa, H.S., The St-Donat, Quebec, earthquake of February 18-23, 1978, Can. J. Earth Sci., 16, 1892-1898, 1979.

[21] Klein, F.W., Hypocenter location program HYPOINVERSE, U.S. Geol. Surv. Open-file Report No. 78-694, 113 pp., 1978.

[22] Leblanc, G., Stevens, A.E., Wetmiller, R.J., and Duberger, R., A microearthquake survey of the St. Lawrence Valley near La Maibaie, Quebec, Can. J. Earth Sci., 10, 42-53, 1973.

[23] Leblanc, G. and Buchbinder, G., Second microearthquake survey of the St. Lawrence Valley near La Malbaie, Quebec, Can J. Earth Sci., 14, 2778-2789, 1977.

[24] Lee, W.H.K. and Lahr, J.C., HYPO71 (revised): A computer program for determining hypocenter, magnitude, and first motion pattern of local earthquakes. U.S. Geol. Surv. Open-file report 75-3111, 1-116, 1975.

[25] Michael, A.J., Gildea, S.P. and Pulli, J.J., A real-time digital seismic event detection and recording system for network applications. Bull. Seis. Soc. Amer., 72, 2339-2348, 1982.

[26] Nabelek, J., Suarez, G., and Toksoz, M.N., Source parameters of the New Brunswick earthquake of January 9, 1982 from inversion of teleseismic body and surface waves (abstract), Earthquake Notes,53, 28b, 1982.

[27] Nuttli, O.W., Seismic wave attenuation and magnitude relations for eastern North America, J. Geophys. Res., 78, 876-885, 1973.

[28] Oliver, J., Johnson, T., and Dorman, J., Post-glacial faulting and seismicity in New York and Quebec, Can. J. Earth Sci., 7, 579-590, 1970.

[29] Overby, W.K.Jr., and Rough, R.L., Surface studies predict orientation of induced formation fractures, Prod. Mon., 32, 16-19, 1968.

[30] Pomeroy, P.W., Simpson, D.W. and Sbar, M.L., Earthquakes triggered by surface quarrying - the Wappinger Falls, New York sequence of June, 1974, Bull. Seis. Soc. Am., 66, 685-700, 1976.

[31] Pulli, J.J., Stewart, R.R., Johnston, J.C., Tubman, K.M., and Michael, A., Field investigation and fault plane solution of the Bath, ME earthquake of April 18, 1979, Earthquake Notes,51(4), 39-46, 1980.

[32] Pulli, J.J. and Guenette, M.J., The Chelmsford-Lowell, MA earthquakes of 1980 and 1938, Earthquake Notes, 52(2), 3-11, 1981a.

[33] Pulli, J.J. and Guenette, M.J., The Chelmsford-Lowell, MA earthquake of November 23, 1980: depth control and fault plane solution,Bull. Seis. Soc. Amer., 71, 1369-1372, 1981b.

[34] Pulli, J.J. and Godkin, C.B., The Long Island Sound, New York earthquake of October 21, 1981, Earthquake Notes, 52(4), 23-27, 1981.

[35] Pulli, J.J. and Toksoz, M.N., Fault plane solutions for northeastern United States earthquakes, Bull.Seis. Soc. Amer., 71, 1875-1885, 1981.

[36] Pulli, J.J., Seismicity, earthquake mechanisms and seismic wave attenuation in the Northeastern United States, PhD Thesis, M.I.T., 1983.

[37] Pulli, J.J., Attenuation of coda waves in New England, Bull. Seis. Soc. Am., 74, 1149-1166, 1984.

[38] Putnam, G.W. and Sullivan, J.W., Granitic pegmatites as indicators of crustal pressures - a test in the eastern Adirondacks, New York, Geol., 7, 549-553, 1979.

[39] Sbar, M.L., Armbruster, J., and Aggarwal, Y.P., The Adirondacks, New York, earthquake swarm of 1971 and tectonic implications, Bull. Soc. Seis. Am., 62, 1303-1317, 1972.

[40] Sbar, M.L., Rynn, J.M.W., Gumper, F.J. and Lahr, J.C., An earthquake sequence and focal mechanism solution, Lake Hopatcong, northern New Jersey, Bull. Seis. Soc. Am., 60, 1231-1243, 1970.

[41] Sbar, M.L. and Sykes, L.R., Contemporary compressive stress and seismicity in eastern North America: an example of intraplate tectonics, Geol. Soc. Amer. Bull., 84, 1861-1882, 1973.

[42] Sbar, M.L. and Sykes, L.R., Seismicity and lithospheric stress in New York and adjacent areas, J. Geophys. Res., 82, 5771-5786, 1977.

[43] Schafer, K., Recent thrust faulting in the Appalachians, Nature, 280, 223-226, 1979.

[44] Schlesinger-Miller, E.A., Barstow, N.L. and Revetta, F.A., Recent earthquakes near Cornwall, Ontario, Earthquake Notes, 53(3), (abstract), 26, 1981.

[45] Seborowski, K.D., Williams G., Kelleher, J.A., and Statton, T.C., Tectonic implications of recent earthquakes near Annsville, New York, Bull. Seis. Soc. Am., 72, 1601-1609, 1982.

[46] Seeber, L. and Armbruster, J.G., A study of earthquake hazards in New York State and adjacent areas, Final Report covering the period 1982-1985, Lamont-Doherty Geological Observatory, NUREG/CR-4750, 1986.

[47] Shakal, A.F. and Toksoz, M.N., Earthquake hazard in New England, Science, 195, 171-173, 1977.

[48] Singh, S. and Herrmann, R.B., Regionalization of crustal coda Q in the continental United States, J. Geophys. Res., 88, 527-538, 1983.

[49] Taylor, S., Crust and upper mantle structure of the Northeastern United States, PhD Thesis, M.I.T., 1980.

[50] Taylor, S.R. and Toksoz, M.N., Three-dimensional crust and upper mantle structure of the northeastern United States, J. Geophys. Res., 84, 7627-7644, 1979.

[51] Taylor, S.R., Toksoz, M.N. and Chaplin, M.P., Crustal structure of the northeastern United States: contrasts between Grenville and Appalachian Provinces, Science, 208, 595-597, 1980.

[52] Taylor, S.R. and Toksoz, M.N., Measurement of interstation phase and group velocity using Wiener filtering, Bull. Seis. Soc. Amer., 72, 73-92, 1982.

[53] Wetmiller, R.J., Adams, J., Anglin, F.M., Hasegawa, H.S., and Stevens, A.E., Aftershock sequences of the 1982 Miramichi, New Brunswick, earthquakes, Bull. Seis. Soc. Amer., 74, 621-653, 1984.

Appendix A: M.I.T. Seismic Network Publications

References

[1] Chaplin, M.P., Taylor, S.R. and Toksoz, M.N., A coda-length magnitude scale for New England, Earthquake Notes, 51(4), 15-22, 1980.

[2] Curtin, P., Pulli, J. and Godkin, C., A new crustal model for central New England - implications for hypocentral calculations and fault plane solutions, Earthquake Notes, 54(3), Abstract, p.16, 1983.

[3] Godkin, C.B. and Pulli, J.J., Application of the "Winding-Number Algorithm" to the spatial sorting of cataloged earthquake data, Bull. Seis. Soc. Am., 74, 1845-1849, 1984.

[4] Michael, A.J., Gildea, S.P. and Pulli, J.J., A real-time digital seismic event detection and recording system for network applications, Bull. Seis. Soc. Amer., 72, 2339-2348, 1982.

[5] Nabelek, J., Suarez, G., and Toksoz, M.N., Source parameters of the New Brunswick earthquake of January 9, 1982 from inversion of teleseismic body and surface waves (abstract), Earthquake Notes,53, 28b, 1982.

[6] Nabelek, J., "The January 9, 1982, New Brunswick, Canada, earthquake", in Determination of Earthquake Source Parameters from Inversion of Body Waves, PhD Thesis, M.I.T., pp 144-181, 1984.

[7] Pulli, J.J., Focal mechanism of the Maine-Quebec border earthquake of June 15, 1973, as determined from the phase spectra of Rayleigh waves (abstract), Earthquake Notes, 48, 24, 1977.

[8] Pulli, J.J. and Benaron, N., Recent earthquake activity in New Hampshire and Massachusetts, Eastern Section SSA, Weston, MA, 1978.

[9] Pulli, J.J. and Graham, T., The earthquake mechanism in New England, Earthquake Notes, 49, (abstract), 86, 1979.

[10] Pulli, J.J., Stewart, R.R., Johnston, J.C., Tubman, K.M., and Michael, A., Field investigation and fault plane solution of the Bath, ME earthquake of April 18, 1979, Earthquake Notes,51(4), 39-46, 1980.

[11] Pulli, J.J. and Guenette, M.J., The Chelmsford-Lowell, MA earthquakes of 1980 and 1938, Earthquake Notes, 52(2), 3-11, 1981a.

[12] Pulli, J.J. and Guenette, M.J., The Chelmsford-Lowell, MA earthquake of November 23, 1980: depth control and fault plane solution,Bull. Seis. Soc. Amer., 71, 1369-1372, 1981b.

[13] Pulli, J.J. and Godkin, C.B., The Long Island Sound, New York earthquake of October 21, 1981, Earthquake Notes, 52(4), 23-27, 1981.

[14] Pulli, J.J. and Toksoz, M.N., Fault plane solutions for northeastern United States earthquakes, Bull.Seis. Soc. Amer., 71, 1875-1885, 1981.

[15] Pulli, J.J., Earthquakes of New England and adjacent areas, Appalachia Journal, 23-24, June, 1982.

[16] Pulli, J.J., Seismicity, earthquake mechanisms and seismic wave attenuation in the Northeastern United States, PhD Thesis, M.I.T., 1983.

[17] Pulli, J.J., Nabelek, J.L. and Sauber, J.M., Source parameters of the January 19, 1982 Gaza, N.H. earthquake, (abstract), Earthquake Notes, 54(3),28-29, 1983.

[18] Pulli, J.J., Attenuation of coda waves in New England, Bull. Seis. Soc. Am., 74, 1149-1166, 1984a.

[19] Pulli, J.J., Nuclear waste disposal and earthquake safety in the White Mountains, New Hampshire, Appalachia Journal, 162-163, June, 1984b.

[20] Shakal, A.F. and Toksoz, M.N., Earthquake hazard in New England, Science, 195, 171-173, 1977.

[21] Suarez, G. and Nabelek, J., The January 9 New Brunswick earthquake: a moment tensor inversion from the amplitude spectra of Rayleigh waves, (abstract), Earthquake Notes, 54(3), 34-35, 1983.

[22] Taylor, S.R. and Toksoz, Inversion of Rayleigh Wave phase velocities in New England, SSA meeting, Golden CO 1979a.

[23] Taylor, S.R. and Toksoz, M.N., Three-dimensional crust and upper mantle structure of the northeastern United States, J. Geophys. Res., 84, 7627-7644, 1979b.

[24] Taylor, S.R. and Toksoz, M.N., Frequency - wavenumber power spectra of fundamental mode Rayleigh waves across southeastern New England, Eastern Section SSA, 51st meeting (abstract), 1979c.

[25] Taylor, S., Crust and upper mantle structure of the Northeastern United States, PhD Thesis, M.I.T., 1980.

[26] Taylor, S.R., Toksoz, M.N. and Chaplin, M.P., Crustal structure of the northeastern United States: contrasts between Grenville and Appalachian Provinces, Science, 208, 595-597, 1980a.

[27] Taylor, S.R., Simmons, G. and Barosh, P., A gravity survey of the Clinton - Newbury and Bloody Bluff fault zones in eastern Massachusetts (abstract), in Abstracts with Programs, Geol. Soc. Am., 12, 86, 1980b.

[28] Taylor, S.R. and Toksoz, M.N., Measurement of interstation phase and group velocity using Wiener filtering, Bull. Seis. Soc. Amer., 72, 73-92, 1982a.

[29] Taylor, S.R. and Toksoz, M.N., Crust and upper mantle velocity structure in the Appalachian orogenic belt: implications for tectonic evolution, Bull. Geol. Soc. Am., 93, 315-329, 1982b.

Appendix B: Linear Velocity Gradient Crustal Model

A LINEAR VELOCITY GRADIENT CRUSTAL MODEL FOR NEW ENGLAND

Carl B. Godkin

Earth Resources Laboratory
Department of Earth, Atmospheric, and Planetary Sciences
Massachusetts Institute of Technology
Cambridge, MA 02139

January 1984

Abstract

A new crustal velocity model for P- and S-waves has been determined for New England. This model has a single layer with a linearly increasing wave velocity overlaying the higher, constant velocity half-space of the upper mantle. The model is obtained by a nonlinear least squares inversion inspired by the method of Mitchell and Hashim (1977). The P-wave model is $V_p(z) = 5.81+0.0430z$ km/s down to 39.5 km with a half-space velocity of 8.08 km/s. For the S-wave data, the best fit is $V_s(z) = 3.45+0.0193z$ km/s, the layer thickness is 31.2 km, and the half-space velocity is 4.33 km/s. The standard deviation of the P-wave fit is .53 seconds, while the S-wave fit is 1.15 seconds and probably not as reliable.

Introduction

Recent efforts to formulate a crustal velocity structure for New England (e.g., Curtin *et al.*, 1983; Taylor, 1980) have all arrived at a set of two or three constant velocity layers over a constant velocity half-space. This paper presents a different kind of model: a single layer with a linear increase in velocity with depth underlain by a constant speed half-space.

To arrive at the new crustal model, a nonlinear least squares inversion was applied to a set of 906 P-wave and 502 S-wave travel times. The travel times were derived from earthquakes and quarry blasts which occurred in and around New England within the last seven years and which were recorded by stations of the Northeastern United States Seismic network. This network is comprised of stations operated by M.I.T., Weston Observatory, Lamont-Doherty Geological Observatory, and cooperatively with the Earth Physics Branch of the Department of Energy, Mines, and Resources in Canada. Additional travel times were provided by Weston Geophysical Corp.

Method

The travel time curve generated by a model having a linear velocity increase with depth underlain by a higher speed half-space is hyperbolic out to the crossover distance where the half-space is first seen, and linear beyond this distance (Dobrin, 1976). The equation for travel time that should be used therefore depends on distance. There is a total of four independent parameters to be determined for this model: V_0, the velocity at the surface; k, the increase in velocity with depth in the layer; V_m, the half-space velocity; and H, the layer thickness.

There are two possible fastest paths a ray may follow from source to receiver. One path is entirely within the single layer. Only V_0 and k are needed to parameterize the single layer velocity:

$$V(z) = V_0 + kz \tag{1}$$

The rays in this layer are circular arcs and the travel time equation is

$$t = \frac{2}{k} \sinh^{-1} \frac{kx}{2V_0} \tag{2}$$

(Dobrin, 1976).

The first order travel time residual is

$$R = t_{observed} - t_{theoretical} = \Delta t = \frac{\partial t}{\partial k}\Delta k + \frac{\partial t}{\partial V_0}\Delta V_0 \tag{3}$$

where Δk and ΔV_0 are small model perturbations to be solved for in an effort to minimize the residual. The partial derivatives are found analytically from the time-distance equation (2). They are:

$$\frac{\partial t}{\partial k} = \frac{x}{kV_0}\left[1 + \left(\frac{kx}{2V_0}\right)^2\right]^{-1/2} - \frac{2}{k^2}\ln\left\{\frac{kx}{2V_0} + \left[\left(\frac{kx}{2V_0}\right)^2 + 1\right]^{1/2}\right\} \tag{4}$$

$$\frac{\partial t}{\partial V_0} = -\frac{x}{V_0^2}\left[1 + \frac{kx}{2V_0^2}\right]^{-1/2} \tag{5}$$

The second possible path descends through the layer and refracts along the top of the half-space. The refracted path is always possible whereas the other path is not seen beyond the critical distance. There is a crossover distance before or at the critical distance after which the refracted path becomes the quicker route. In calculations involving the refracted path, all four free parameters come into play. From Dobrin (1976) again, the expression for travel time beyond the crossover is

$$t = \frac{x}{V_m} + \frac{2}{k}\left\{\cosh^{-1}\frac{V_m}{V_0} - \cosh^{-1}\frac{V_m}{V_0 + kH} - \left[1 - \left(\frac{V_0}{V_m}\right)^2\right]^{1/2} + \left[1 - \left(\frac{V_0 + kH}{V_m}\right)^2\right]^{1/2}\right\} . \tag{6}$$

The travel time residual to first order in this case is

$$R = t_{observed} - t_{theoretical} = \Delta t = \frac{\partial t}{\partial k}\Delta k + \frac{\partial t}{\partial V_0}\Delta V_0 + \frac{\partial t}{\partial V_m}\Delta V_m + \frac{\partial t}{\partial H}\Delta H . \tag{7}$$

Here, again, Δk, ΔV_0, ΔV_m and ΔH are small corrections to the model and the partial derivatives can be found analytically:

$$\frac{\partial t}{\partial k} = -\frac{2}{k^2}\left[\cosh^{-1}\frac{V_m}{V_0} - \cosh^{-1}\frac{V_m}{V_0 + kH} - \left[1 - \left(\frac{V_0}{V_m}\right)^2\right]^{1/2} + \left[1 - \left(\frac{V_0 + kH}{V_m}\right)^2\right]^{1/2}\right] + \frac{2}{k}\left[\frac{\frac{H}{V_0 + kH}}{\left[1 - \left(\frac{V_0 + kH}{V_m}\right)^2\right]^{1/2}} - \frac{\frac{H}{V_m}}{\left[\left(\frac{V_m}{V_0 + kH}\right)^2 - 1\right]^{1/2}}\right] \tag{8}$$

$$\frac{\partial t}{\partial V_0} = \frac{2}{k}\left[\frac{\frac{1}{V_m} - \frac{V_m}{V_0^2}}{\left[\left(\frac{V_m}{V_0}\right)^2 - 1\right]^{1/2}} - \frac{\frac{1}{V_m} - \frac{V_m}{(V_0 + kH)^2}}{\left[\left(\frac{V_m}{V_0 + kH}\right)^2 - 1\right]^{1/2}}\right] \tag{9}$$

$$\frac{\partial t}{\partial V_m} = -\frac{x}{V_m^2} + \frac{2}{k}\left[\frac{1-\left(\frac{V_0}{V_m}\right)^2}{[V_m^2 - V_0^2]^{1/2}} - \frac{1-\left(\frac{V_0+kH}{V_m}\right)^2}{[V_m^2 - V_0 + kH^2]^{1/2}}\right] \tag{10}$$

$$\frac{\partial t}{\partial H} = \frac{2}{k}\left[\frac{\frac{k}{V_0+kH}}{\left[1-\left(\frac{V_0+kH}{V_m}\right)^2\right]^{1/2}} - \frac{\frac{k}{V_m}}{\left[\left(\frac{V_m}{V_0+kH}\right)^2 - 1\right]^{1/2}}\right] \tag{11}$$

After a series of observations are made, a set of m equations in four unknowns is obtained. In matrix form they are:

$$\begin{bmatrix} \frac{\partial t_1}{\partial k} & \frac{\partial t_1}{\partial V_0} & \frac{\partial t_1}{\partial V_m} & \frac{\partial t_1}{\partial H} \\ \frac{\partial t_2}{\partial k} & \frac{\partial t_2}{\partial V_0} & \frac{\partial t_2}{\partial V_m} & \frac{\partial t_2}{\partial H} \\ \vdots & \vdots & \vdots & \vdots \\ \vdots & \vdots & \vdots & \vdots \\ \frac{\partial t_m}{\partial k} & \frac{\partial t_m}{\partial V_0} & \frac{\partial t_m}{\partial V_m} & \frac{\partial t_m}{\partial H} \end{bmatrix} \begin{bmatrix} \Delta k \\ \Delta V_0 \\ \Delta V_m \\ \Delta H \end{bmatrix} = \begin{bmatrix} R_1 \\ R_2 \\ \vdots \\ \vdots \\ R_m \end{bmatrix} \tag{12}$$

Since m may get very large, these matrices may grow too large to be easily manipulated. It is useful to proceed as follows to save space. Rewrite the matrix equation as

$$\mathbf{A}\underline{\Delta x} = \underline{r} \tag{13}$$

and multiply both sides by $\mathbf{A}^T$:

$$\mathbf{A}^T\ \mathbf{A}\underline{\Delta x} = \mathbf{A}^T\ \underline{r}\,. \tag{14}$$

Now $\mathbf{A}^T\ \mathbf{A}$ is a more tractable 4×4 matrix and $\mathbf{A}^T\ \underline{r}$ is a four component vector. The perturbations are found by

$$\underline{\Delta x} = (\mathbf{A}^T\ \mathbf{A})^{-1}\ \mathbf{A}^T\ \underline{r} \tag{15}$$

and are then added to the model parameters.

The actual computer coding is carried out by premultiplying out $\mathbf{A}^T\ \mathbf{A}$ and $\mathbf{A}^T\ \underline{r}$ so that the elements may be simply accumulated as is done in any least squares problem. In this case

$$\mathbf{A}^T\ \underline{r} = \begin{bmatrix} \sum R_i \frac{\partial t_i}{\partial k} \\ \sum R_i \frac{\partial t_i}{\partial V_0} \\ \sum R_i \frac{\partial t_i}{\partial V_m} \\ \sum R_i \frac{\partial t_i}{\partial H} \end{bmatrix} \tag{16}$$

and

$$\mathbf{A}^T\,\mathbf{A} = \begin{bmatrix} \sum\left(\frac{\partial t_i}{\partial k}\right)^2 & \vdots & \vdots & \vdots \\ \sum\left(\frac{\partial t_i}{\partial V_0}\right)\left(\frac{\partial t_i}{\partial k}\right) & \sum\left(\frac{\partial t_i}{\partial V_0}\right)^2 & \vdots & \\ \sum\left(\frac{\partial t_i}{\partial V_m}\right)\left(\frac{\partial t_i}{\partial k}\right) & \sum\left(\frac{\partial t_i}{\partial V_m}\right)\left(\frac{\partial t_i}{\partial V_0}\right) & \sum\left(\frac{\partial t_i}{\partial V_m}\right)^2 & \vdots \\ \sum\left(\frac{\partial t_i}{\partial H}\right)\left(\frac{\partial t_i}{\partial k}\right) & \sum\left(\frac{\partial t_i}{\partial H}\right)\left(\frac{\partial t_i}{\partial V_0}\right) & \sum\left(\frac{\partial t_i}{\partial H}\right)\left(\frac{\partial t_i}{\partial V_M}\right) & \sum\left(\frac{\partial t_i}{\partial H}\right)^2 \end{bmatrix} \tag{17}$$

Matrix $\mathbf{A}^T\,\mathbf{A}$ is symmetric. Note that the partial derivatives $\frac{\partial t}{\partial V_m}$ and $\frac{\partial t}{\partial H}$ are equal to zero identically before the crossover distance.

The crossover distance for each model iteration must be found so that the partial derivatives for a given distance may be calculated correctly. There is no easy way to do this since it involves equating the pre- and post-crossover distance travel time equations (2 and 6) and solving for x, the distance at which the two curves intersect. This is difficult since equation (2) involves the arc hyperbolic sine of distance x. Numerical methods must be used to solve this equation empirically.

This is avoided by computing both possible fastest travel times before the critical distance and using the smaller. This method is easier to use because the critical distance can be found analytically. Working from the knowledge that raypaths in the layer are circular arcs an expression for distance x as a function of the depth of greatest penetration can be derived. See Figure 1.

The Pythagorean Theorem says

$$\left(\frac{x}{2}\right)^2 + \left(\frac{V_0}{d}\right)^2 = r^2\,. \tag{18}$$

The radius of the circular arc path is $1/kp$ (Dobrin, 1976) and since $p = 1/V_{bottom}$, the radius is then $r = V_{bottom}/k$. So:

$$\frac{x^2}{4} = \frac{1}{k^2}(V_{bottom}^2 - V_0^2)\,. \tag{19}$$

The velocity at the bottom of the arc is, in this model,

$$V_{bottom} = V_0 + k z_{\max}\,. \tag{20}$$

Thus, after some algebra,

$$x = 2\left[\frac{2V_0 z_{\max}}{k} + z_{\max}^2\right]^{1/2}\,. \tag{21}$$

As distance x is increased, the last ray to travel solely in the variable velocity layer is that ray which penetrates just deep enough to skim the top of the higher speed half-space. The range of this ray is the critical distance x_c.

To find x_c, substitute $z_{\max} = H$ into (21). Now

$$x_c = 2\left[\frac{2V_0 H}{k} + H^2\right]^{1/2}\,. \tag{22}$$

Data Anlaysis

906 P-wave and 502 S-wave travel times were used in this analysis. All data had to meet several criteria. Only data whose entire raypath lay within the rectangle extending from 40°to 46°N and 67°to 74°W were used. Figure 2 shows all of the raypaths used in the P-wave analysis. To minimize the effect on travel time of source depth, data from earthquakes deeper than 5 km were not included. The effect on the travel times of assuming a surface focus in these calculations is always less than one second for close-in events and disappears by 40 km (S.R. Taylor, 1980). To avoid having to deal with earth curvature for distant events, source to receiver distances were restricted to less than 500 km.

The earthquake locations used to compute the travel times and epicentral distances came from three sources: The N.E.U.S.S.N. *Bulletins* (1976–1983) published by Weston Observatory and covering the years 1975–1981, the M.I.T. Seismic Network's *Quarterly Bulletins* (1981–1984), and unpublished locations computed by the M.I.T. Seismic Network. The seismic stations used in this study are shown in Figure 3.

The travel time data are shown plotted in Figure 4. The prompting for the paper was the difficulty in finding clear "breaks" in the slope of the travel time plot (other than the break at about 200 km) which correspond to crossovers. To formulate a plane layered model of two or three constant velocity layers over a constant velocity half-space, it is important to pick the crossovers correctly. Since the travel time curve out to about 200 km seems to smoothly increase, it is very difficult to pick crossovers with any certainty. The monotonically increasing inverse hyperbolic sine in equation (2) seems a more natural fit than the series of straight lines a plane layered model produces.

A computer program caled MARKR was written and used to invert the travel time data in the manner described in the previous section. Since the method is iterative and the point of convergence is partially determined by the starting values of k, V_0, V_m,and H, several runs were made and the (nearly identical) results were averaged. The best fit to the P-wave data comes from the model

Layer velocity: $5.81 \pm .017) + (0.0430 \pm .002)z$ km/s

Layer thickness: 39.5 ± 1.9 km

Half-space velocity: $8.08 \pm .06$ km/s

For the S-wave data, the best fitting model is

Layer velocity: $(3.45 \pm .017) + (0.0193 \pm .002)z$ km/s

Layer thickness: 31.2 ± 3.6 km

Half-space velocity: $4.33 \pm .05$ km/s

These models' fits to the travel time data are shown in Figure 5 and Figure 6 shows the theoretical travel time curves. Figure 7 shows velocity versus depth diagrams plotted in comparison with other models for the region.

To get an idea of the reliability of the S-wave model versus the P-wave model (which is assumed to be more accurate since there are more points and because P-wave arrivals are usually more easily picked on seismograms), V_p/V_s versus depth is plotted in Figure 8. A Poisson solid has a V_p/V_s ratio of $\sqrt{3}$. The dashed line in Figure 8 represents this Poisson solid. The dashed line falls within the uncertainty of the models in only part of the figure.

The fit of the theoretical time-distance curve to the data is very close. The root mean squared (RMS) travel time residual of the fit, σ, is given by

$$\sigma^2 = \sum_{i=1}^{m} \frac{(t_{observed} - t_{theoretical})^2}{m-4} \tag{23}$$

(J.R. Taylor, 1982) where m is the number of observations and $m-4$ is the number of degrees of freedom of the system (since it has 4 parameters) $\sigma = 0.533$ seconds for the P-wave model and 1.15 seconds for the S-wave model. The P-wave fit is quite close considering that the RMS error for a fifth order polynomial fit to the P-wave data is a shade more, .537 seconds. By comparison, the RMS errors associated with the various regional layer-cake models of the Northeast have RMS errors of between .544 and .629 seconds. These values were calculated from the data used in this study which came from all over New England, while some of these models were derived for only certain parts of the Northeast.

Conclusion

A new crustal velocity model is useful only if it can be applied to problems of the region being modeled. A model with a linearly increasing velocity with depth over a constant velocity half-space is sufficiently different from the other models for the Northeast that it is not possible to simply substitute it into existing algorithms for finding earthquake locations, fault plane solutions, etc. Instead, these algorithms must be modified and in some cases, such as the problem of determining take-off angles, even simplified. Since this model provides the best fit of any tested to at least this data set, some of these algorithms should be formulated.

REFERENCES

Curtin, Patricia L., Jay J. Pulli, and Carl B. Godkin, A new crustal model for central New England—Implications for hypocentral calculations and fault plane solution, presented at the 1983 Annual Meeting of the Eastern Section Seis. Soc. of Am.

Dobrin, Martin B., *Introduction to Geophysical Prospecting*, 3rd ed., McGraw Hill, New York, 1976.

M.I.T. Seismic Network *Quarterly Bulletins*. Published by the M.I.T.S.N., Cambridge, MA, 1981–1984.

Mitchell, Brian J. and Braik M. Hashim, Seismic velocity determinations in the New Madrid Seismic Zone: A method using local earthquakes, *Bull.. Seis. Soc. Am., 67*, 413–424, 1977.

Northeastern United States Seismic Network, *Bulletins, 1–25*. Published by Weston Observatory, Weston, MA, 1976–1983.

Taylor, John R., *An Introduction to Error Analysis*. University Science Books, Mill Valley, CA., 1982.

Taylor, Steven R., Crust and Upper Mantle Structure of the Northeastern United States, Ph.D. Thesis, M.I.T., Cambridge, MA, 1980.

Taylor, Steven R. and M. Nafi Toksöz, Three-dimensional crust and upper mantle structure of the northeastern United States, *J. Geophys. Res., 84*, 7627–7644, 1979.

ACKNOWLEDGMENTS

This work was supported by U.S. Nuclear Regulatory Commission Contract NRC-04-76-209

Figure Captions

Figure 1. Diagram of raypaths for a model with a linear increase in wave velocity with depth. The center of the circular path lies on the dashed line above the surface which is where $V(z) = V_0 + kz = 0$.

Figure 2. P-wave paths used in this study. Most of the data came from paths crossing the center of New England.

Figure 3. Stations of the N.E.U.S.S.N. and cooperating networks.

Figure 4. Travel time vs. distance plots of the P-wave and S-wave data used in this study.

Figure 5. Fit of the new model's time-distance curve to the P- and S-wave data.

Figure 6. Travel time curves generated by the new model.

Figure 7. Velocity vs. depth plots comparing the new model with other models for the Northeast. The new model is shown as a dotted line on each plot.
(a) Curtin *et al.* (1983). P-wave model for central New England. (b) N.E.U.S.S.N. (1976–1983). P-wave model for New England. (c) Taylor (1980). P-wave model for New England. (d) Taylor and Toksöz (1979). P-wave model for eastern Massachusetts and southern New Hampshire. (e) Curtin *et al.* (1983). S-wave model for central New England. (f) Taylor (1980). S-wave model for New England.

Figure 8. Plot of V_p/V_s vs. depth for the new model. Maximum and minimum values are shown by the dotted lines. The vertical dashed line represents the value for a Poisson solid.

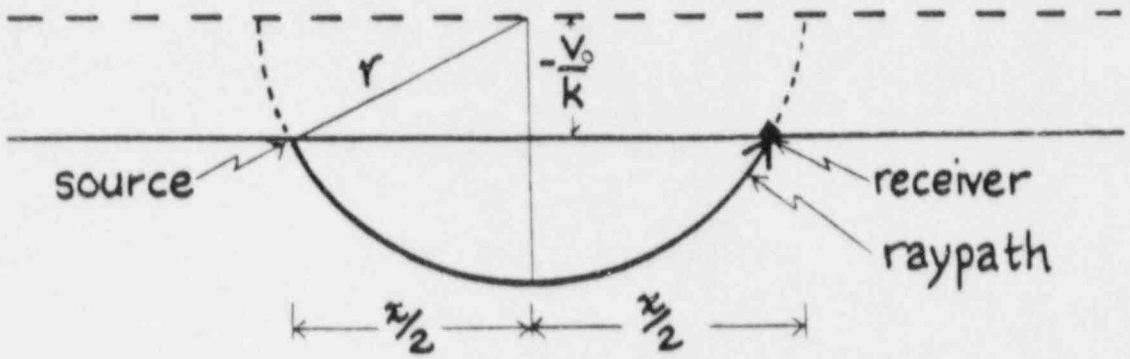

Figure 1

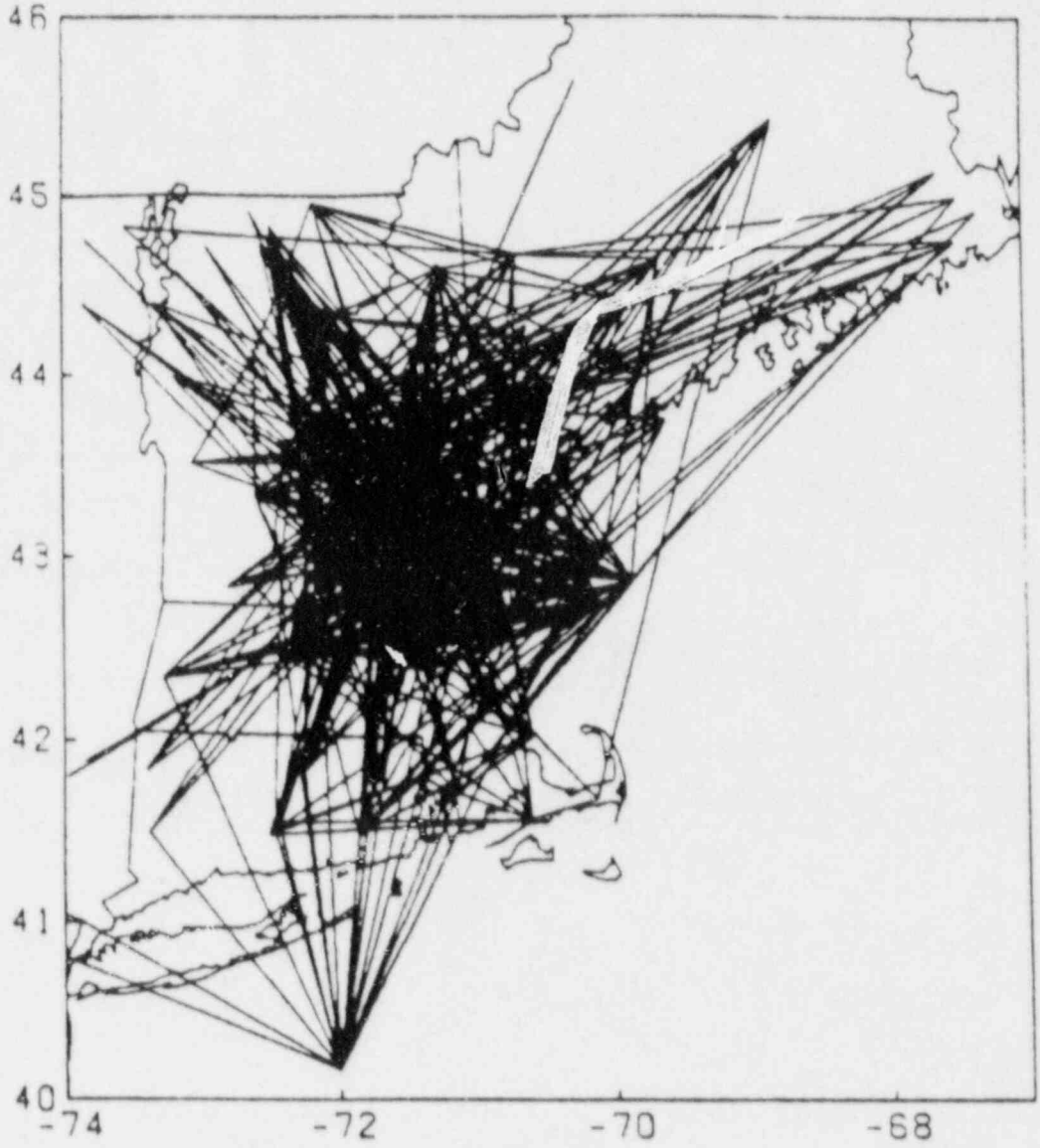

Figure 2

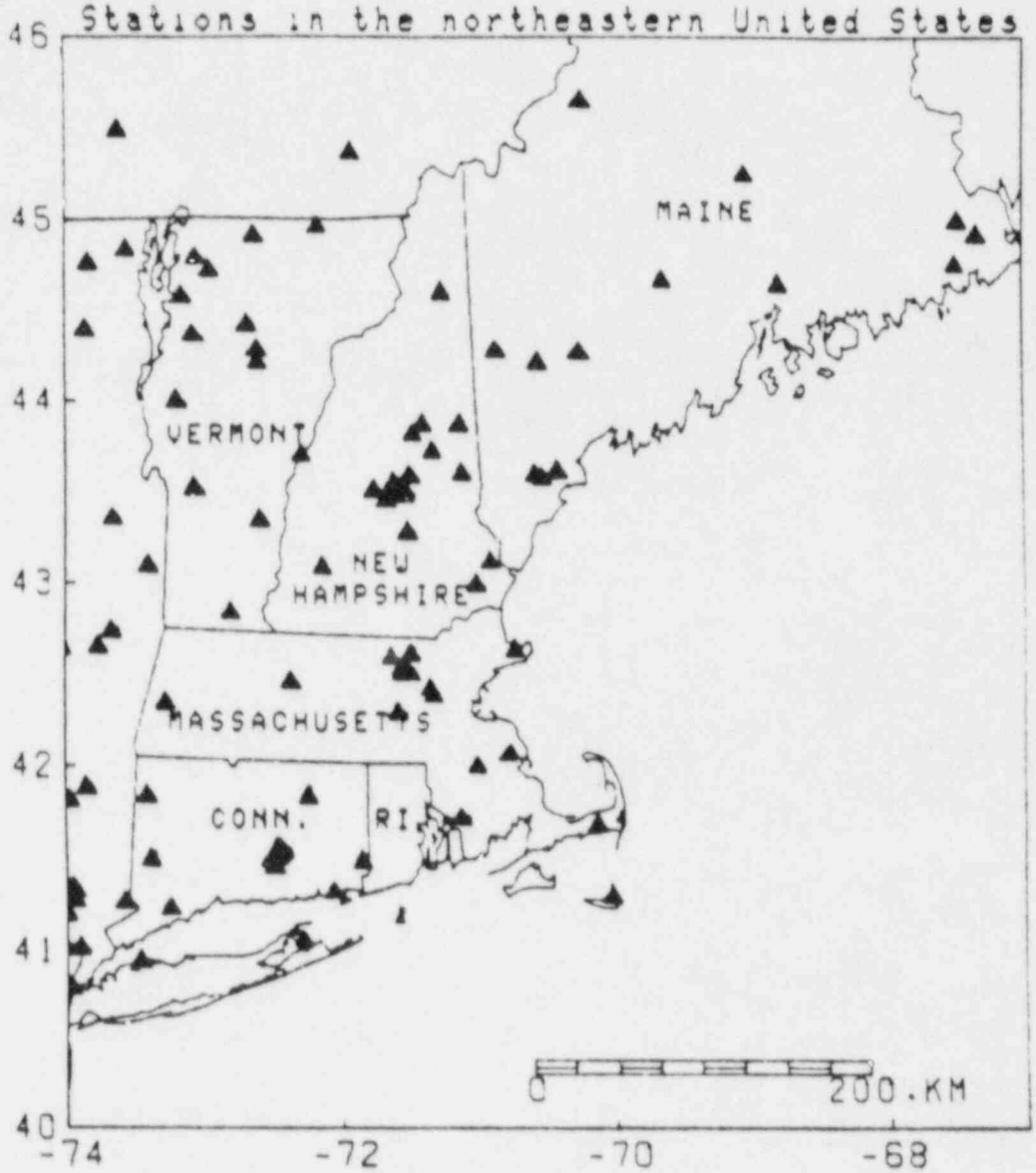
Stations in the northeastern United States
MAINE
VERMONT
NEW HAMPSHIRE
MASSACHUSETTS
CONN.
RI
0
200. KM
46
45
44
43
42
41
40
-74
-72
-70
-68

Figure 3

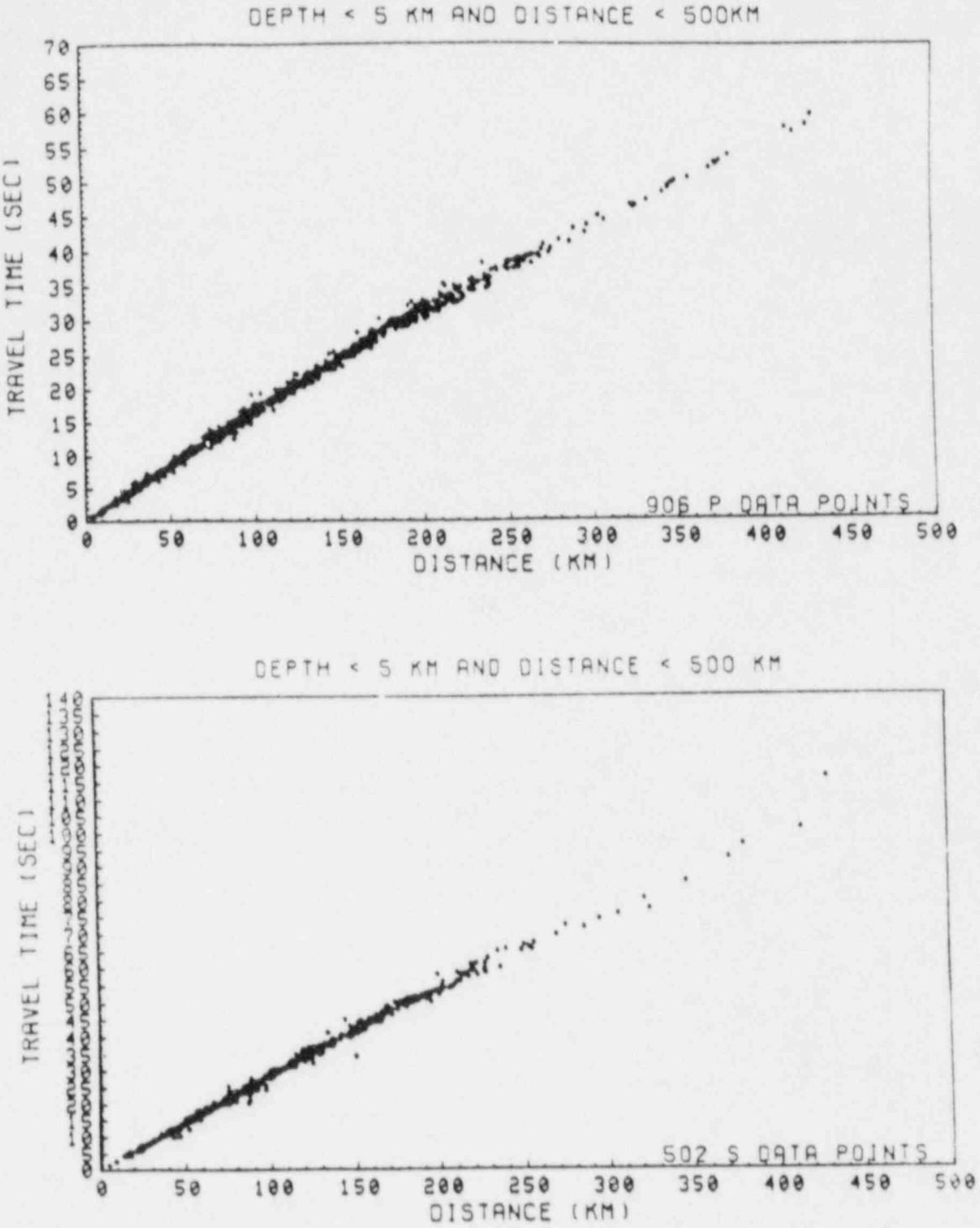
DEPTH < 5 KM AND DISTANCE < 500KM
TRAVEL TIME (SEC)
DISTANCE (KM)
906 P DATA POINTS
DEPTH < 5 KM AND DISTANCE < 500 KM
TRAVEL TIME (SEC)
DISTANCE (KM)
502 S DATA POINTS

Figure 4

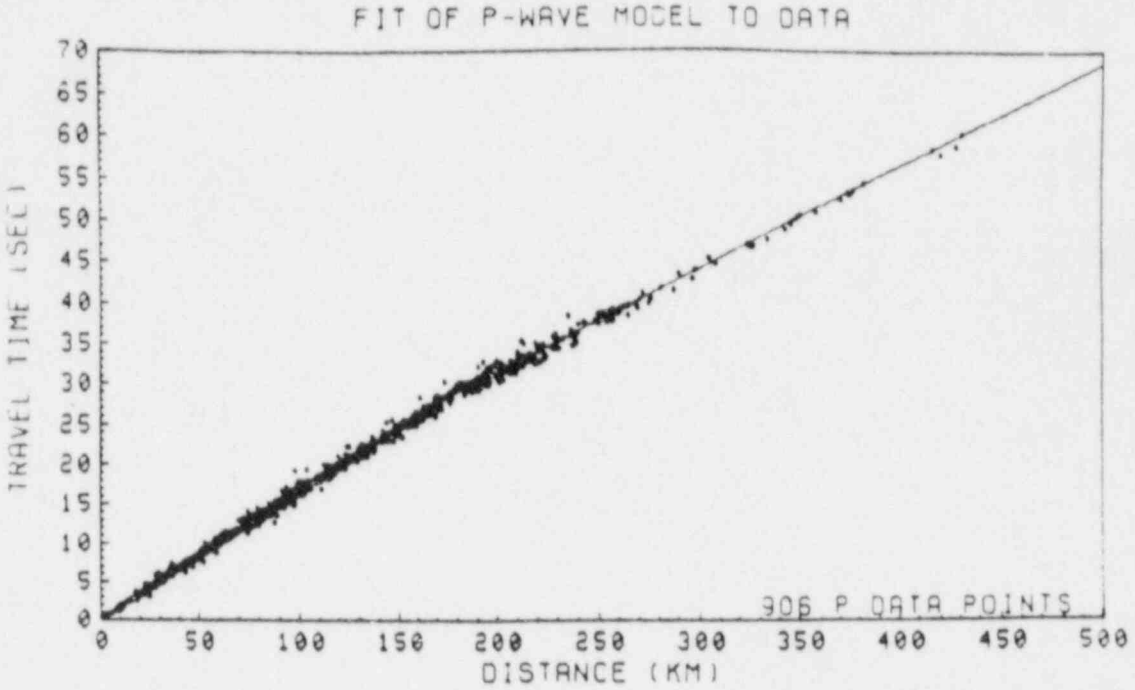
FIT OF P-WAVE MODEL TO DATA
TRAVEL TIME (SEC)
0
5
10
15
20
25
30
35
40
45
50
55
60
65
70
306 P DATA POINTS
0
50
100
150
200
250
300
350
400
450
500
DISTANCE (KM)

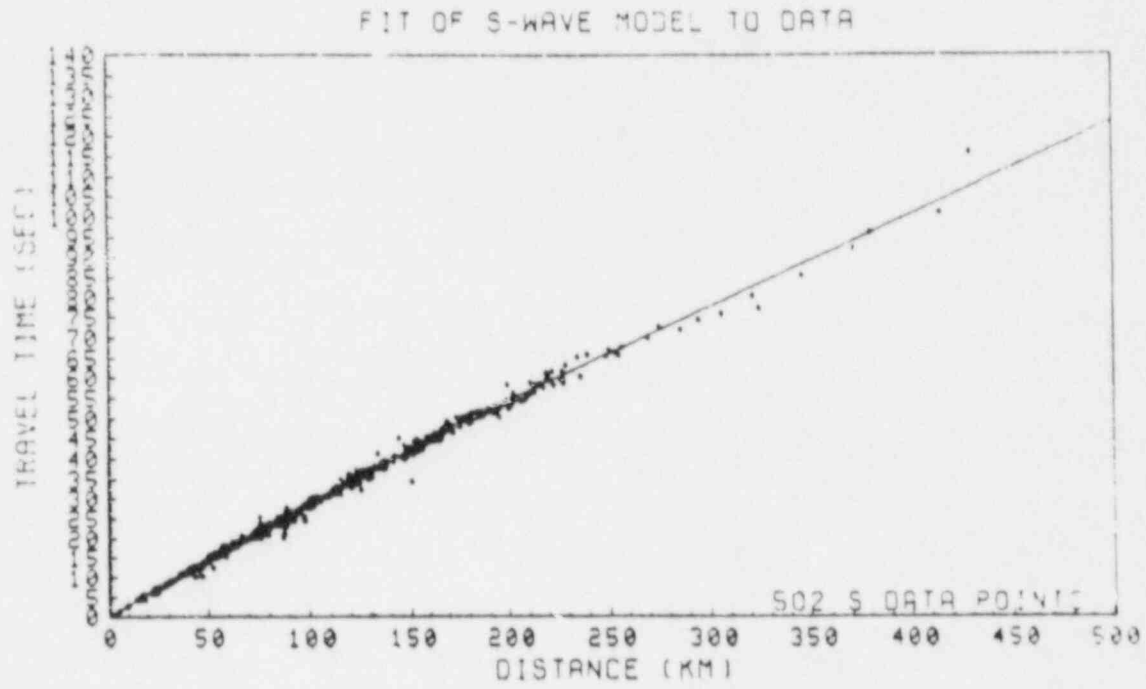
FIT OF S-WAVE MODEL TO DATA
TRAVEL TIME (SEC)
502 S DATA POINTS
0
50
100
150
200
250
300
350
400
450
500
DISTANCE (KM)

Figure 5

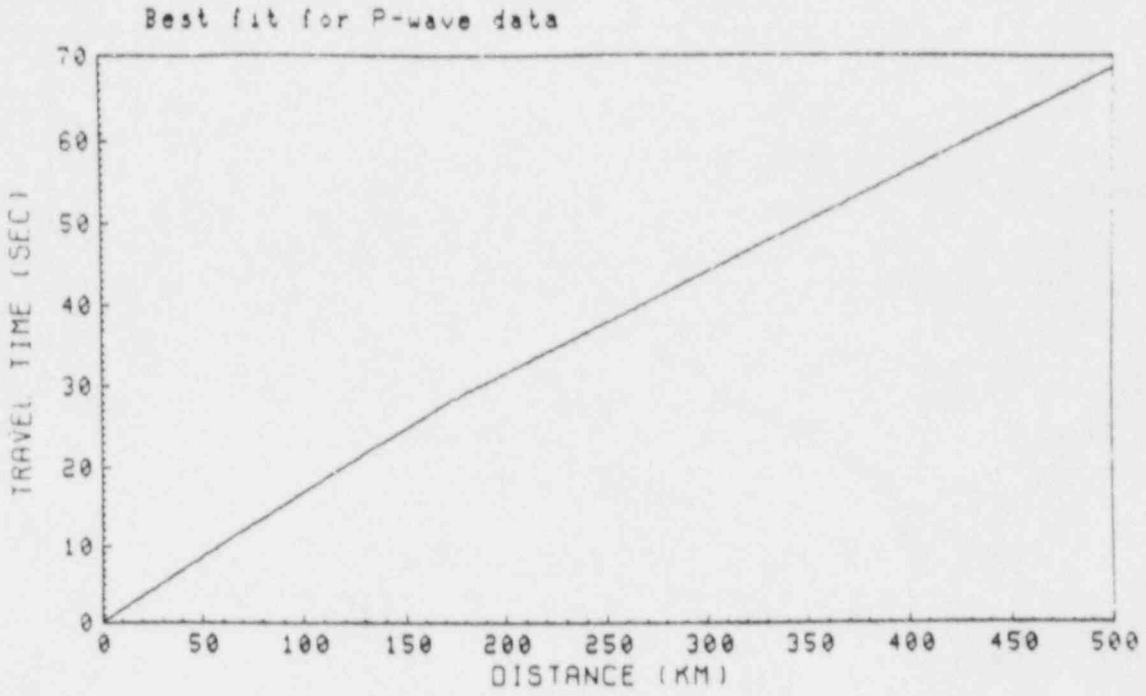
Best fit for P-wave data
TRAVEL TIME (SEC)
0
10
20
30
40
50
60
70
0
50
100
150
200
250
300
350
400
450
500
DISTANCE (KM)

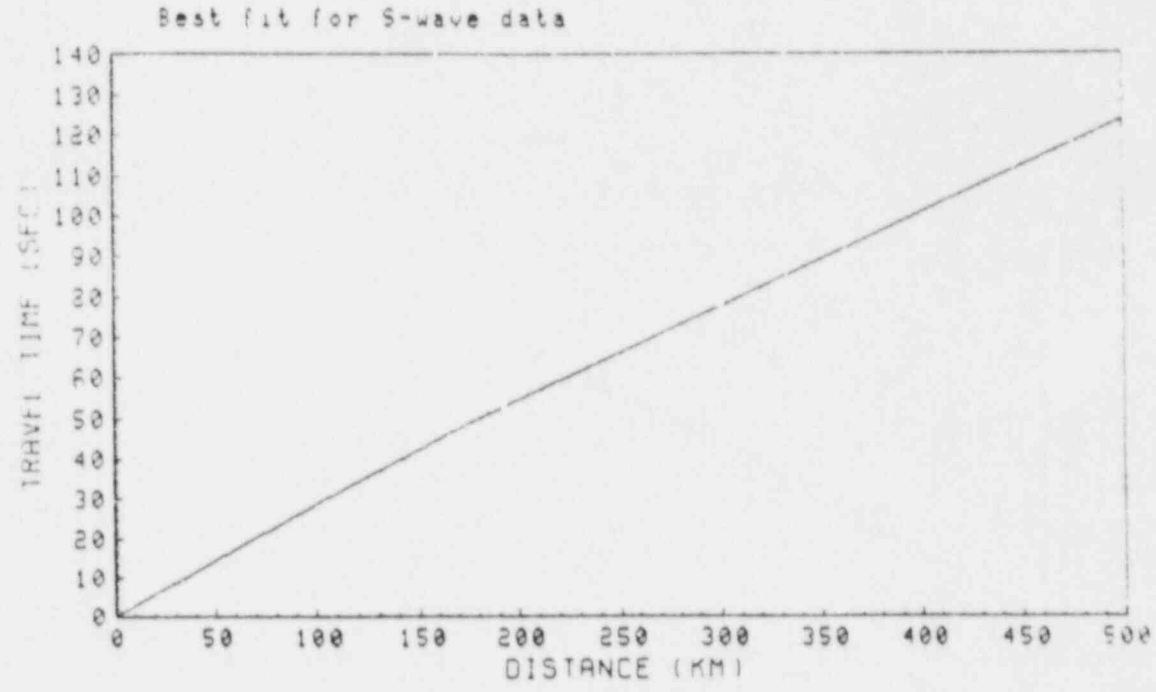
Best fit for S-wave data
0
10
20
30
40
50
60
70
80
90
100
110
120
130
140
0
50
100
150
200
250
300
350
400
450
500
DISTANCE (KM)

Figure 6

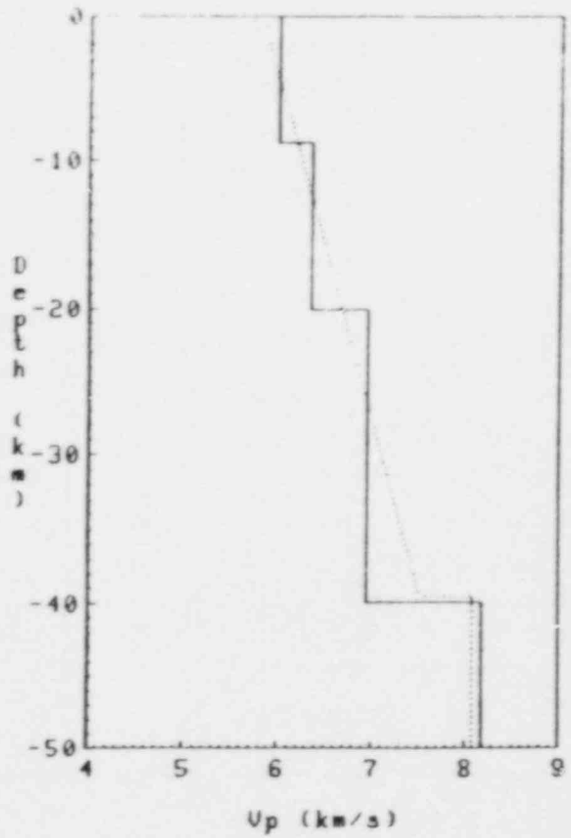

Figure 7 a

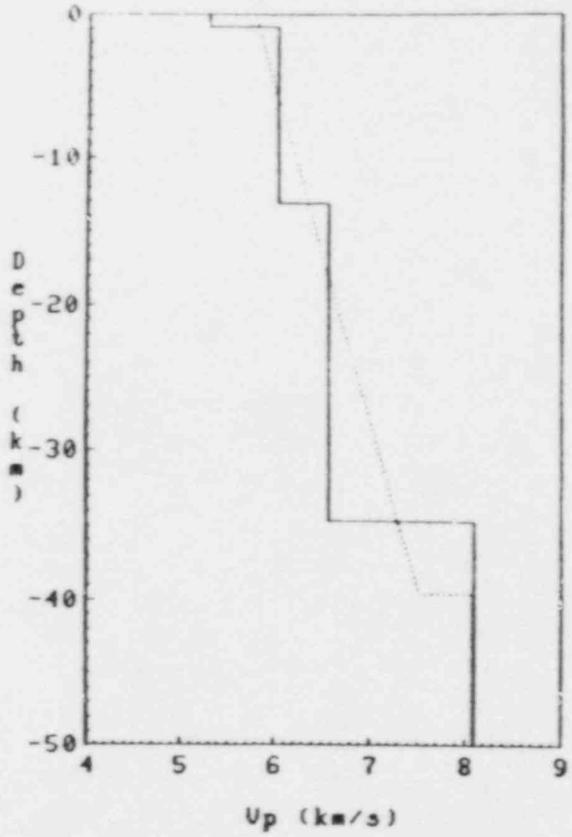

Figure 7b

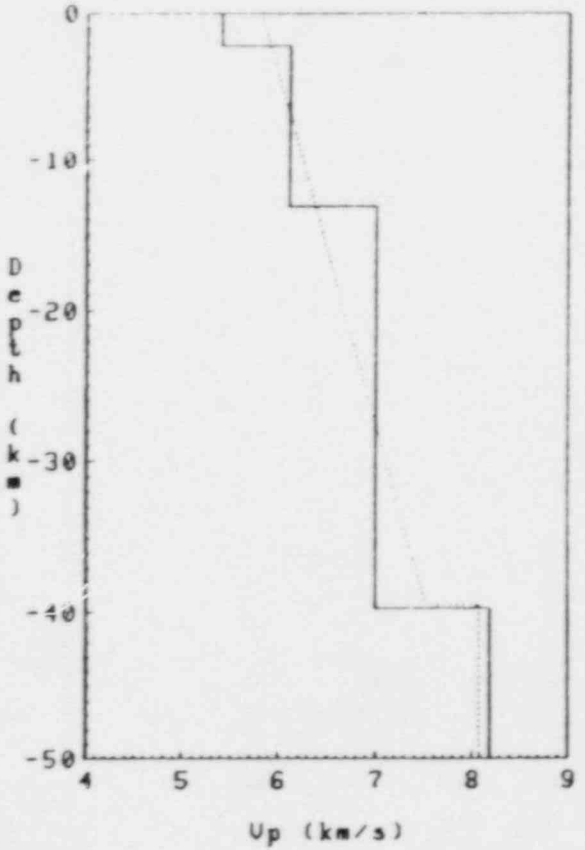

Figure 7 c

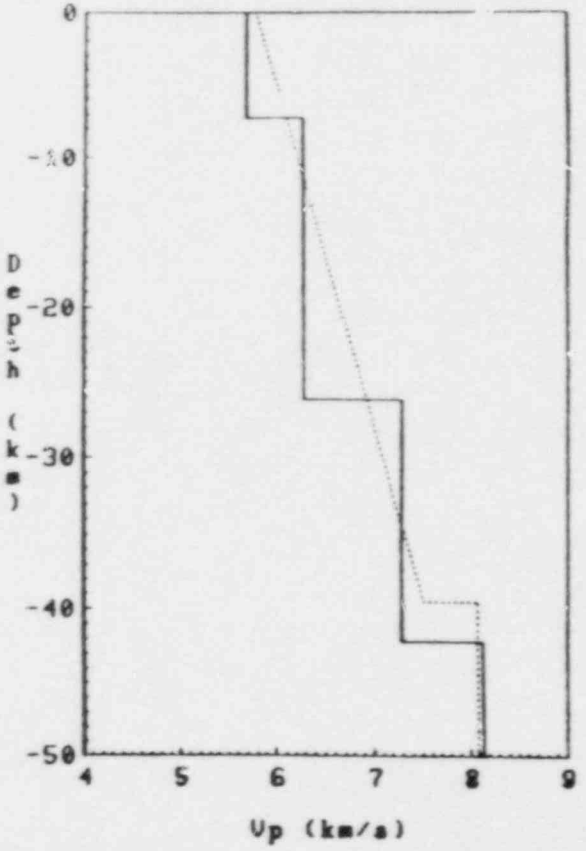

Figure 7 d

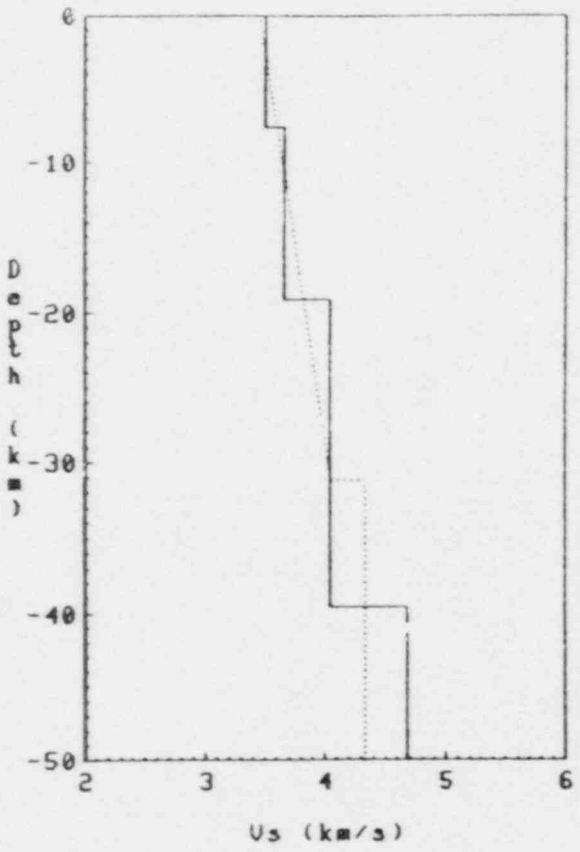

Figure 7e

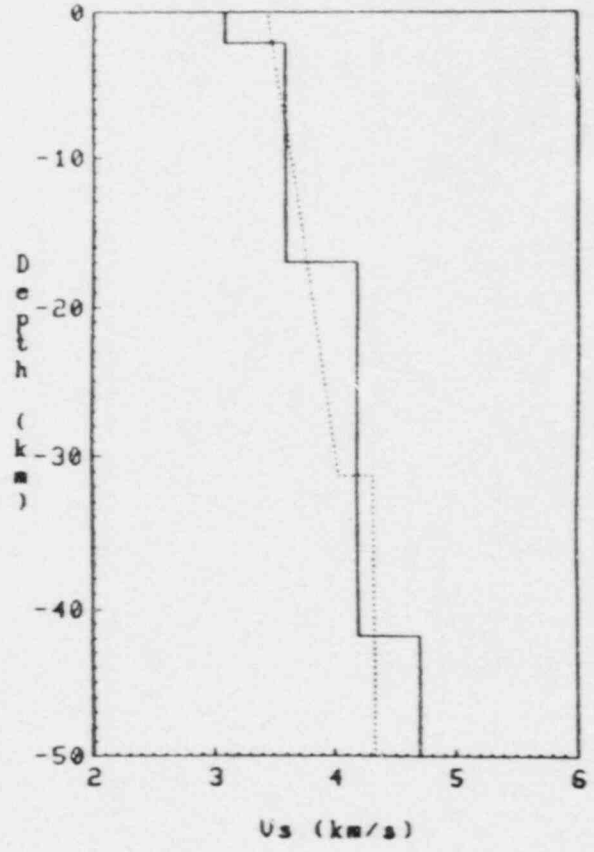

Figure 7f

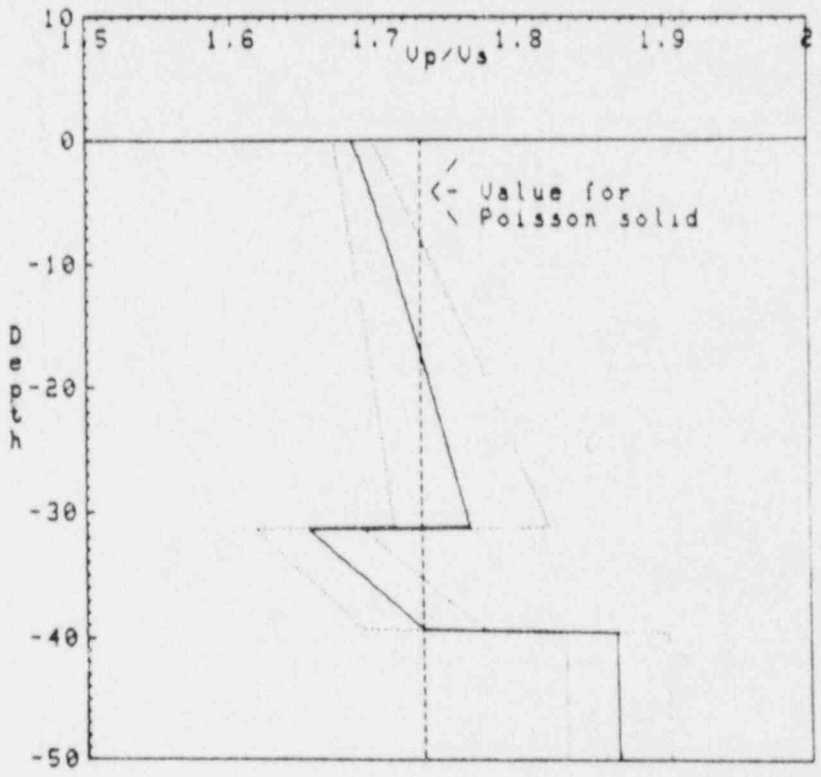
10
1.5
1.6
1.7
Vp/Vs
1.8
1.9
2
0
<- Value for
\ Poisson solid
-10
Depth
-20
-30
-40
-50

Figure 8

Appendix C: 1982 New Brunswick Earthquake

THE JANUARY 9, 1982, NEW BRUNSWICK, CANADA EARTHQUAKE

by

J. Nabělek

Earth Resources Laboratory
Department of Earth, Atmospheric, and Planetary Sciences
Massachusetts Institute of Technology
Cambridge, MA 02142

INTRODUCTION

The New Brunswick earthquake, although of only intermediate size (m_b =5.7 ; 12:53:52 GMT; 47.0° N, 66.7° W), is an important event because it is the first event in eastern North America since the inception of the major global seismic network that has been large enough to be recorded globally. Because the propagation of regional phases in eastern North America is still poorly understood, source parameters of smaller earthquakes are subject to large uncertainties [Aggarwal and Sykes, 1978; Yang and Aggarwal, 1981; Pulli and Toksöz, 1981; Pulli, 1983]. Prior to the New Brunswick earthquake the best recorded event was the m_b =5.2 1980 Sharpsburg, Kentucky earthquake [Herrmann *et al.*, 1982]. The New Brunswick earthquake provides the first opportunity to study an event from this region using well developed techniques of teleseismic source analysis, thus permitting a more reliable estimate of the source parameters which can be directly compared with the results of similar source studies in other regions.

Eastern North America has been the site of infrequent but large and potentially damaging earthquakes in the past (e.g. 1886 Charleston, m_b =6.8; 1925 Grand Banks, M_s =7.2; 1925 St. Lawrence, M_s =6.7). Because of the high population density in this region, it is important to estimate the potential hazard from such large events. Studies of typical source properties for smaller events, especially stress drop, can provide important clues to the potential hazard from larger events.

This paper presents the results of modeling the short- and long-period body waveforms (P and SH) and Rayleigh wave spectra of the New Brunswick earthquake, using data from the GDSN, WWSSN, and Canadian networks. The dataset spans periods of about 0.1 to 80 s. The use of short-period data is particularly important because it allows much better resolution of the source duration, which is usually shorter than 2 s for an earthquake of this size. The minimum resolvable source duration using data from long-period WWSSN instruments is about 1.5-2 s. A major obstacle in using short-period wave to infer source properties is that they are quite sensitive to variations in anelastic attenuation. Observed values of t^* (travel time/Q average) for P-waves seem to vary from about 1.5 to about 0.3 s depending on the propagation path and location of the source [Helmberger and Hadley, 1981; Der *et al.*, 1982] and may also be frequency dependent, with lower values at higher frequencies [Lundquist and Cormier, 1980; Der *et al.*, 1982; Cormier, 1982]. Therfore, one of our tasks will be to determine the appropriate value(s) of t^* for paths from the New Brunswick region.

Our results demonstrate that the New Brunswick earthquake was caused by thrust faulting at a depth of 7 km on a fault plane striking in the north-south direction. The seismic moment was $1.6 \pm 0.1 \times 10^{24}$ dyne-cm, released over a period of about 0.6 s, from which a stress drop of 960 bars is inferred. The short period waveforms indicate the presence of a small precursor about 1 s before main rupture, but the parameters of the precursor are not well resolved. Its moment is approximately 10 times smaller than that of the main event, and its orientation appears to be slightly different. The average value of t^* for paths to stations used in the short-period P wave analysis appears to be approximately 1 s, but with large azimuthal variations. The largest values (1.2-1.3 s) were observed in the western U.S. and the smallest values (0.6-0.8 s) were observed for South American stations.

The site of the New Brunswick earthquake has been a region of scattered seismicity with events of magnitude up to 3 in the past (Figure 1). The epicenter was located in the middle of a granitic pluton of the Miramichi Anticlinorium, at a site with no observable geologic faulting (Figure 2). The nearest significant geologic fault is the Catamaran Fault, an east-west trending lineament about 20 km south of the epicenter (Figure 2). From the offset of geologic features cut by the Catamaran Fault, it appears that the sense of displacement is mainly right-lateral strike slip, but it is not known if the fault is still active.

INVERSION AND MODELING OF TELESEISMIC BODY WAVES

The inversion procedure has been described in Chapter II and Appendices A and B of Nabelek [1984]. I shall again make use of the two objective functions (i.e. measures of misfit)

$$o_i - s_i \tag{1}$$

and

$$o_i / \left(\sum_j o_j^2\right)^{1/2} - s_i / \left(\sum_j s_j^2\right)^{1/2} \tag{2}$$

which are minimized in a least squares sense. The second objective function, which is insensitive to the absolute amplitudes, will be particularly useful in the analysis of the short-period data, where poorly understood variation in t^* and other path effects dominate the amplitude signature of the source. In preliminary inversions of the short-period data, positivity constraints (Chapter II; Appendix 3) were applied to the source time function. This stabilized the inversion and facilitated rapid convergence.

LONG-PERIOD P- and SH-WAVES

The dataset for the long-period body-wave inversion included seismograms from the GDSN, WWSSN and Canadian seismic networks (Table 1). To remove very long-period noise and D.C. offset, the GDSN seismograms were high-pass filtered with a three-pole (zero phase) Butterworth filter with a cut-off period of 60 s, well outside of the dominant period range of the observed body waves. The analog WWSSN and Canadian network seismograms were hand digitized at 0.5 s intervals. The S-wave seismograms were rotated in order to retrieve the transverse component for the SH analysis.

To deal with variations in data quality at different stations, we implemented a weighting scheme which reflects our ability to predict the contributions of the various sources of error in the data. The signal S generated by the source and recorded on receiver R is affected along its path by the crustal structure, in the source region C^s, anelastic attenuation A, geometrical spreading and other losses G, and receiver crustal structure C^r. The recorded signal d can be considered as a convolution of these terms,

$$d = R * C^r * G * A * C^s * S \tag{3}$$

The errors in d are mainly due to imprecise knowledge of the path effects, the presence of some background microseismic noise, incomplete parameterization of the source, error in the assumed source crustal structure and misalignment of the data with the synthetics (it is sometimes difficult to determine exactly where the observed seismogram begins). The errors due to path effects and background noise can be estimated in advance and are reflected directly in our weighting scheme. The other errors are difficult to determine in advance and are investigated after the best estimate of the model parameters is made.

To first order, the errors in R, C^r, and G are amplitude factors (small phase errors, to first order, are also reflected in amplitude fluctuation; Chapter III) which are independent of each other and can be summed in quadrature. The error in attenuation is negligible for long-period data. The background noise level can be estimated from the seismogram trace prior to the arrival of the signal. The fractional error of the individual data points due to these uncertainties is,

$$\frac{\Delta d_i}{|d_i|} = \sqrt{\left(\frac{\Delta R}{|R|}\right)^2 + \left(\frac{\Delta C^r}{|C^r|}\right)^2 + \left(\frac{\Delta G}{|G|}\right)^2} + \frac{N}{|d_i|} = M + \frac{N}{|d_i|}, \tag{4}$$

where N is the estimated background noise level. When the background noise is small, d_i can be approximated by the observed signal x_i. The final expression for the estimated error of data point d_i at station s becomes

$$\Delta d_i^s = M|x_i^s| + N^s \tag{5}$$

The error increases linearly with amplitude of the signal from a minimum determined by the background noise, N^s. The errors in C^s are not random and cannot be treated statistically. These will be discussed later.

The uncertainty in the instrument magnification is assumed to be about 5%. At long periods, the effect of likely variations in the receiver crustal structure for angles of incidence corresponding to the distance range of 30 to 80° is also about 5%, and the uncertainty in the geometrical spreading and other losses is assumed to be about 10-15%. The combined error M is therefore approximately 15%. The weight,

$$w_i^s = w^s / \Delta d_i^s \tag{6}$$

assigned to each data point is inversely proportional to the estimated error. The term w^s allows additional weighting and can be used to compensate for biases such as poor station distribution or systematic variations in the amplitudes of different phases. In this study, w^s was 1.0 for P-waves and 0.7 for SH-waves. SH-waves were given lower weight because of their larger average amplitudes.

For the long-period analysis the source time function is parameterized by a series of box functions of 1.5 s duration. This is approximately the time resolution limit of the long-period WWSSN and Canadian network instruments. The assumed

source and receiver crustal structure is a halfspace with compressional velocity of 6.0 km/s, shear velocity of 3.46 km/s and density of $2.8 g/cm^3$. Five sets of inversions were performed: (1) both P- and SH-waves were inverted simultaneously using moment tensor parameterization of the source; (2) after confirming that the source is well-characterized as a pure double couple (as one would expect for an earthquake) the inversion was repeated using a double-couple constraint; (3) and (4) in order to test the stability of the inversion, P- and SH-waves were inverted individually; and (5) the inversion was performed using the second objective function (eq. 5), which is sensitive to the shapes but not to the absolute amplitudes of the seismograms. The results are summarized in Table 2. The synthetic waveforms for the joint P- and SH inversion (2) (Table 2) are compared with the observed data in Figure 3. The matches are within the estimated uncertainty in the data. The worst matches are obtained for the noisiest stations (e.g. ANMO), which also carried the least weight in the inversion.

The data indicate essentially pure thrust faulting at a depth of 7 km on a fault striking in the north-south direction. The dips of the P-wave nodal planes are approximately 54 ° west and 30 ° east. The seismic moment is 1.6×10^{24} dyne-cm. The source time function obtained from the inversion is only 1.5 s (1 unit) long, implying that the far-field time function was essentially an impulse with respect to long-period instruments.

The P- and SH-waves complement each other in constraining the orientation. Because of deficient station distribution and dip-slip source mechanism, the P-waves alone provide little constraint on the strike and rake of the fault. This is reflected in large standard errors of the strike and rake angles when only P-waves are used in the inversion (Table 2). Since three of the four lobes of the SH radiation pattern are sampled by the data, the SH-waves are much more sensitive to changes in these angles. The SH-waves alone, however, cannot distinguish between a vertical strike-slip and a 45° dipping normal or thrust fault.

The *a posteriori* standard deviation of the weighted data (for definition, see Appendix B) is approximately one, which indicates that the *a priori* data error estimates were reasonably accurate and that the source is sufficiently parameterized. The formal standard errors of the source parameters for the combined P and SH inversion are very small and most likely underestimate the true uncertainty in the estimated parameters. The estimated errors do not include uncertainties in the source crustal structure and misalignment of the synthetics with the observed data.

Although the effect of misalignment tends to average out when a large number of stations is used, it can cause a sbstantial bias in the estimated source parameters if it is azimuthally dependent. In this study, the onset of the waveform was first assumed to be the theoretical arrival time. After convergence to a solution, it was allowed to vary by up to 2 s if a better cross-correlation between the observed and synthetic waveforms could be found. The computation was then restarted, resulting in the final solution.

To obtain a more realistic picture of the uncertainties in the source parameters, I performed additional inversions using different source crustal models, longer time function elements, and altered weighting of individual stations. The effect of misalignment was investigated by varying the assumed initial time of the observed seismograms. The misalignment of the P-waves was minimized by comparing the long- and short-period P-wave arrival times. The results of these inversions suggest that more realistic uncertainties in the estimated source parameters inferred from the

long-period body wave data are: strike ± 10 °, dip ± 3 °, rake ± 10 ° and depth ± 1 km. The time function duration appears to be less than 2.0 s (with the strongest constraints coming from stations of the WWSSN and Canadian network), but the long-period data cannot resolve how much shorter it might be.

The long-period description of the source within the above uncertainties is certainly sufficient for most geotectonic studies. In order to estimate the stress drop or displacement on the fault, however, we must improve the resolution of the fault dimensions. For this it is necessary to consider shorter period data.

SHORT-PERIOD P-WAVES

Because of the small size of the event and some instrument malfunctions, the azimuthal coverage of the long-period P-wave data was poor. The azimuthal distribution of well recorded short-period P-waves is considerably better. After high-pass filtering with a cut-off at 0.4 Hz, the short-period waveforms at adjacent stations show remarkable coherency. The wave shapes change smoothly across the focal sphere, suggesting that the source radiation pattern is the dominant factor (good coherency of short-period records has been noted and successfully utilized by Hartzel [1980], Cipar [1981], and Ebel and Helmberger [1982] in studies of other events). The high-pass filtering was done only on the GDSN data to remove D.C. offset and long-period noise present at some stations. Stations with good signal-to-noise ratio were not visibly affected by this filtering. The observed data and the best-fit theoretical seismograms are shown in Figure 4. Because the absolute amplitudes of the waveforms appear to be mainly controlled by path effects, only the wave shapes were inverted. The inversion was performed on the first 6 s of the waveform after the onset of the direct P arrival. The inferred source parameters and their formal uncertainties are summarized in Table 3.

With the improved time resolution of the short-period records, we can see that the earthquake is composed of two discrete subevents 0.7 s apart. The seismic moment of the first subevent is approximately 10 times smaller than the second and it can be identified only as a small oscillation prior to the larger arrivals at stations in the northern, southern, and western quadrants of the focal sphere. This oscillation is not observed at eastern stations, suggesting that the dip of the first subevent was slightly different from that of the second. The mechanism of this small precursor is poorly resolved and was fixed in the inversion. The dip was adjusted to satisfy the amplitude and the polarity of the initial part of the records, while the strike and rake were kept approximately equal to the strike and rake of the second subevent. The exact duration of the first subevent is not well determined. The main portion of the energy appears to be released in about 0.2-0.4 s. The seismic moment is 0.15×10^{24} dyne-cm. The source depth is poorly resolved because the depth phases (pP, sP) are buried in the signal from the second subevent. The inversion indicates two possible depths: one at 8 km, and one at 6 km (Figure 5). For the reasons discussed below, I prefer the deeper solution as the more likely of the two.

An emergent character of the small precursory event and background noise make it difficult to identify the initial time of the seismograms at some stations. In these cases, the initial time was determined by correlation with less noisy stations (e.g. DUG, ALE, BOCO). A comparison with the signal from an aftershock, which will be discussed later, helped distinguish source effects from path effects and helped determine the initial time of the direct arrival at the Albuquerque, N.M. stations ANMO

and AKQ. It will be shown that the energy arriving prior to the assumed initial time at ANMO and ALQ is probably related to a crustal or mantle heterogeneity below these stations.

The parameters of the second subevent are well resolved by the short-period data and agree with those determined from the long-period records. The best-fitting double-couple orientation has strike 174°, dip 54°, and rake 85°; the seismic moment is 1.4×10^{24} dyne-cm; the average (centroidal) depth is 6.9 km; the time delay with respect to the origin time of the first subevent is 0.7 s; and the rupture duration is 0.4 s. The centroidal depth is particularly well resolved by the short-period dataset. The inferred moment and rupture duration are very sensitive to the assumed value of t^*. These results assume a value for t^* of 1.0 s at all stations. The reasons for this choice will be discussed in the next section.

In order to obtain a better estimate of the fault dimensions and to determine if directivity is resolvable in the observed waveforms, the source was modeled as a propagating line source. Because of the steep take-off angles of the rays contributing to the seismograms at teleseismic distances and the small size of the event, the waveforms are expected to be sensitive mainly to the vertical component of rupture. The effect of rupture propagation along the dip of the fault is introduced into our formulation by varying the time function duration of each elementary seismogram $H_i(t)$ according to the formula

$$\Delta\tau_i = \Delta\tau\{1 - v^\delta[-\eta_i \sin\delta + p\cos\delta\sin(\varphi - 0)]\} \qquad (7)$$

$H_i(t)$ and all other parameters are defined in Chapter II and Appendix A. The term containing the ray parameter p represents the directivity due to the horizontal component of the propagating line source, and is very small. It was kept in the formulation because, if observable, it could help in distinguishing the fault plane from the complementary plane of the double couple. The assumed rupture velocity v^δ is 2.5 km/s. Figure 6 illustrates the effect of source finiteness on the short-period waveforms. Up-dip propagating rupture increases the amplitude of the reflected phases and decreases the amplitude of the direct arrival. The reverse is observed for down-dip rupture. (Due to narrow bandwidth of the short-period data, the effect on the pulse width is less apparent.) The residual relative to the observed waveforms is essentially identical for the upward propagating line source models and the point-source model, but the downward propagating models are inferior (Figure 6). A scenario that is consistent with these results and the bounds on the possible depths of the two subevents (Figure 5) is that the precursor occurred at a greater depth than the main event and the rupture propagated upward, but the evidence is far from being conclusive. The data cannot resolve which P-wave nodal plane corresponds to the actual fault plane. I choose to present the results in terms of the west-dipping fault plane because it is preferred by some other investigators [Wetmiller *et al.*, 1982; Choy *et al.*, 1983] and thus allows an easier comparison with their results.

t_p^* FOR MANTLE TRAVEL PATHS FROM THE NEW BRUNSWICK REGION

Values of t^* for P-waves at 1 Hz are known to vary between 1.3 and 0.5 s depending on the propagation path [Der *et al.*, 1982; Cormier, 1982]. At higher frequencies, t^* is much less certain because in order to generate enough energy to be observed at teleseismic distances, the source has to be of considerable size, and the source time function cannot be considered to be an impulse, even for explosions.

All t^* measurements at frequencies higher than 1 Hz, therefore, depend strongly on assumptions about the behavior of the source. Many studies indicate, however, that t^* may decrease with frequency, dropping to values of 0.2-0.3 s at about 8 Hz for some paths [Der et al., 1982; Cormier, 1982].

The results of modeling constrain the duration of the main subevent to less than 1 s. This result is independent of the assumed t^* within the bounds of the values discussed above. Due to the lack of t^* measurements for paths from eastern North America, we must be able to estimate the correct value from our data if better constraints on the source time function are desired. Because of the trade-off between the source time function and t^*, certain assumptions about their behavior are necessary. The first assumption is that t^* is constant from long periods to a period of about 1 s; the second assumption is that the source has a flat amplitude spectrum from long periods to about 2-1.5 s (the longest significant periods in the short-period records). The second assumption is crucial, because it implies that the seismic moments determined from the long- and short-period records should be equal. The moment determined at long periods is not very sensitive to the assumed attenuation and can be used as a standard for the shorter periods if this assumption is correct.

After the best match to the waveshapes of the short-period data was determined, the seismic moment was estimated by matching the absolute amplitudes in the least squares sense. An excellent match between the long- and short-period moments can be obtained when the average t^* to all stations is about 1 s. For a t^* of 0.6 s, the short-period moment is under-estimated by about 40%. The t^* of 1 s is average in a crude sense, because the scatter in the absolute amplitudes of the short-period seismograms with respect to the average model is large (that was why we inverted only wave shapes when originally determining the source mechanism). The match of the best-fitting average model (Table 3 and t^* = ls for all stations) to the absolute amplitude short-period data is shown in Figure 17. Also shown are the matches after the correction to t^* for individual stations was made, assuming the amplitude differences are mainly due to attenuation along a given path. The highest attenuation (t^* of 1.2-1.3s) is observed for paths to stations in California (JAS) and New Mexico (ANMO and ALQ). The least attenuation (t^* of 0.6-0.8 s) occurs for stations in South America (BOCO and ZOBO). Since the power of the short-period data is concentrated around a period of 1 s, the t^* determined here applies only for those periods. Although the absolute values of t^* quoted in Figure 7 are probably less certain because they depend on the assumption we made about the source (i.e. that the long- and short-period moments should be equal), the relative differences in t^* among stations are probably correct because the source orientation and its radiation pattern are well constrained by the waveforms of the observed records.

BROAD-BAND P-WAVES

Because of the response characteristics of the long-period and short-period instruments (further accentuated by high-pass filtering of the short-period data) there is little information about the behavior of the source at very short periods and periods in the range of about 1.5-3 s. Thus any source complexities in these bands might have gone undetected. These undesirable instrumental characteristics strongly limit our view of the true ground motion and must be removed by deconvolving the instrument response. Since we are primarily interested in periods shorter than 5 s, only deconvolution of the short-period traces is necessary. Due to background noise, only stations ZOBO and BOCO could be successfully deconvolved.

The resulting broad-band traces (flat in the period range of 0.1 to 10 s) of the ground displacement and velocity are shown in Figure 8 . Nearly all of the energy arrives in the first 5 s at these stations. According to our model, the observed positive displacement pulse corresponds to the direct P arrival and the negative pulse to the pP; the sP is very small and is difficult to identify. The precursor blends with the main event in the displacement records but can be easily distinguished in the velocity records.

Since the source mechanism was well constrained in the previous analysis, the mechanisms of both the precursor and the main event were fixed during the analysis of the broad-band records. Fortunately, the sP phase is nodal for these two stations, thus reducing interference between phases and improving the resolution of the source time function. Although the sP corresponding to the overall best-fitting source mechanism is close to being nodal, its amplitude is somewhat larger than that actually observed at these two stations (a discrepancy possibly due to a small error in the ray parameter or small inclination of the free surface in the source region [Langston, 1977]. Such errors become significant only when a phase is near its node; the P and P, being further from the nodes, should not be as sensitive to local structural deviations with respect to the average earth model). Care must be taken not to alias this discrepancy into the estimate of the source time function. In order to avoid this problem, only the time window before the arrival of the sP was considered.

Both displacement and velocity records were inverted simultaneously. The velocity records were given half the weight of the displacement records, because of their larger amplitude. A t^* of 0.7 s, (the average value for these two stations determined in the previous analysis) was used (Figure 7). Because these two stations do not show significant directivity, the point source model was used. The source time function determined in this inversion is very similar to that obtained from the standard short-period records (Figure 8). The duration of the main event (0.4 s) remains unchanged. The main difference between the results of the broad-band and short-period analyses is the partitioning of the moments between the subevents. The broad-band data requires a relatively larger moment for the precursor (0.4 : 1.2 x 10^{24} dyne-cm; which may simply be an artifact of errors in the mechanism for the precursor and limited station distribution). The total moment of the two events is 1.6 x 10^{24} dyne-cm.

In view of the possibility that t^* decreases at high frequencies, the constant t^* attenuation operator [Futterman, 1962] was replaced by a band-limited attenuation operator [Liu *et al.* 1976; Minster, 1978] in which at high frequencies $t^* \approx t_m^* \frac{2}{\pi} \tan^{-1}\left(\frac{1}{2\pi f \tau_m}\right)$. I take $t_m^* = 0.8s$ and $\tau_m = 0.08s$; thus the t^* at 1 Hz is 0.7 s and falls to 0.12 s at 10 Hz (these values approximately satisfy the results of the previous analysis and Der *et al.* [1982]). The inversion using this frequency dependent t^* indicates a somewhat longer source duration (0.6 s) while the match to the data is indistinguishable from that obtained for the constant t^* case (Figure 9). Because the attenuation at periods longer than 1 s is not affected by this operator, the seismic moment estimate was unchanged.

Had we assumed a constant t^* of 0.4 s (the value used by Choy *et al.* [1983]), the moment would be underestimated by about 30%. Because we are working with a broad-band signal, one might expect that it should contain long enough periods to be insensitive to the assumed attenuation, but the presence of the pP free surface reflection causes a peaked spectrum even in the broad-band signal. The power of

the broad-band signal at these two stations is concentrated between periods of 2 to 4 s, causing the absolute amplitudes of the synthetics to be scaled mainly to the signal at those periods. If we assume that the long-period seismic moment determined in section 6 should be equal to the seismic moment determined here, the t^* of 0.4 s at periods of 4-2 s is inadmissible.

Based on the results discussed above it can be concluded that the duration of the rupture of the main subevent was 0.4-0.6 s. The rupture duration of 0.8 s obtained by assuming the constant (frequency independent) t^* of 0.4 s is probably a conservative upper bound.

COMPARISON WITH THE SURFACE WAVE DATA

In this section we will check the consistency of the source model inferred from short- and long-period body waves with the observed surface wave radiation. The New Brunswick earthquake has an ideal magnitude and location for a surface study. The data quality is high, with good azimuthal coverage and paths which are shorter than 40° and generally cross only a single tectonic province. The station coverage is displayed in Figure 9. The dataset consists of the digital GDSN data, supplemented by hand-digitized WWSSN and Canadian Network seismograms. The consistency of the dataset can readily be seen from Figure 10; the seismograms in this figure were equalized to a common distance, phase velocity dispersion, and seismometer type and magnification. The equalization was accomplished in the frequency domain using the formula:

$$u_0(\omega) = u(\omega)\ F(\omega)\ \frac{\sqrt{\sin \Delta / a}}{\sqrt{\sin \Delta_0 / a}}\ e^{i\omega\left(\frac{\Delta}{c} - \frac{\Delta}{c_0}\right)}\ e^{\frac{\omega}{2Q(\omega)}\left(\frac{\Delta}{u} - \frac{\Delta_0}{u_0}\right)}\ \frac{R_0(\omega)}{R(\omega)} \qquad (8)$$

$u(\omega)$ spectrum of the observed Rayleigh waves
$F(\omega)$ 3-pole Butterworth band-pass filter with cutoff periods of 80 and 20 s
ω angular frequency
$c(\omega)$ phase velocity
$u(\omega)$ group velocity
$Q(\omega)$ quality factor
$R(\omega)$ receiver response
Δ epicentral distance in km
a Earth radius (6371 km)

The reference values are indicated by a subscript of zero. The phase and group velocity model assumed for the continental paths as well as the reference model, are for the Gutenberg continental structure [Aki and Richards, 1980]. For the oceanic paths, we assumed the velocity dispersion model of Weidner [1974] (normal ocean basin). The Q model is from Tsai and Aki [1969]. The reference distance and instrument are 40° and SRO, respectively. This equilization is analogous to that of Kanamori and Stewart [1976] except that we have accounted for the significantly different phase velocity dispersion in the period range considered between oceanic paths and continental paths.

The spectra of the wavetrains appear to be flat, except for the obvious hole in the mid-periods at JAS in California. This spectral hole is apparently due to passage across the low-Q Basin and Range Province, since DUG, with similar azimuth but on the

near side of the Basin and Range Province (Figures 9 and 10), does not show such a hole. Using spectral ratios between these two stations, values of Q in the range 15-30 were obtained for periods between 25 and 40 s, with the lowest values occurring at T ≈ 30 s. This result correlates with P-waves, which also showed high attenuation for the path to JAS ($t^* = 1.3$ s, the largest recorded value).

The azimuthal variation of amplitudes of the wavetrains shown in Figure 10 is clearly two-lobed and consistent with a north-south oriented thrust-type source mechanism. This observation is further confirmed in Figure 11, where the theoretical T=50 Rayleigh-wave radiation pattern matches the data very well (using the P-wave solution as the source model). The seismic moment ($2\text{-}2.2 \times 10^{24}$ dyne-cm) at T=50 s is somewhat larger than was obtained in the body wave analysis. Using the same dataset but a moment-tensor inversion procedure over a wider period range, Suarez [1982] obtained a moment of 1.1×10^{24} dyne-cm. His estimate of the source mechanism is in good agreeement with the one obtained in this study. Discrepancies of this size in the seismic moment are expected when entirely different datasets or wave types are compared, and mainly reflect biases introduced into the analysis by making different assumptions about the earth response.

THE STRESS DROP

The stress drop (Chapter II) is very difficult to estimate because it depends on the least certain quantity we could directly determine: the far-field source time function, which must be further interpreted (with great uncertainty) in terms of the fault geometry. The situation is further complicated by the presence of the precursor. Does the asperity model [Kanamori, 1978] or the barrier model [Das and Aki, 1977] apply? Can we distinguish between the two? Although the asperity model [Kanamori, 1978] and the barrier model in which all barriers (strong areas in the fault zone) break during an earthquake (model P-SV-3 of Das and Aki [1977]) differ in details, they cannot be distinguished either by the teleseismic radiation or the final static displacements. In both models, passage of the rupture releases a portion of the accumulated tectonic stress, and the residual stress is equalized over the entire fault area. Therefore, the average stress drop for both models is well represented by a single crack model [Madariaga, 1979]. Since both models lead to the same static stress-drop estimate, for our purposes the distinction between them is not important (hereafter, I will refer to both of these models as model A). Model A must, however be distinguished from the barrier model in which the barriers are left unbroken by th slip on the fault (model P-SV-2 of Das and Aki [1977]). This model results in a drastically different slip distribution on the fault (this model will hereafter be referred to as model B).

Figure 12 depicts the slip displacement which would result from the precursor (first subevent) and the main (second) subevent of the New Brunswick earthquake using both model B and model A. The rupture durations in both cases would be approximately the same. For the same moment, however, the displacement and the stress drop associated with the second subevent would be about 4 and 8 times larger in model B, respectively. Perhaps the strongest argument that can be presented against model B for the New Brunswick earthquake is that if this model applied, the stress drop associated with the main event would be more than 6 kilobars, which would most likely be sufficient to break the barrier. I shall continue the analysis under the premise that model A is a better representation for this event.

Although it appears that the centroidal depth of the precursor was different from that of the main subevent (Figure 5), the confidence in the precursor's depth is insufficient to give a reliable constraint on the fault dimensions. By taking advantage of the fact that the second subevent was much larger than the first, a more reliable estimate of the fault size can be obtained from the duration of the pulse of the second subevent. Guided by model A (Figure 12), we can see that all information about the total fault dimension is contained in the pulse shape of the second subevent, since the large stress release from it most likely resulted in a slip across the entire fault surface. The duration and the relative timing of the small precursor is therefore irrelevant. For the estimate of the average slip displacement and stress drop resulting from both the precursor and the main subevent, however, the total moment of both must be used.

In the analysis of the broad-band records we found that the source time function of the main subevent had a duration of about 0.6 s or less, assuming the values of t^* determined in this study are correct. For a circular rupture, the fault radius r can be obtained simply from

$$r = \frac{v_r v_h}{v_r + v_h} t_d \tag{9}$$

where v_r is the velocity of the rupture front, v_h is the velocity of the healing front and T_d is the duration of the source time function [Madariaga, 1976]. If $v_r = 0.75\beta$ and $v_h = \beta$, we obtain a fault radius of 0.9 km. For this radius and the moment of 1.6 x 10^{24} dyne-cm, we obtain the stress drop of 960 bars and average fault displacement of 190 cm. Since the results are sensitive to errors in the assumed attenuation, we also calculated stress drop and displacement using the time function duration of 0.8 s (obtained by assuming a frequency independent t^* of 0.4s) as its upper bound. The corresponding values of 400 bars for average stress drop and 100 cm for average displacement are probably a good representation of the lower bounds for these parameters. Thus we must conclude that, for an event of this size, the New Brunswick earthquake had above average stress drop [Kanamori and Anderson, 1975]. That this event is unusual is also evident from the m_b v.s. M_s plot shown in Figure 13. The m_b vs M_s ratio increases with increasing stress drop, and the New Brunswick earthquake clearly falls outside of the field defined by North American earthquakes. The implications of the high stress drop will be discussed further in the conclusions.

COMPARISON WITH PREVIOUS BODY WAVE STUDIES

The source mechanism of the New Brunswick earthquake has been studied by Dziewonski and Woodhouse [1983] and Choy *et al.* [1983]. These mechanisms differ from the detailed source model derived in this study. Because of the importance of this earthquake for understanding the seismicity of eastern North America I will examine the other proposed models in some detail. Figures 14a-d compare the match to the data by the preferred model of this study with the matches produced by the preferred models of the above studies. The average model from this study is a pure double-couple with the following parameters: strike 175°, dip 54°, rake 85°, depth 7 km, and moment 1.6 x 10^{24} dyne-cm. I will refer to this model as model N. I will first discuss the Dziewonski and Woodhouse model, followed by the Choy *et al.*, model. To facilitate a better comparison between different source mechanisms, the seismic moment (i.e. the scale factor) determined in this study was used for theoretical seismograms (unless otherwise stated in the figure captions).

The seismic moments determined in the other studies, especially the moment preferred by Choy *et al.* results in a much larger misfit.

The Dziewonski and Woodhouse model

Dziewonski and Woodhouse [1983] presented their result as a part of a larger study of global seismicity. Their preferred source moment tensor for the New Brunswick earthquake is characterized by quite a large linear-vector-dipole component (16%). Its best double-couple component has the orientation: strike 202°, dip 61°, rake 129°, and moment 1.9 x 10^{24} dyne-cm. They set the depth arbitrarily to 10 km. This double-couple orientation implies a large strike-slip component of displacement on the fault. The synthetics corresponding to this model (model DW) tend to substantially underestimate the observed long-period P wave amplitudes, especially those for the northern stations (Figure 14a), while the long-period SH-wave amplitudes are generally overestimated (Figure 14b). The short-period P-wave misfit is markedly large for the northern and southern stations (Figure 14c). The solution produces a large sP arrival in the broad-band records of the southern stations (Figure 14d).

The Dziewonski and Woodhouse technique is designed to obtain a rough estimate of the mechanism of a large earthquake in "real" time, i.e. for rapid distribution to various agencies. It involves matching the entire body wave seismogram up to the arrival of surface waves. In order to avoid large phase misalignments resulting from deviations of the body-wave travel times with respect to the average earth model, they must work only with a very long period signal. For the New Brunswick earthquake they applied a low-pass filter with the cut-off at T = 45 s. Because of this filtering and the small size and shallow focus of the New Brunswick event, this earthquake is at the lower limit of applicability of their method.

Event though it is more time consuming, the approach taken in our study, which involved working with data with periods shorter than 45 s is more appropriate for an event of this size. In order to avoid the phase mismatch, I had to treat each body wave phase individually and allow adjustment for variations in their travel time. For small, shallow events, the resolution in the Dziewonski and Woodhouse method is much worse than that of the analysis presented here. The similarity between our results is a testimony to the utility of their method for obtaining a first estimate of fault mechanism.

The Choy et al. model

The Choy *et al.* [1983] investigation of the source mechanism involved two independent studies: visual analysis of the long-period and broad-band body wave data, and inversion of the long-period body waves (similar to one presented in section 6 of this paper). I will refer to the results of the former as model CBDS1 and of the latter as model CBDS2. The discrepancies between the Choy *et al.* study and mine are troubling, because essentially the same dataset was used in both.

The CBDS2 model, based on inversion of long-period P- and SH-waves, is the most similar to the model obtained in this study. It is characterized by a pure double-couple mechanism with a strike of 169°, dip of 65°, rake of 81°, and moment of 3.2 x 10^{24} dyne-cm (a value of 5.3 x 10^{24} dyne-cm was obtained when only P waves were considered). The depth of 9 km was found by trial-and-error. This

solution indicates a slightly larger strike-slip component of displacement and a somewhat steeper dip of the west-dipping nodal plane than the solution N. The moment is considerably larger than that determined here by Dziewonski and Woodhouse [1983] or by Suarez [1982].

There are serious problems with CBDS2. The synthetics presented are clearly not compatible with the source orientation they are supposed to represent (for example, the P synthetic waveform for ANMO has a clear upward first motion when--allowing for the uncertainty in the take-off angle--the first motion should be negative or at most nodal. Similarly, the SH synthetic for KEV clearly has an incorrect first motion polarity). According to S. Sipkin [personal communication] the error occurred in the last stage of the inversion, in which only the final waveforms and moment are calculated. The inferred orientation should not be affected, although the moment is significantly smaller. The difference in the source orientation between our two models may be due to several factors, including slightly different data handling (I filtered the signals with a high-pass filter with the cut-off at T = 60 s), different alignment of seismograms and different source depth (they did not invert for the source depth).

What I believe to be the correct synthetics for CBDS2 are shown in Figure 14. Visually, the CBDS2 model matches the long-period P waveforms quite well, although because of the steeper dip of the fault plane the amplitudes are somewhat underestimated at the western stations and overestimated at the eastern stations (Figure 14a). For the long-period SH-waves, the mismatch is largest at KEV and BOCO (Figure 14b). The amplitude mismatch is also particularly large at COL (not shown in the figure). Due to the steeper dip of CBDS2, the amplitude of direct P-waves is significantly underestimated in the western short-period waveforms (e.g., JAS, Figure 14c). Of all models presented, CBDS2 produces the smallest sP arrival for the broad-band r cords (Figure 14d), but because the P/pP amplitude ratio is not correct, the residual is larger than for N or CBDS1.

Choy *et al.* [1983] place considerable weight on the CBDS1 model, which is based on a visual examination of waveforms. The model is characterized by a strike of 195°, a dip of 65°, a rake of 70°, a moment of 4.7×10^{24} dyne-cm, and a focal depth of 9 km. For this model, their dataset consisted of short-period and broad-band P-waves and long-period SH waves. The P, pP, sP, S, and sS were identified and their polarities read directly from the seismograms. The stations used are not specified, but it appears from the distribution of the readings on their focal sphere plots that the P-waves from the western stations were completely disregarded. Considering the extremely long-period response of the long-period GDSN stations it is quite difficult to believe that unambiguous polarity picks are possible, not only of the direct S arrivals but also the free surface reflections. Moreover, such picks are presented for the high-noise stations such as ANMO and BOCO, but not for KEV--the station with one of the clearest signals.

The CBDS1 model underestimates amplitudes of the western long-period P waves and overestimates those of the eastern long-period P-waves (Figure 14a). The matches to the long-period SH-waveforms--as well as their amplitudes--are particularly poor (Figure 14b). The amplitude of the direct P-wave in the short-period records is clearly underestimated (Figure 14c). Choy *et al.* [1983] put considerable weight on the fact that the sP appears to be nodal on the broad-band records at BOCO and ZOBO, but model CBDS1 does not fit this feature any better than model N of this study (Figure 14d). Choy *et al.* also obtained an estimate of the moment, apparently based on the area under the pulses of these stations. The value of 4.7 x

10^{24} dyne-cm appears to be a severe overestimate. Since Choy *et al.* [1983] assumed a much lower attenuation than that used in this study, an overestimate of the seismic moment is especially puzzling.

Using directivity arguments Choy *et al.* [1983] determined the westward dipping plane of the double-couple to be the actual fault plane. Based on visual comparison of the models shown in Figure 5, one could perhaps argue that some upward directivity appears to be present, e.g. upward propagating models match the waveform better at ALE. Based on residuals, the evidence is not convincing. For their source mechanism, which has one very steeply dipping and one very shallow dipping fault plane, such a conjecture would perhaps be justified. In the source mechanism found in this study, the westward dipping double-couple plane starts with a dip of 45° for the precursor and ends with a dip of 54° for the main subevent. The corresponding values for the eastward dipping plane are 45° and 35°, respectively. The selection of the west-dipping plane as the fault plane therefore depends on aspects of the focal mechanism with which this study is in conflict. Rupture propagation along either plane of solution of this study could produce the observed directivity. (Although the choice of the fault plane is arbitrary for models in this study, the model parameters presented in this paper are for the westward dipping nodal plane, to provide an easier comparison with the previous investigations.)

One of the major discrepancies between Choy *et al.* and the present study concerns the estimate of stress drop. In spite of the fact that they used a moment three times larger in their calculation, the estimated stress drop is only 41 bars, and would be 14 bars if a moment of 1.6×10^{24} dyne-cm determined in this study were used. The source of this discrepancy is the difference in fault dimensions which were estimated from the source time function. The different attenuation assumed in these studies is clearly one of the factors leading to a different estimate of the source time function duration, but, as was shown in the previous section, the assumption of the constant $t^* = 0.4$s still resulted in a time function duration of approximately 0.8 s and a stress drop of several hundred bars. The main reason for the discrepancy between the two studies is the different treatment of the precursor. Although Choy *et al.* [1983] recognize the precursor and point out that the P-SV-3 model of Das and Aki [1977] probably applies, in their calculations they treat both the small precursor and the main subevent as a continuous breaking of a single asperity. In other words, they take the total time from the initiation of the rupture of the recursor to the stopping of the main subevent as representative of the dimension of the fault area, although, as I have argued in the previous section, only the duration of the main subevent should be considered. To stress this point, consider a case in which the small precursor occurs 10 minutes prior to the much larger main event. Clearly, one would not assume that the rupture had a radius of 1500 km. Since the main event would most likely cause additional motion on the fault plane ruptured by the precursor, the total dimension of the fault plane would be entirely given by the dimension of the main event, but the total displacement would be the sum of the two. On the basis of the above arguments, I believe that the stress drop of 14 bars, which one would obtain using the Choy *et al.* fault dimensions and moment of 1.6×10^{24} dyne-cm obtained in this study, is substantially underestimated.

THE JANUARY 11, 1982 AFTERSHOCK

The January 11, 1982 event is the largest aftershock ($m_b = 5.4$) of the New Brunswick earthquake, but it is too small for a long-period study. An analysis of the

short-period P-waves, identical to that described for the main shock, was performed. The data and the synthetics for the best fit solution are shown in Figure 15 and the inferred source parameters are summarized in Table 4. The event has a similar mechanism to the main shock but is simpler and shallower. The aftershock distribution has been used to infer that the eastward dipping nodal plane was the actual fault plane [Wetmiller *et al.*, 1982]. Because fewer stations were available, the inferred parameters for this event are less certain. The main reason to study this event is that it helps distinguish source effects from structural effects in the observed waveforms of the January 9 earthquake. By comparing these two events, we see that the initial oscillation in the waveforms of the January 9 event (which we identified as the first of two subevents), was indeed a source effect, because it is not observed for the aftershock. On the other hand, structurally related coda is observed for both events at station ZOBO, while at BOCO (with similar azimuth) the waveforms are consistently simpler. Note also an arrival at the Albuquerque stations (ALQ and ANMO) at about 1 s ahead of what has been identified as the direct arrival. This arrival appears to be caused by multipathing near the receiver, since nearby noise-free stations DUG (Figure 4) and JAS (Figure 5) do not exhibit this phenomenon.

DISCUSSION AND CONCLUSIONS

In this study I have derived a detailed model of the source process of the New Brunswick earthquake. The body and surface wave data considered in this study covered periods from 0.1 to 80 s. The best constrained parameters of the model are the average source mechanism (pure double-couple with strike 172-182°, dip 53-55°, rake 80-95°), seismic moment ($1.6 \pm 0.1 \times 10^{24}$ dyne-cm) and the average depth (6.9 ± 0.1 km). The presence of a small precursor (first subevent) of slightly different orientation is indicated by the short-period and broad-band data. The duration of the source time function of the main (second) subevent is clearly less than 1 s, but a precise determination would require a precise estimate of the attenuation along individual propagation paths rather than simply assuming a worldwide average t^* for paths from a source in New Brunswick.

Based on the assumption that the source has a flat spectrum down to periods of 1-1.5 s, we concluded that the average t^* for the paths from New Brunswick is about 1 s. The t^* at T=1 s appears to fluctuate between high values of 1.2-1.3 s for the western North American stations and low values of 0.65-0.8 s for the South American stations. Intermediate values were obtained for the European stations. Based on the less stringent assumption that the source has a flat spectrum down to periods of 2-4 s we concluded that the constant $t^* = 0.4$ s for the paths to the South American stations is probably not correct, instead a value of 0.7-0.8 s appears more appropriate for those periods. Assuming a frequency dependent t^* [Liu *et al.*, 1976] with $t^*_m = 0.8$ s and $\tau_m = 0.08$ s in the analysis of the broad-band South American records, a time function duration of 0.6 s was inferred for the main subevent, leading to a stress drop estimate of 960 bars. A larger value than this is acceptable by the data. A conservative lower bound on the stress drop, found by assuming frequency independent $t^* = 04$ s, is about 400 bars.

The stress drop of the New Brunswick earthquake is large when compared with the average stress drops commonly found for large events [Kanamori and Anderson, 1975; Hanks, 1980]. It is not, however, inconsistent with stress drops found in some studies of events similar in magnitude to the New Brunswick earthquake [Fletcher *et*

al., 1980] or in studies of local stress concentrations on fault planes of some large events [Hanks, 1974; Bouchon, 1978; Hanks, 1980; Papageorgiou and Aki, 1983b].

The coseismic stress drop is of interest because it has a direct bearing on the magnitude of strong ground motion felt in the epicentral area. A critical question is whether the average stress drop value found for this event would also apply to a larger, potentially more damaging earthquake. I believe it would not, since many studies indicate that the average stress drop of events with fault radii of more than a few kilometers never attains a level as high as that found for the New Brunswick event [Kanamori and Anderson, 1975; Hanks, 1980]. Nevertheless, local stress drop concentrations as large as the one found for the New Brunswick earthquake can occur and should be included in models for predicting strong ground motion for larger events in eastern North America (e.g. the patch model of Aki *et al.* [1977] or Papageorgiou and Aki [1983a]). It is possible, of course, that the stress drop associated with the New Brunswick earthquake may not be typical of the earthquakes in the region, since the event occurred in a pluton with no apparent prior faulting.

The causes of seismic activity in the eastern U.S. are poorly understood. Although historical records show several large events [Street and Turcotte, 1977], the seismicity of the past two hundred years has been characterized by scattered small and intermediate events. Several concentrations of seismic activity do occur, e.g., the New Madrid region, the Charlevoix zone, the Ottawa northern New York region [Stauder *et al.*, 1976; Basham *et al.*, 1979; Yang and Aggarwal, 1981; Pulli, 1983] but the activity can seldom be associated with any well-defined fault system. There have been attempts to identify linear trends (e.g., Alabama-New Brunswick, St. Lawrence River, Boston-Ottawa [Woollard, 1969, Sbar and Sykes, 1973]), but their existence remains controversial. A controversy also exists about correlations of the seismic activity with such features as mafic and ultramafic intrusive bodies [Kane, 1976; McKeown, 1978], alkaline intrusions, or oceanic fracture zones extending into the continental margins [Sykes, 1978]. Recently, Yang and Aggarwal [1981] proposed two distinct seismotectonic provinces, 1) the Adirondack-western Quebec province and 2) the Appalachian province, which responds to two distinctly different stress systems (see also Zoback and Zoback [1980]). They also suggest that intrusive bodies tend to inhibit earthquake activity.

The New Brunswick earthquake occurred within an intrusive body. Therefore, it may be a result of local thermal stresses caused by the cooling of the body. On the other hand, the orientation of the principal compression appears to be consistent with the east-west compression generally found for earthquakes throughout eastern North America (Figure 16), indicating that the earthquake may be a response to a regional stress field.

One of the striking aspects of the New Brunswick earthquake is the simplicity and coherency of the short-period records. Because of the location of the event within a granitic pluton and the lack of sediment cover, the structural complexity of the source region is minimal. The fact that some stations show significant coda but a few, such as BOCO or ALE (Figures 4, 15), show practically no coda suggests that, to a large extent, the teleseismic coda is generated by reverberations within the crustal layering at the source and the receiver. The multipath arrival at the Albuquerque stations (ANMO and ALQ), prior to what was identified as the direct P arrival from the January 9th and 11th events, is interesting and probably results from structural heterogeneity below these two stations.

Notwithstanding some unexplained complexities, the short-period waveforms were matched with reasonable success and led to important constraints on the source process of the New Brunswick earthquake and its largest aftershock. This success suggests the possibility of studying intermediate size events using short-period teleseismic body waves and techniques developed for long-period studies of larger events. The recent availability of well-calibrated short-period data (that can be easily filtered to suitable frequency bands) should facilitate teleseismic studies of remote regions characterized by intermediate size earthquakes.

REFERENCES

Aggarwal, Y.P., and L.R. Sykes, Earthquakes, faults and nuclear power plants in southern New York - northern New Jersey, Science, 200, 425-429, 1978.

Aki, K., M. Bouchon, B. Chouet, and S. Das, Quantitative prediction of strong motion for a potential earthquake fault, Ann. Geophys., XXX, 341-368, 1977.

Aki, K., and P.G. Richards, Quantitative Seismology: Theory and Methods, W.H. Freeman, San Francisco, 1980.

Basham, P.W., D.H. Weichert, and M.J. Berry, Regional assessment of seismic risk in eastern Canada, Bull. Seis. Soc. Am., 69, 1567-1602, 1979.

Boatwright, J., A spectral theory for circular seismic sources; simple estimates of source dimensions, dynamic stress drop, and radiated seismic energy, Bull. Seis. Soc. Am., 70, 1-27, 1980.

Bouchon, M., A dynamic source model for the San Fernando earthquake, Bull. Seis. Soc. Am., 68, 1555-1576, 1978.

Choy, G., J. Boatwright, J.W. Dewey, and S.A. Sipkin, A teleseismic analysis of the New Brunswick earthquake of January 9, 1982, J. Geophys. Res., 88, 2199-2212, 1983.

Cipar, J., Broadband time domain modeling of earthquakes from Friuli, Italy, Bull. Seis. Soc. Am., 71, 1215-1231, 1981.

Cormier, V.F., The effect of attenuation on seismic body waves, Bull. Seis. Soc. Am., 72, S162-S200, 1982.

Das, S., and K. Aki, Fault plane with barriers: A versatile earthquake model, J. Geophys. Res., 82, 5658-5670, 1977.

Der, Z.A., T.W. McElfresh, and A. O'Donnell, An investigation of the regional variations and frequency dependence of anelastic attenuation if the mantle under the United States in the 0.5-4 Hz band, Geophys. J.R. Astr. Soc., 69, 67-100, 1982.

Douglas, A., Seismic source identification: A review of past and present research efforts, in Identification of Seismic Sources, eds. E.S.Husebye and S. Mykkeltveit, D. Reidel, Dordrecht, Holland, 1-48, 1981.

Dziewonski, A.M., and J.H. Woodhouse, An experiment in systematic study of global

seismicity: Centroid-moment tensor solutions for 201 moderate and large earthquakes of 1981, J. Geophys. Res., 88, 3247-3271, 1983.

Ebel, J.E., and D.V. Helmberger, P-wave complexity and fault asperities; the Borrego Mountain, California, earthquake of 1968, Bull. Seis. Soc. Am., 72, 413-437, 1982.

Fletcher, J.B., A.G. Brady, and T.C. Hanks, Strong-motion accelerograms of the Oroville, California, aftershocks: Data processing and the aftershock of 0350 August 6, 1975, Bull. Seis. Soc. Am., 70, 243-267, 1980.

Futterman, W.I., Dispersive body waves, J. Geophys. Res., 67, 5279-5291.

Hanks, T.C., The faulting mechanism of the San Fernando earthquake, J. Geophys. Res., 78, 1215-1229, 1974.

Hanks, T.C., Crustal earthquake stress drops, Proc. of Conference IX, Magnitude of Deviatoric Stress in Earth's Crust and Upper Mantle II, 491,518, 1980.

Hartzell, S., Faulting process of the May 17, 1976 Gazli, USSR, earthquake, Bull. Seis. Soc. Am., 70, 1715-1736, 1980.

Helmberger, D.V., and D.M. Hadley, Seismic source functions and attenuation from local and teleseismic observations of the NTS events JORUM and HANDLEY, Bull. Seis. Soc. Am., 71, 51-67, 1981.

Herrmann, R.B., C.A. Langston, and J.E. Zollweg, The Sharpsburg, Kentucky earthquake of 27 July 1980, Bull. Seis. Soc. Am., 72, 1219-1239.

Kanamori, H., Use of seismic radiation to infer source parameters, Proceedings of Conference III, Fault Mechanics and Its Relation to Earthquake Prediction, Geol. Surv. Open File Rep. U.S., 78-380, 283-318, 1978.

Kanamori, H., and G.S. Stewart, Mode of strain release along the Gibbs fracture zone, mid-Atlantic ridge, Phys. Earth Planet. Int., 11, 312-332, 1976.

Kane, M.F., Correlation of major eastern U.S. earthquake centers with mafic/ultramafic masses, EOS Trans. AGU, 57, 963, 1976.

Langston, C.A., The effect of planar dipping structure on source and receiver responses for constant ray parameters, Bull. Seis. Soc. Am., 4, 1029-1050.

Liu, H.-P., D.L. Anderson, and H. Kanamori, Velocity dispersion due to anelasticity: Implications for seismology and mantle composition, Geophys. J.R. Astr. Soc., 47, 41-58, 1976.

Lundquist, G.M., and V.F. Cormier, Constraints on the absorption band model of Q, J. Geophys. Res., 85

Madariaga, R., Dynamics of an expanding circular fault, Bull. Seis. Soc. Am., 66, 639-666, 1976.

Madariaga, R., On the relation between seismic moment and stress drop in the presence of stress and strength heterogeneity, J. Geophys. Res., 84, 2243-2250, 1979.

McKeown, F.H., Hypothesis: Many earthquakes in the central and southeastern United States are causally related to mafic intrusive bodies, J. Res. U.S. Geol. Surv., 6, 41-50, 1978.

Minster, J.B., Transient and impulse responses of a one-dimensional linearly attenuating medium - I. Analytical results, Geophys. J.R. Astr. Soc., 52, 479-501, 1978.

Nabelek, J.L. (1984), Determination of earthquake source parameters from inversion of body waves, PhD thesis, MIT.

Papageorgiou, A.S., and K. Aki, A specific barriar model for the quantitative description of inhomogeneous faulting and the prediction of strong ground motion. Part I. Description of the model, Bull Seis. Soc. Am., 73, 693-722, 1983a.

Papageorgiou, A.S., and K. Aki, A specific barrier model for the quantitative description of inhomogeneous faulting and the prediction of strong ground motion. Part II. Applications of the model, Bull. Seis. Soc. Am., 73, 953-978, 1983b.

Pulli, J.J., Seismicity, earthquake mechanisms, and seismic wave attenuation in the northeastern United States, Ph.D. Thesis, Massachusetts Institute of Technology, Cambridge, Mass., June, 1983.

Pulli, J.J., and M.N. Toksöz, Fault plane solutions for northeastern United States earthquakes, Bull. Seis. Soc. Am., 71, 1875-1882, 1981.

Sbar, M.L., and S.R. Sykes, Contemporary compressive stress and seismicity in eastern North America: An example of intraplate tectonics, Geol. Soc. Am. Bull., 84, 1861-1882, 1973.

Stauder, W., M. Kramer, G. Fisher, S. Schaefer, and S.T. Morrissey, Seismic characteristics of southeast Missouri as indicated by a regional telemetered microearthquake array, Bull. Seis. Soc. Am., 66, 1953-1964, 1976.

Street, R.L., and F.T. Turcotte, A study of northeastern North American spectral moments, magnitudes, and intensities, *Bull. Seis. Soc. Am., 67*, 599-614, 1977.

Suarez, G., Seismicity, tectonics, and surface wave propagation in the central Andes, Ph.D. Thesis, Massachusetts Institute of Technology, Cambridge, Mass., December, 1982.

Sykes, L.R., Intraplate seismicity, reactivation of preexisting zones of weakness, alkaline magmatism, and other tectonism postdating continental fragmentation, Rev. Geophys. Space Phys., 16, 621-688, 1978.

Tsai, Y.B., and K. Aki, Simultaneous determination of the seismic moment and attenuation of seismic surface waves, Bull. Seis. Soc. Am., 59, 275-287.

Wetmiller, R.J., J. Adams, A.E. Stevens, H.S. Hasegawa, and J. Berube, Aftershock sequence for the New Brunswick earthquakes of January 9th and 11th, March 31st, and June 16th, 1982, Earthquake Notes 53, 41, 1982.

Woolard, G.P., Tectonic activity in North America as indicated by earthquakes, in the

Earth's crust and upper mantle, Geophys. Monogr. Ser., 13, ed. P.J. Hart, 125-133, AGU, Washington, D.C., 1969.

Yang, J.P., and Y.P. Aggarwal, Seismotectonics of northeastern United States and adjacent Canada, J. Geophys. Res., 86, 4981-1998, 1981.

Zoback, M.L., and M. Zoback, State of stress in the conterminous United States, J. Geophys. Res., 85, 6113-6156, 1980.

Table 1

Stations used in the Analysis of the New Brunswick Earthquake

Stat	Type[2]	Δ (deg)	φ_{ES} (deg)	φ_{SE} (deg)	$P_{1st\ mot}$	Waveforms[1]
DIGITAL						
ALQ	WWSN	32.0	262.5	55.7	Ce	P_{sp}, R
ANMO	SRO	32.0	262.5	55.7	Ce	P_{sp}, P_{lp}, SH
BER	WWSSN	42.4	44.3	285.4		P_{lp}, R
BOCO	SRO	42.8	190.9	7.5	Cl	P_{sp}, SH, R
COL	WWSN	45.1	323.6	72.3	Ce	P_{sp}, SH
GRFO	SRO	49.5	56.4	298.6	Ce	P_{sp}, P_{lp}, SH, R
JAS	WWSSN	39.9	277.1	59.2	Ce	P_{sp}, P_{lp}, R
KEV	WWSSN	48.0	27.8	293.7		P_{lp}, SH
KONO	ASRO	44.6	45.5	289.1	Ce	P_{sp}, P_{lp}, SH, R
LON	WWSSN	37.0	290.5	68.8		SH, R
SCP	WWSSN	10.2	236.6	48.8	Ce	R
TOL	WWSSN	44.9	75.2	300.7	Ce	P_{sp}, P_{lp}, R
ZOBO	SRO	63.1	181.6	1.1	Cl	P_{sp}
ANALOG						
ALE	CN	35.6	1.0	185.0	Cl	P_{sp}, P_{lp}, SH, R
BEC	WWSSN	14.7	173.4	354.7		R
DAG	WWSSN	35.3	17.1	241.2	Cl	
DUG	WWSSN	33.7	275.6	62.8	Cl	P_{sp}, [illegible]
FCC	CN	20.1	315.9	113.7	Cl	
DIGITAL						
FRB	CN	16.8	357.2	175.7	Cl	
FVM	WWSSN	19.6	251.4	55.2	Ce	
GEO	WWSSN	11.1	272.1	40.0	C	
GOL	WWSSN	28.8	269.7	62.5	Cl	R
INK	CN	39.0	327.1	88.0	Cl	R
KBL	WWSSN	89.4	35.1	331.5	C	P_{lp}
LHC	CN	15.3	283.7	86.9		R
MBC	CN	36.1	341.2	112.7	C	R
PNT	CN	34.7	293.9	73.1	Ce	P_{sp}, R
PHC	CN	39.1	298.6	71.0		R
SCH	CN	7.8	359.5	179.4	Ce	
SES	CN	29.1	293.3	79.2	Cl	R
STJ	CN	9.5	81.3	271.6	De	
STU	WWSSN	48.8	58.3	298.3	C	
WES	WWSSN	5.7	217.6	34.3	Ce	
YKC	CN	30.9	320.2	99.7	Ce	

Δ is the distance between station and the epicenter; φ_{ES} is the azimuth of station from the epicenter; φ_{SE} is the azimuth of the epicenter from the station.

* C, D, i and e indicate compressive, dilatational, impulsive and emergent readings. Except for KBL all first motions were determined from the short-period records.

(1) P_{sp} indicates short-period P wave, P_{lp} indicates long-period P wave, SH indicates long-period SH wave, and R indicates Rayleigh wave.

(2) CN is abbreviation for the Canadian network stations.

Table 2

Summary of Long-Period Body Wave Inversions

MOMENT TENSOR

Depth = 7.0 ±0.1 km

Normalized moment-tensor components:

M_{xx} =	0.05 ±0.01	M_{xy} =	-0.00 ±0.01
M_{yy} =	-0.64 ±0.01	M_{xz} =	0.05 ±0.01
M_{zz} =	0.69 ±0.01	M_{yz} =	0.22 ±0.01

Moment-tensor norm = $2.32 \pm 0.09 \times 10^{24}$ dyne-cm

Principal axes:

	Eigenvalue	Azimuth	Plunge
P:	-0.68 ±0.01	269 ±1°	9 ±1°
B:	-0.05 ±0.01	179 ±1°	4 ±1°
T:	0.73 ±0.01	67 ±6°	80 ±1°

Decomposition:* 93% double-couple 7% linear vector-dipole

Best double-couple:

Scalar moment = 1.6×10^{24} dyne-cm
Strike = 176° Dip = 54° Rake = 86°

Residual = 0.48(2)

CONSTRAINED DOUBLE-COUPLE

	P AND SH	P ONLY	SH ONLY	P AND SH WAVE SHAPE ONLY
Depth (km)	7.1 ±0.1	7.0 ±0.2	7.1 ±0.1	7.0 ±0.1
Scalar moment (10^{24} dyne-cm)	1.57 ±0.03	1.76 ±0.06	1.48 ±0.05	1.52 ±0.24(1)
Strike (deg)	175 ±1	170 ±4	175 ±1	176 ±0
Dip (deg)	55 ±1	54 ±1	56 ±1	54 ±0
Rake (deg)	84 ±1	104 ±4	82 ±1	90 ±0
Residual	0.85	0.82	0.81	0.86

Conventions as in Aki and Richards (1980). Quoted uncertainties represent one standard deviation. Residuals are normalized to the RMS amplitude of the data. The source time function was a box-car of 1.5 s duration. * Moment tensor was constrained to be purely deviatoric. (1) Moment was determined after the last iteration.

Table 3

Summary of Short-Period P-wave Inversion

Event	Depth** (km)	Strike	Dip (deg)	Rake
1	8.41±0.02 (8.06)	177	45	90(2)
2	7.34±0.00 (6.90)	174±3	54±0	85±1

Event	Source Time Function* w_1	w_2	Time Delay(1)	Moment (dyne-cm)
1	1.00			$0.15 \pm 0.02 \times 10^{24}$
2	0.44±0.09	0.66±0.09	0.72±0.01	$1.38 \pm 0.04 \times 10^{24}$

* Each element of the source time function had a duration of 0.2s.
(1) Time delay of the second subevent is with respect to the origin time of the first subevent.
(2) Orientation (strike, dip, rake) of the first event was determined by trial-and-error by matching the amplitudes and polarities of the first motions.
** Depth of the initial point of the rupture; rupture propagated up-dip with velocity of 2.5 km/s. Numbers in the parenthesis indicate the centroidal depth.

Table 4

Summary of Short-Period P-wave Inversion for the 11 Jan. 1982 Aftershock

MOMENT TENSOR

Depth = 5.25±0.01 km

Normalized moment-tensor components:

M_{xx} =	-0.34±0.03	M_{xy} =	-0.22±0.05
M_{yy} =	-0.37±0.03	M_{xz} =	0.08±0.02
M_{zz} =	0.71±0.01	M_{yz} =	-0.26±0.01

Moment-tensor norm = 6.1±0.7 × 10^{23} dyne-cm

Principal axes:

	Eigenvalue	Azimuth	Plunge
P:	-0.59±0.05	50±3°	6±1°
B:	-0.20±0.05	141±3°	14±1°
T:	0.79±0.01	296±3°	75±1°

Decomposition:* 78% double couple 22% linear vector dipole

Best double-couple:

Scalar moment = 4.2 × 10^{23} dyne-cm
Strike = 332° Dip = 53° Rake = 108°

Source time function: 1.16±0.03, −0.16±0.04

RMS residual = 0.059

CONSTRAINED DOUBLE-COUPLE

Depth = 5.30±0.02 km

Scalar moment = 4.1±0.3 × 10^{23} dyne-cm

Strike = 345±4° Dip = 53±1° Rake = 98±3°

Source time function: 0.92±0.01, 0.002±0.01

RMS residual = 0.059

Quoted uncertainties respresent one standard deviation.
Each element of the source time function had a duration of 0.2 s.
*Moment tensor was constrained to be purely deviatoric.

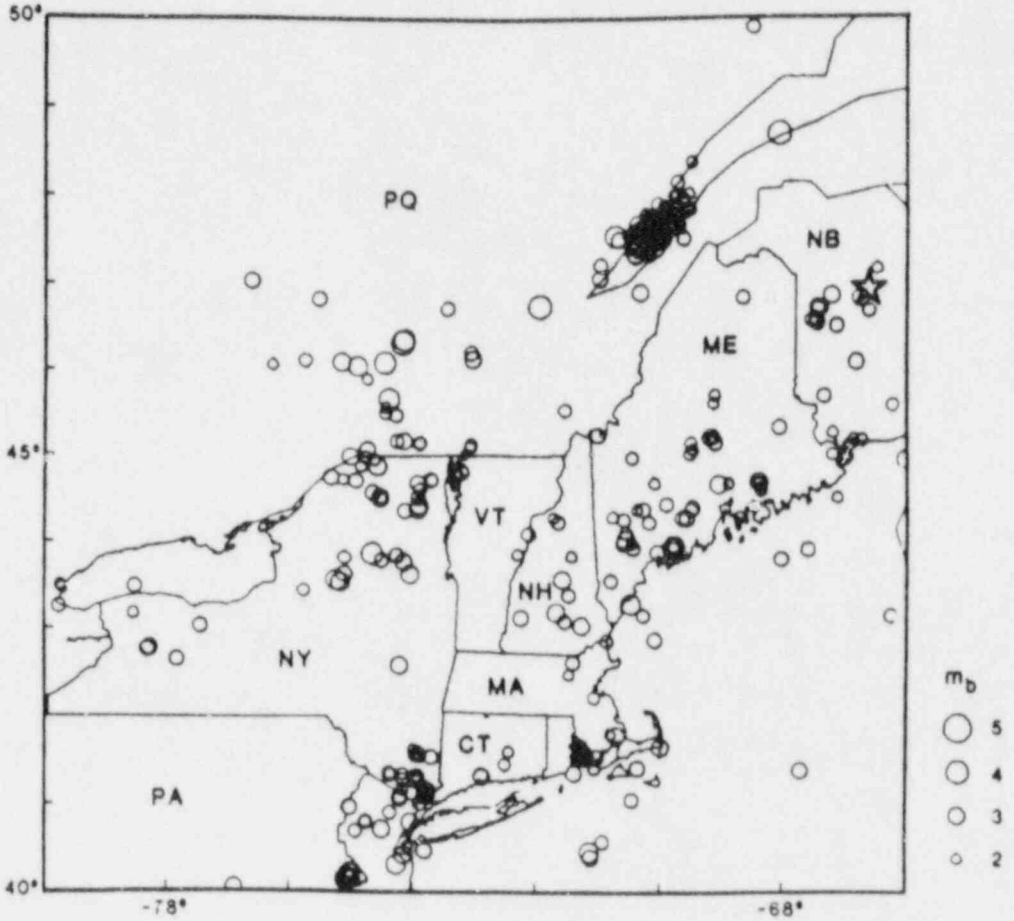

Figure 1. Seismicity map of the northeastern United States and Canada for the period 1975 to 1981. The epicenter of the New Brunswick earthquake (m_b =5.7) is indicated by the star.

Figure 2 Geotectonic map of the epicentral region. The earthquake epicenter (star) falls within the granitic pluton of the Miramichi Anticlinorium (the north-east trending structure in the center of the map).

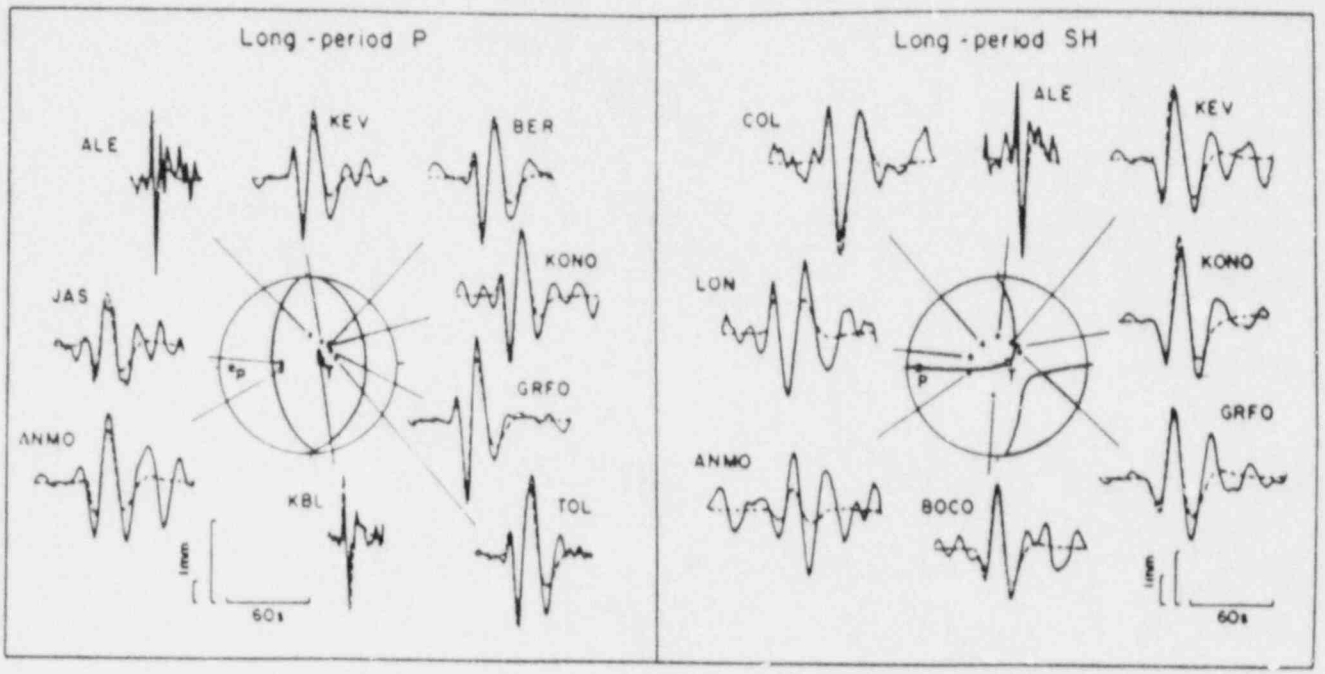

Figure 3. The observed (solid lines) and the corresponding theoretical (dashed lines) long-period P- and SH-wave seismograms. The longerperiod waveforms are the GDSN data, the shorterperiod waveforms are analog recordings. The theoretical seismograms are for the joint P and SH double-couple inversion (Table 4). All seismograms were normalized to an instrument magnification of 5000 and epicentral distance of 40°. Larger vertical scales are for the digital data, the smaller ones are for the analog data.

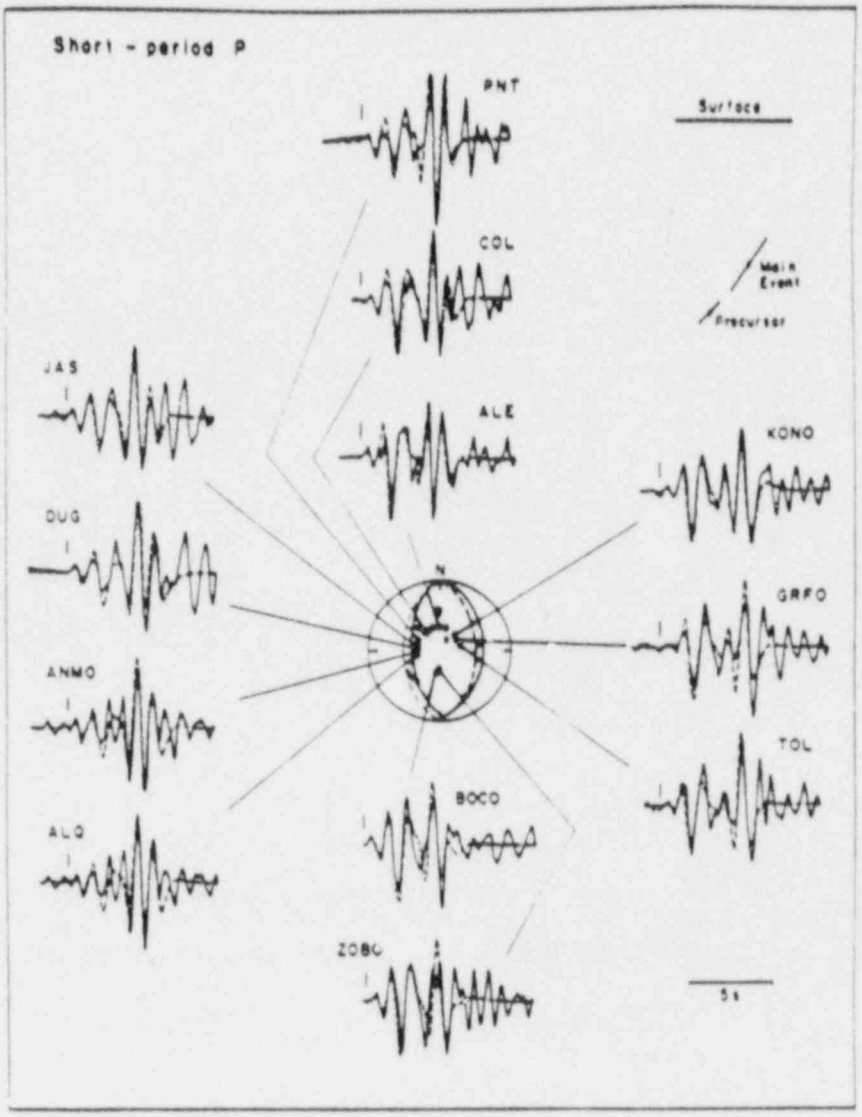

Figure 4 The observed (solid lines) and the corresponding theoretical (dashed lines) short-period P-wave seismograms. The sketch in the upper right-hand corner shows the geometry of the model; further details are given in Table 5. The assumed first arrivals are indicated by the vertical marks. The presumed precursor causes the first small oscillation immediately following the marks. The arrival prior to the mark at ANMO and ALQ is real and appears to be due to some earth heterogeneity (see also Figure 18); a similar arrival at JAS is an artifact of the zero phase filtering (it is not observed on the original record). The arrival time of P, pP and sP of the main subevent is also indicated. All traces are normalized to the power 1/2.

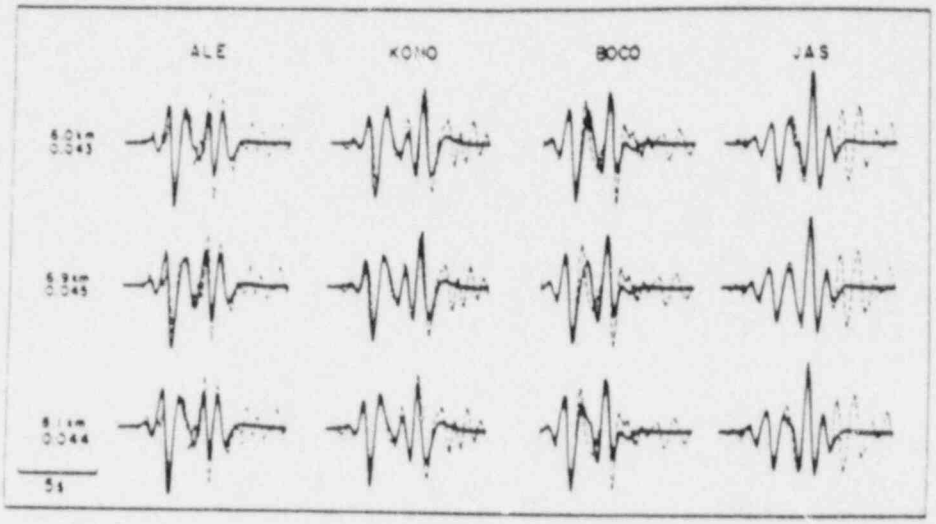

Figure 5 Effect of the depth of the precursor on the short-period waveforms (dashed lines are the data, solid lines are the synthetics). In each row, synthetics were calculated using the indicated depth of the precursor. In all examples, the depth of the main event was 7 km. Point sources on other parameters given in Table 3 were used in all calculations. The RMS residual for each model using all stations is also shown. The models with the precursor depth of 6 and 8 km correspond to the two relative minima found in the inversion.

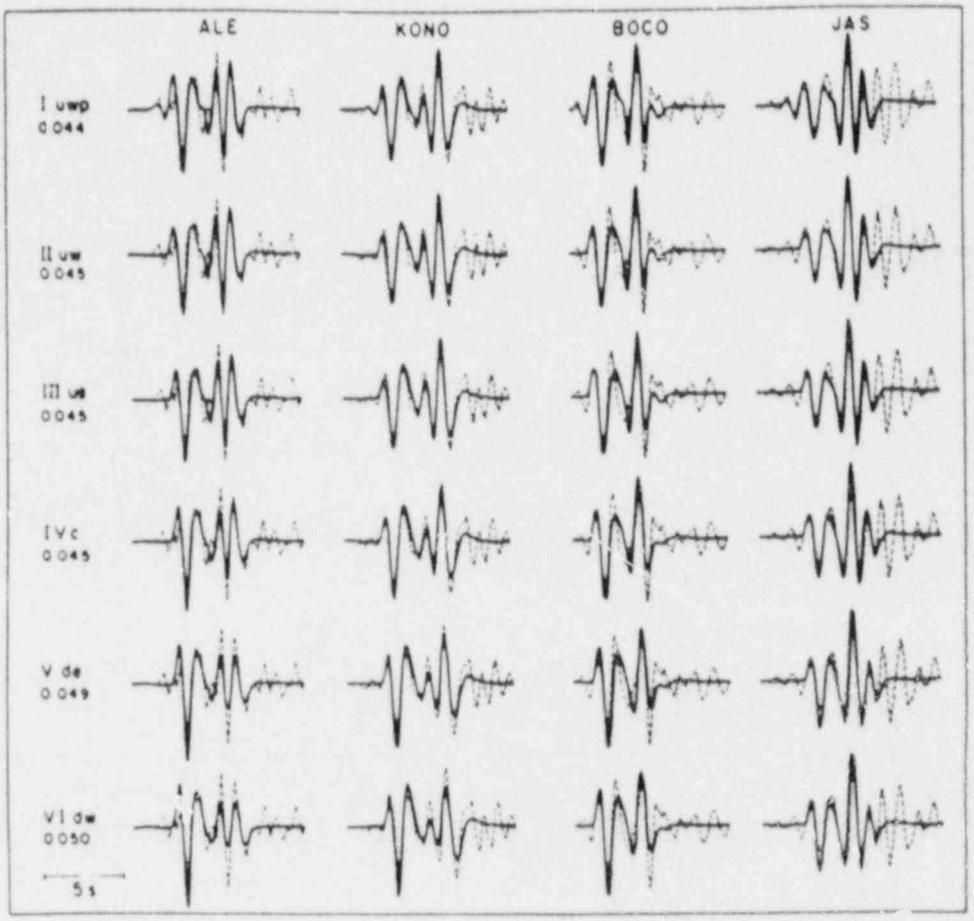

Figure 6 Effect of the source finiteness and rupture propagation on the short-period waveforms (dashed lines are the data; solid lines are the synthetics). Model I is for an upward propagating westward dipping line source with precursor (the best-fit model). In the subsequent models the small precursor was not included. Model II is for the same geometry as I; III is for an upward propagating eastward dipping line source; IV is for a point source; V is for a downward propagating eastward dipping line source; and VI is for a downward propagating westward dipping line source. The numbers are the RMS residuals using all stations. We cannot distinguish between the point and the upward propagating models from the residuals, but the downward propagating models are clearly inferior.

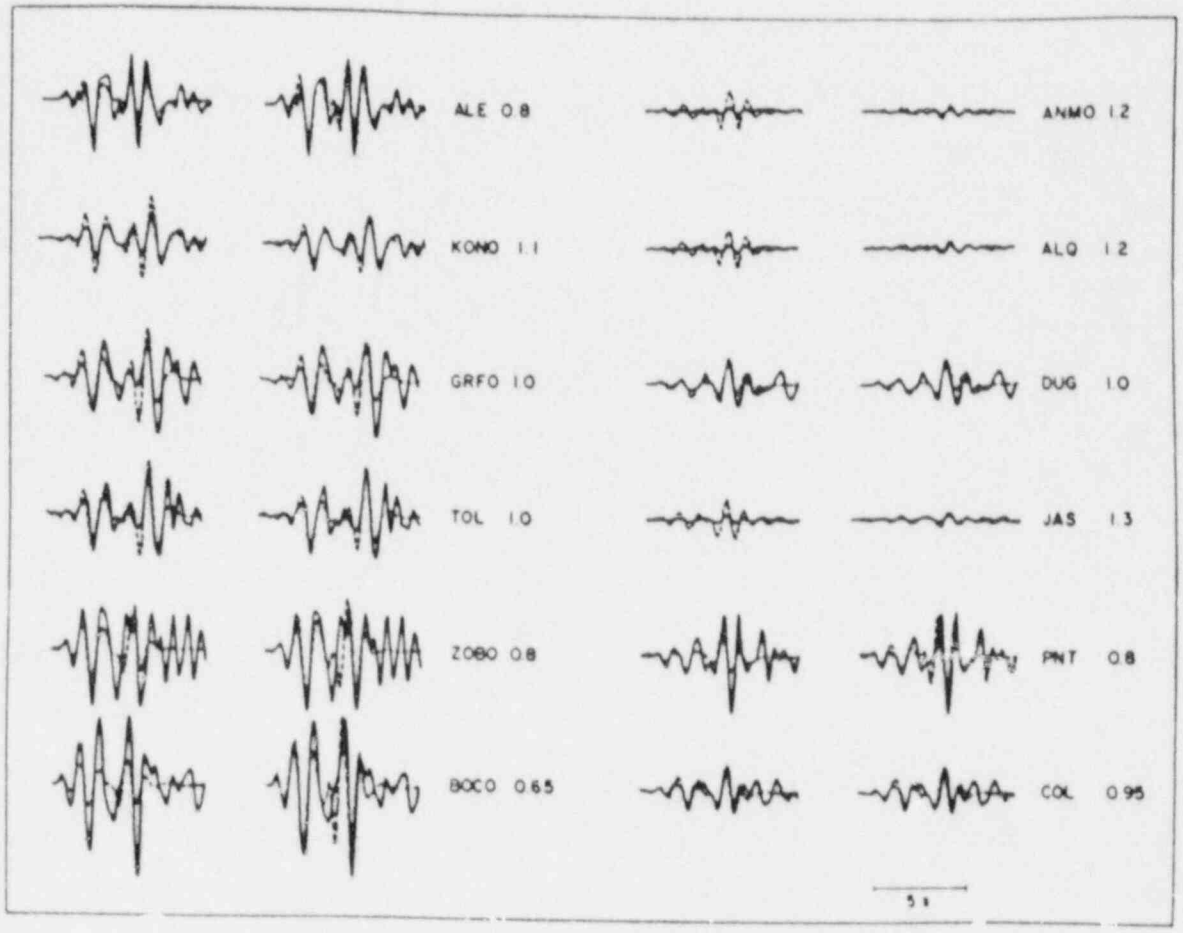

Figure 7 Traces on the left show the fluctuations of the short-period absolute amplitudes with respect to the average model with a $t^* = 1$s (solid lines are the data, dashed lines are the synthetics). Traces on the right were generated with the same source model, but the t*s were adjusted to fit the absolute amplitude at each station. The t*s used are indicated.

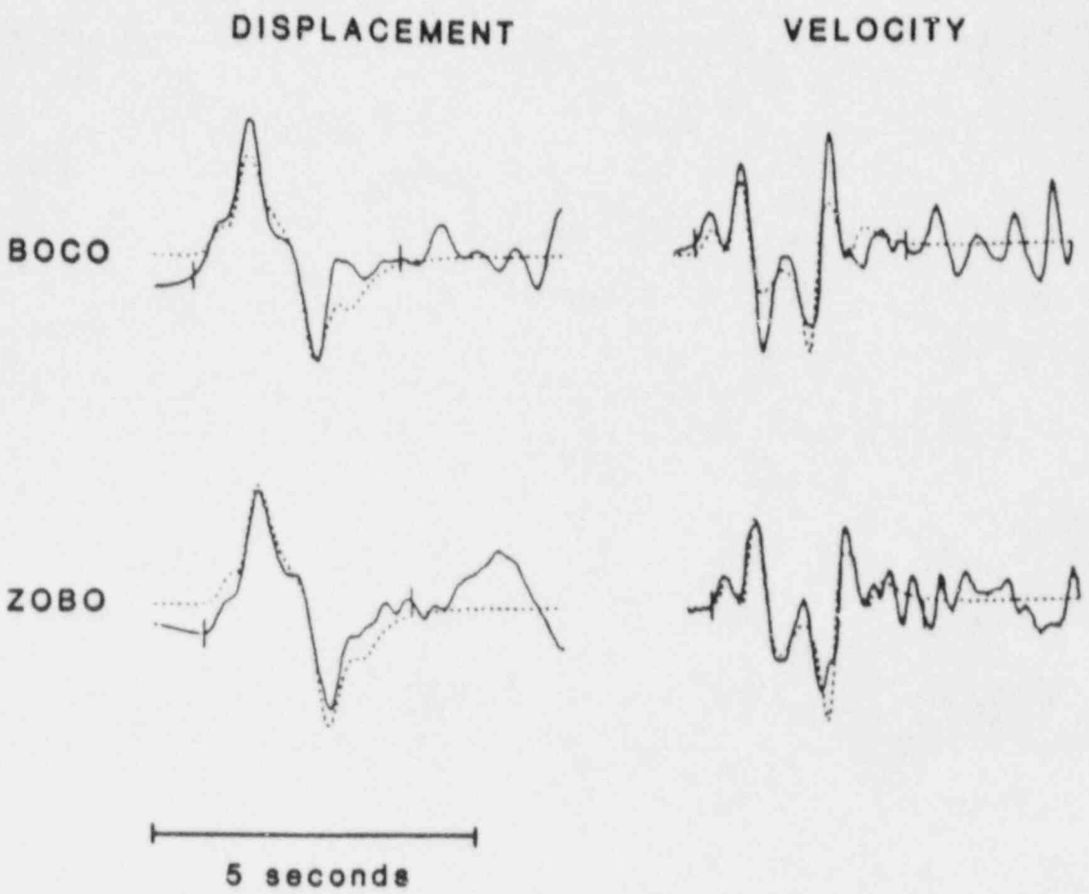

Figure 8 The broad-band records of the ground displacement and velocity due to P-waves at the South American stations (solid lines are the data, dashed lines are the synthetics). The amplitudes are normalized to a distance of 40°. The source time functions shown were obtained by matching the shapes of the observed P and the pP pulses at these stations.

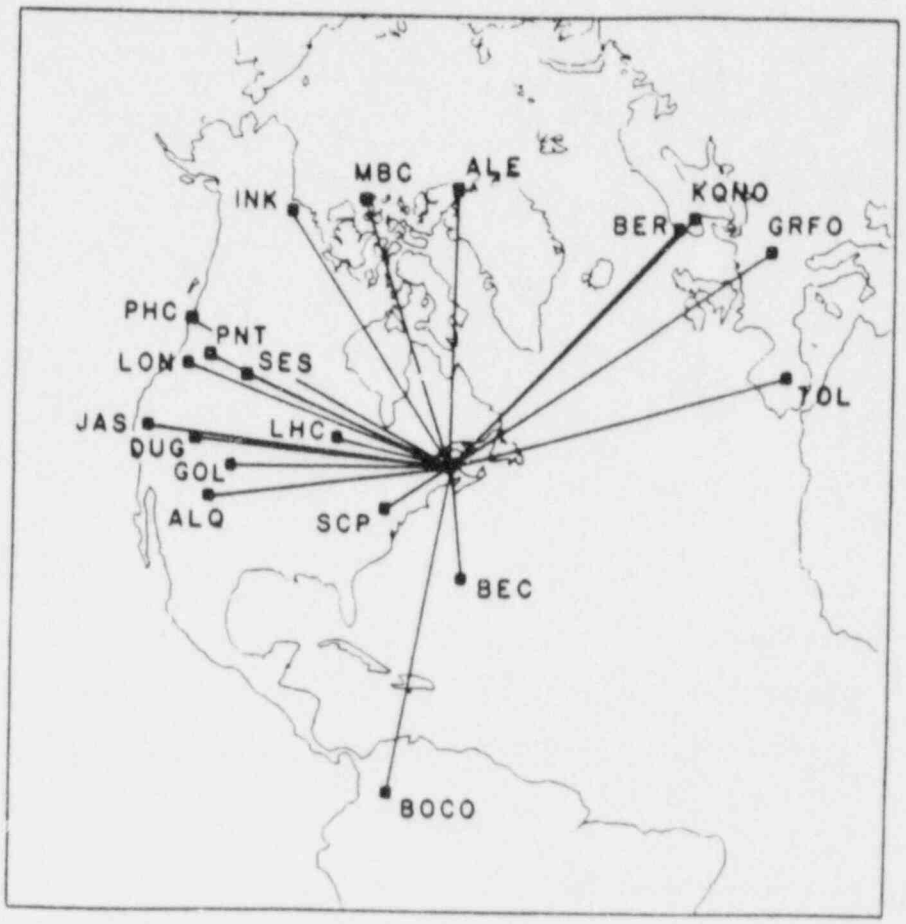

Figure 9 The surface wave paths to the stations used in the analysis (equal distance equal angle projection).

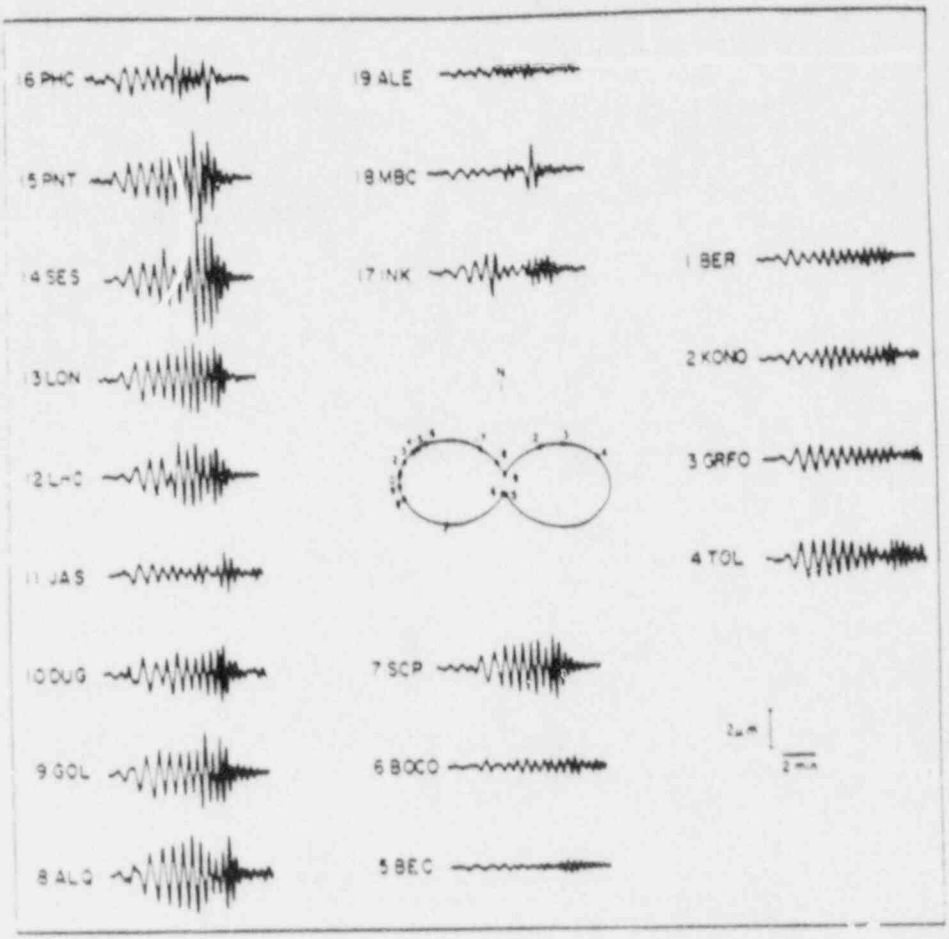

Figure 10 Equalized Rayleigh wave traces for the New Brunswick earthquake. The azimuthal amplitude variation is consistent with north-south striking thrust faulting. Note the spectral hole in the mid-periods at JAS, most likely due to high attenuation in the region between DUG and JAS.

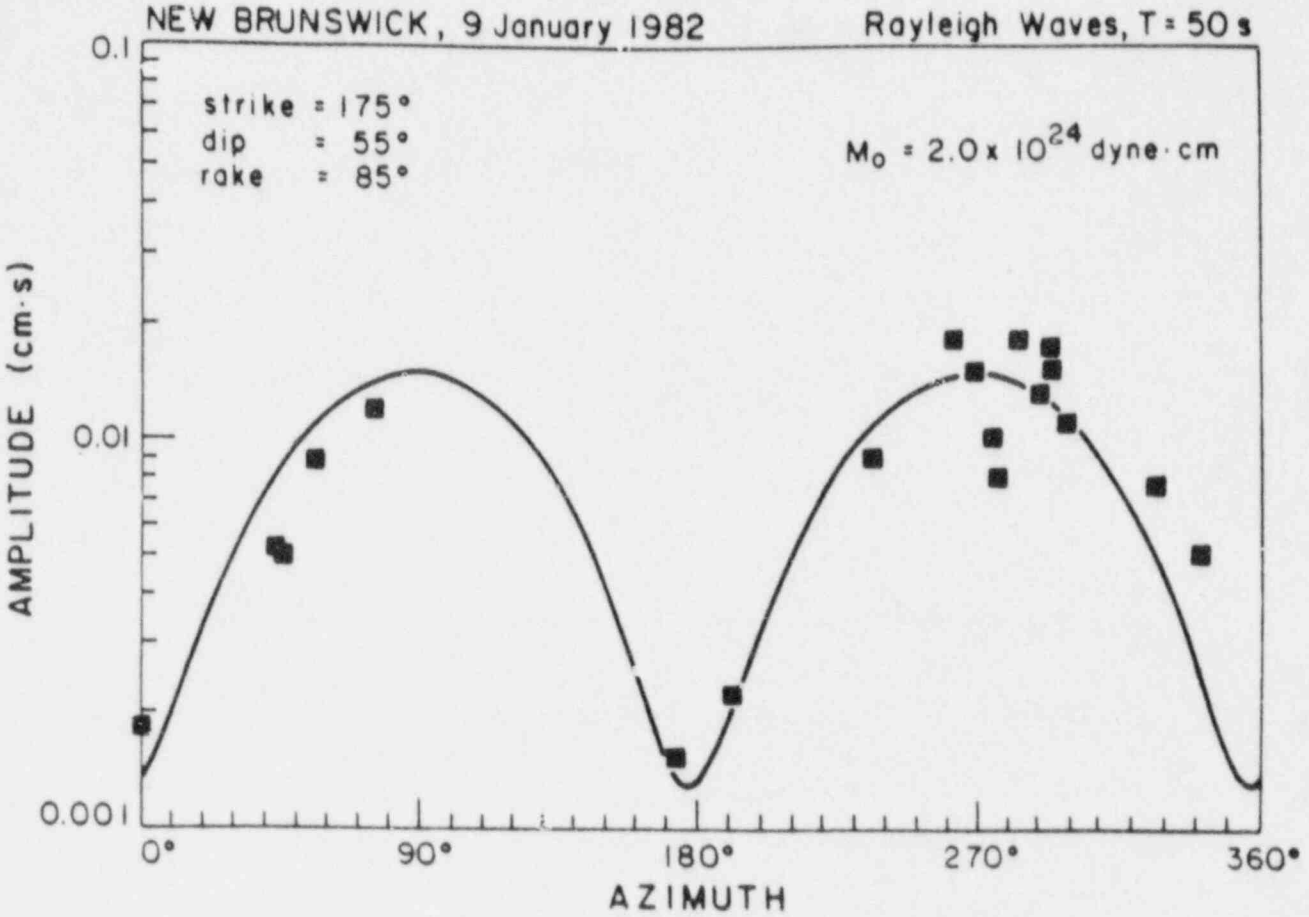

Figure 11 The observed (square) and the theoretical (solid line) radiation pattern of Rayleigh waves at a period of 50 s. The theoretical radiation pattern was calculated for the source mechanism and the moment determined in the body wave analysis.

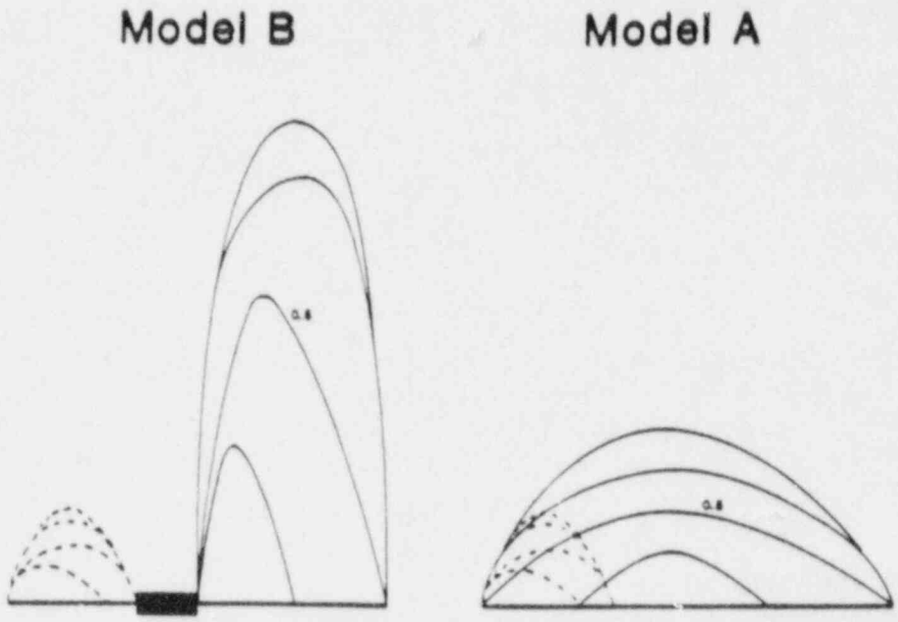

Figure 12. Interpretation of the source time function of the New Brunswick earthquake in terms of the barrier and asperity models of faulting. The concentric lines depict the growth of the slip displacement along the fault. The slip resulting from the precursor is indicated by dashed lines. In the asperity model [Kanamori, 1978] or barrier model P-SV-3 of Das and Aki [1977] (here shown together as a single model A), the slip due to the precursor and the main subevent become distributed over the whole fault surface, but in the barrier model P-SV-2 of Das and Aki (here shown as model B), high stress areas with no slip remain on the fault surface even after the passage of the rupture. "0.5" marks the displacement distribution at the time when the stopping (healing) phase is initiated, approximately at the half-time of the duration of motion [Boatwright, 1980].

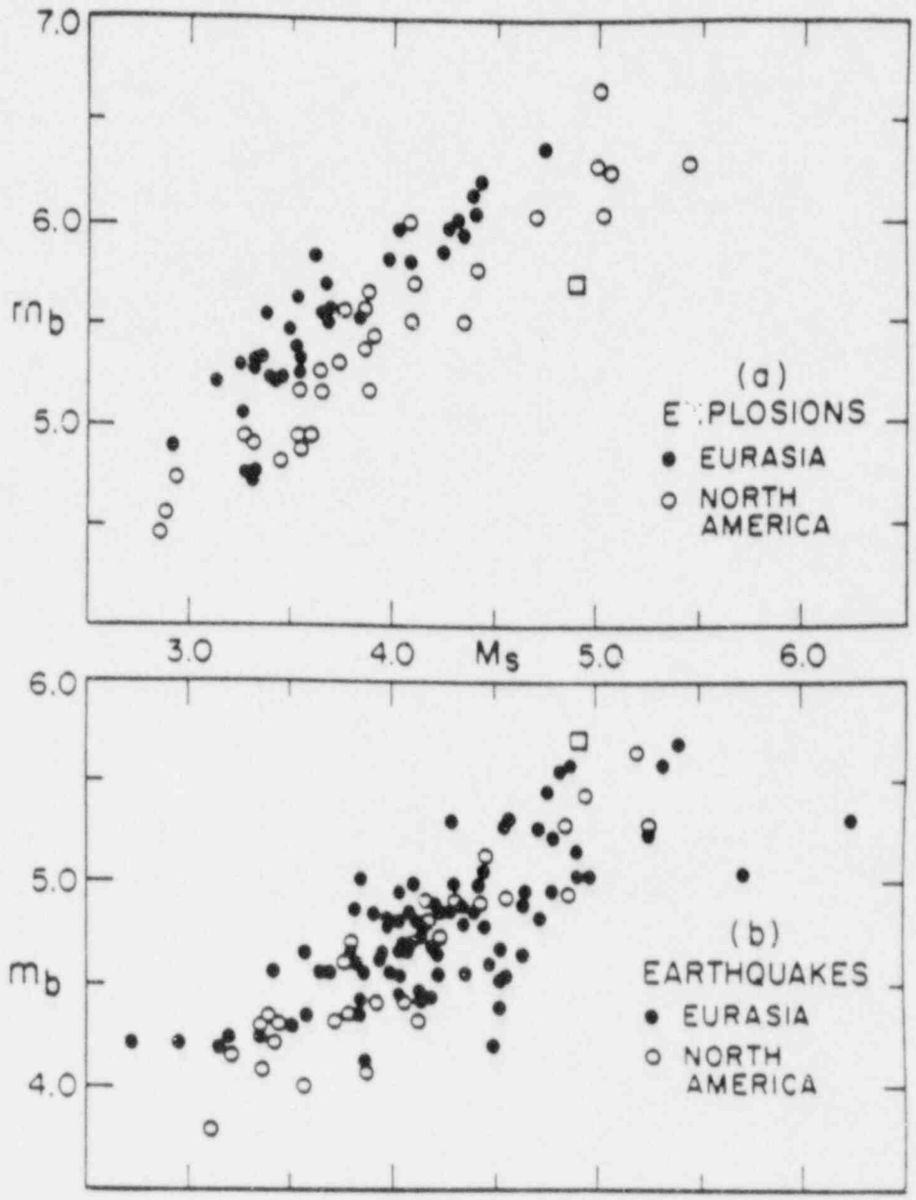

Figure 13 The m_b v.s. M_s plots for earthquakes and explosions. The New Brunswick earthquake is indicated by the squares. (Adapted from Douglas [1980].)

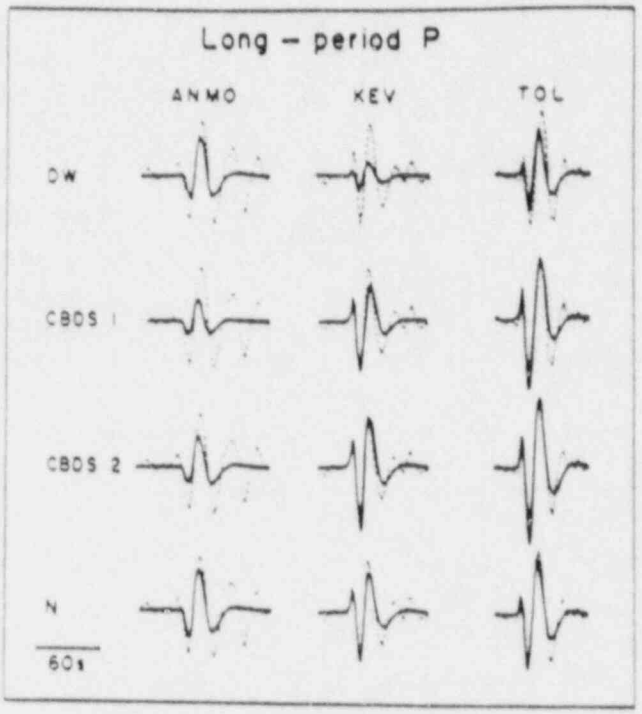

Figure 14 (a) Examples of the fit to the long period P-wave data by the DW model (Dziewonski and Woodhouse [1983], the CBDS1 and CBDS2 models (Choy *et al.* [1983]), and the N model (present study). Dashed lines are the data and solid lines are the theoretical seismograms. To facilitate a better comparison between different source mechanisms, the seismic moment (i.e. the sale factor) of 1.6×10^{24} dyne-cm was used for all theoretical seismograms (the preferred moments, especially those for CBDS1 and CBDS2, result in a very large misfit). The source depths are those determined in each study.

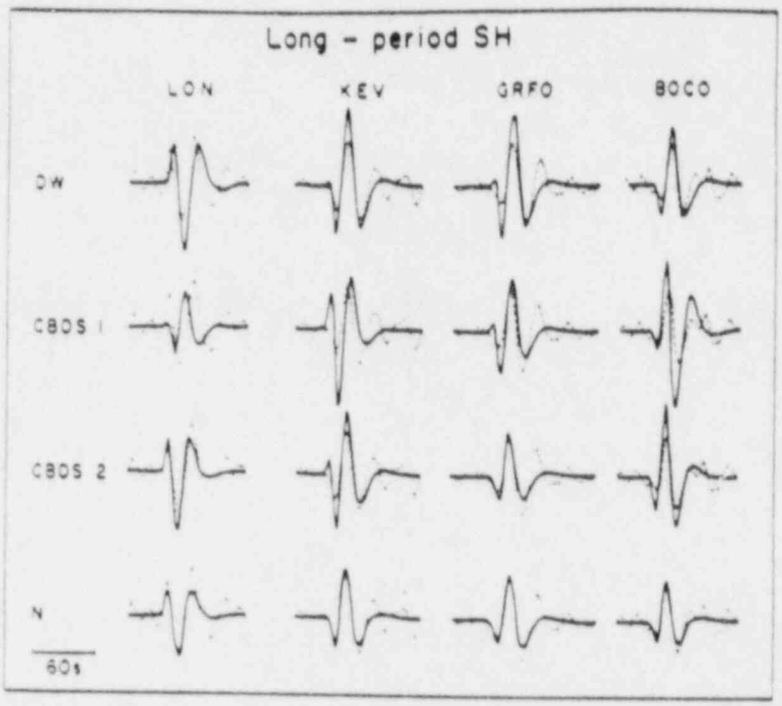

Figure 14 (b) Examples of the fit to the long-period SH data by the DW, CBDS1, CBDS2, and N models. The seismic moment of 1.6×10^{24} dyne-cm was used for all theoretical seismograms.

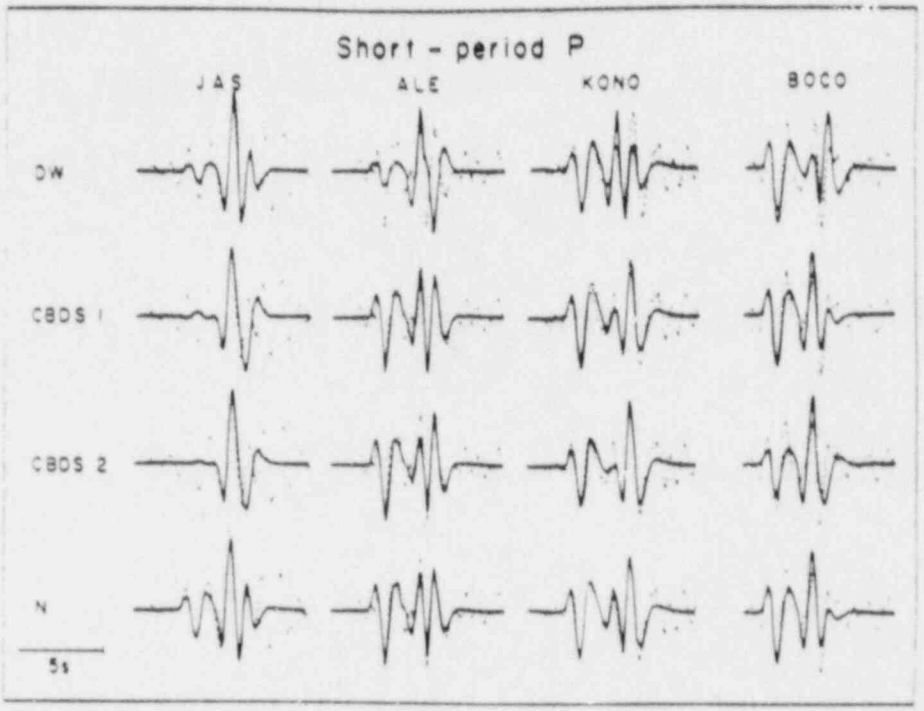

Figure 14 (c) Examples of the fit to the short-period P-wave data by the DW, CBDS1, CBDS2, and N models. Only the main subevent is modeled. Because the source depths determined in the previous studies were not sufficiently precise for a meaningful comparison, the source depth determined in this study was used in all models. The source time function determined in this study was used. The absolute amplitudes of all traces were normalized to the power of 1/2 of each trace.

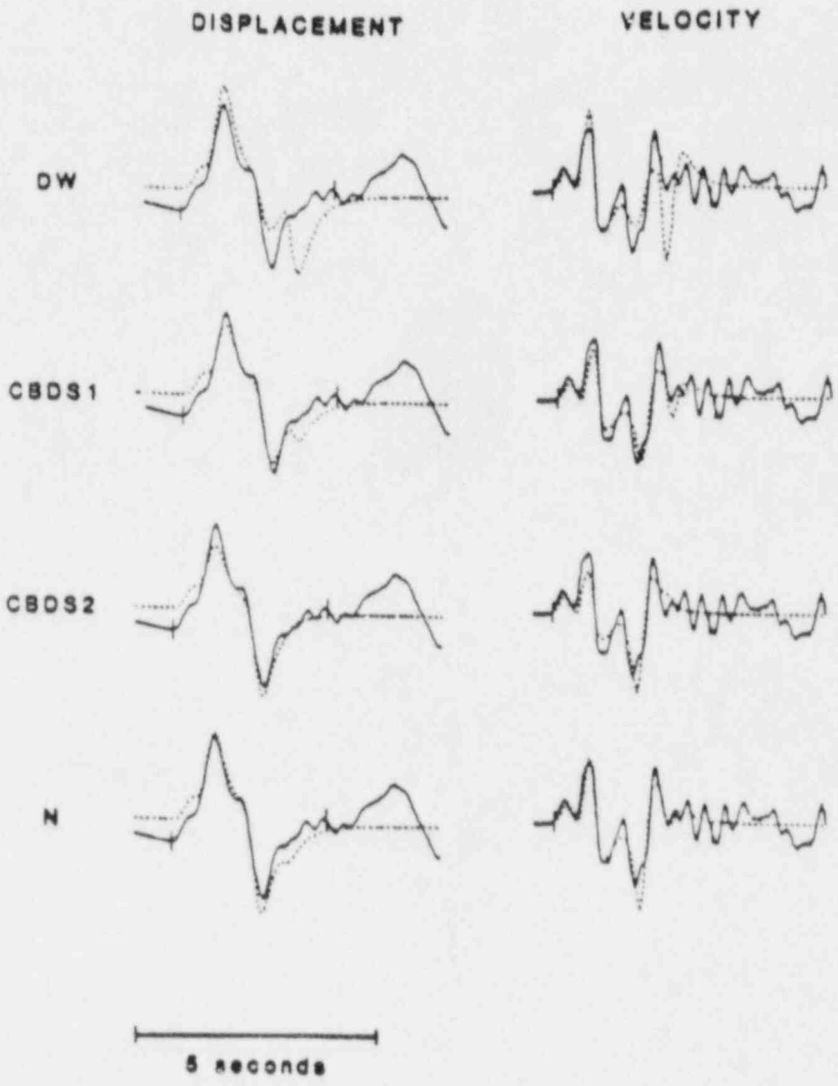

Figure 14 (d) Examples of the fit to the broad-band P-wave data by the DW, CBDS1, CBDS2, and N models. The source time function depth and seismic moment determined in this study were used in all theoretical seismograms.

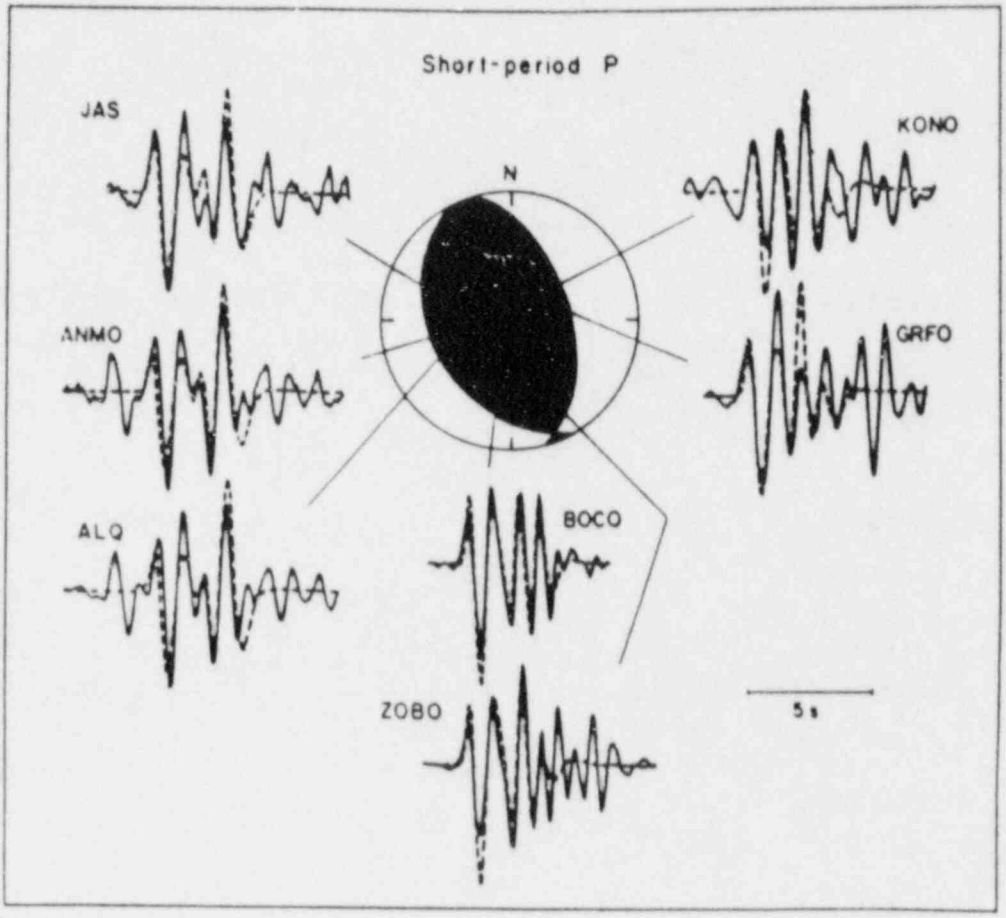

Figure 15 The observed (solid lines) and the corresponding theoretical (dashed lines) short-period P-wave seismograms for the January 11, 1982 aftershock. The constrained double-couple model given in Table 4 is used for the theoretical seismograms. The arrival prior to the direct arrival at ANMO and ALQ is identical to that observed for the January 9, 1982 event (Figure 4).

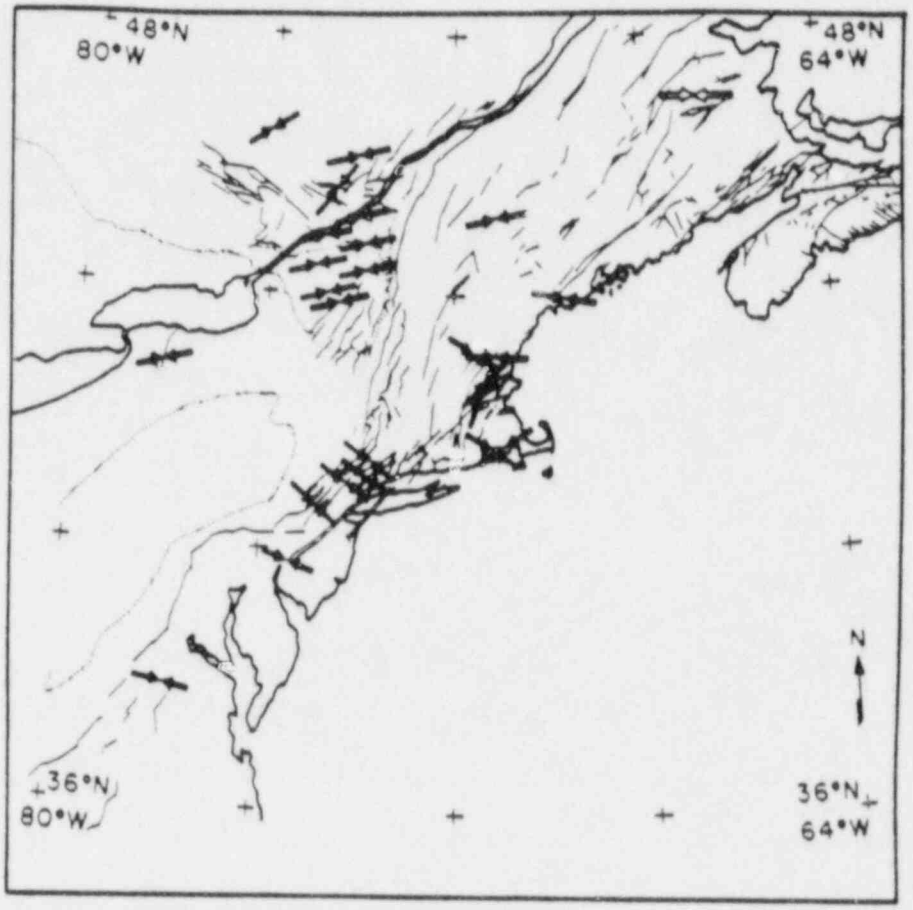

Figure 16 The orientation of the principal compression for the eastern North American earthquakes. The New Brunswick earthquake is indicated by the open symbol. (Adapted from Yang and Aggarwal [1981])

Appendix D: 1982 New Hampshire Earthquake

THE JANUARY 19, 1982 GAZA, NEW HAMPSHIRE EARTHQUAKE

by

Jeanne Sauber

Earth Resources Laboratory
Department of Earth, Atmospheric, and Planetary Sciences
Massachusetts Institute of Technology
Cambridge, MA 02142

ABSTRACT

On January 19, 1982, a magnitude 4.6 earthquake occurred in Gaza, New Hampshire. This moderate sized event was well recorded on a large number of regional stations, on strong ground motion instruments at Franklin Falls, NH, and at teleseismic distance on SRO station ANMO. These data were used to estimate source parameters such as source orientation, depth, scalar seismic moment, source extent, and stress drop.

From P-wave first motion data a strike-slip mechanism was determined. Results of using teleseismic P-waves to invert for scalar seismic moment and source depth give estimates of ~3 km for depth and $3.\times10^{22}$ dyne*cm for seismic moment (Pulli *et al*, 1983). Using strong ground motion records from Franklin Falls, NH, the seismic moment was estimated from the displacement amplitude spectrum to be 6.2×10^{22} dyne*cm and from time domain modeling of the records to be $5.6-17.7\times10^{22}$ dyne*cm. Using the spectral corner frequency and the source duration from modeling of the direct S wave, a circular source radius of .6 km was determined. Static stress drop estimates ranged from ~100-350 bars.

INTRODUCTION

On January 19, 1982 a magnitude 4.6 earthquake occurred in Gaza, New Hampshire (Figure 1). This event was the largest magnitude earthquake (m_b =4.6) to occur in central NH since the 1940 Ossipee event (m_b =5.4). The Gaza earthquake produced intensity V effects in the epicentral area. To locate this earthquake and its aftershocks, Pulli *et al.* (1983) used the crustal model of Curtin *et al.* (1983). The location they obtained was: lat. 43.523, long. -71.612, depth 3.0 km. This location is 43 km southwest of the site of the 1940 earthquake. Using the main shock as a master event for a joint hypocentral location of the largest aftershocks, the aftershocks were found to fall within an area of 2 km in extent and trending NE. The focal depths of the aftershocks were all less than 2 km.

This moderate sized event was well recorded on a large number of regional stations, on strong ground motion instruments at Franklin Falls, NH, and at teleseismic distance on SRO station ANMO. The data includes digital recordings from the RSTN, ECTN, MIT, and GDSN networks. Although a large number of regional stations recorded this event much of this data was from short-period, vertical instruments. Additionally,

three component stations, such as RSNY (RSTN station in upstate New York), PAL (station near New York City), and WES (at Weston, MA), showed a spurious long period pulse. Figure 2 shows the intermediate period record from the RSTN station, RSNY. Table 1 gives the station distance and azimuth. The long-period pulse in the record occurs shortly after the surface wave arrival. The very large amplitude of this feature is attributed to instrument nonlinearity (Dale Breding, Sandia Labs, personal communication).

The strong ground motion, regional, and teleseismic data were used to estimate source parameters such as source orientation, depth, scalar seismic moment, source extent, and stress drop.

SOURCE MECHANISM

P-Wave First Motion Data

Twenty-four reliable P-wave first motions were used to determine the focal mechanism of the main shock (Figure 3). One fault plane strikes N19E and dips 68 ° to the east. This fault plane is parallel to the structural grain of the area and the trend of instrumentally located earthquakes. The other plane strikes N100E and dips 75 ° to the north.

First motions at two stations are inconsistent with the solution, ONH and WNH. For an earthquake of this size discernible P-wave first motions are observed out to a distance of ~300 km on regional short-period records. Even at these distances, however, there is still some ambiguity in determining first motions due to weak Pn arrivals. Additional uncertainty in the first motion of the P-wave occurs due to possible reversals in instrument polarity.

Teleseismic Modeling

Using the method of Nabelek (1984), teleseismic P-waves at the short-period SRO station ANMO were used to invert for scalar seismic moment and source depth (Pulli *et al*., 1983). Figure 4a shows the original short-period,vertical seismogram from ANMO. ANMO is at a distance of 28.1° and azimuth of 264.2°. This record was high pass filtered using a zerophase 3-pole Butterworth filter. Figure 4b compares the filtered seismogram with the synthetic fit. Using the source mechanism determined from the P-wave first motion study as a source orientation, and assuming a $t^*=1.0$, a focal depth of 3.4 km and a scalar seismic moment (3×10^{22} dyne*cm) were calculated. A focal depth of 3.4 km is consistent with the depth determined using local stations. The estimated source time function is shorter or equal to the resolution limit of the data, which is about 0.2 s. Due to uncertainty in attenuation associated with the path to ANMO, the uncertainty in the source time function estimate is large.

STRONG GROUND MOTION DATA

The U.S. Army Corps of Engineers Division, New England has strong-motion accelerographs at 12 dams in New England (Chang,1983). Eleven three-component accelerographs at five dams, plus an instrument at a Veterans Administration hospital

recorded the Gaza earthquake (Figure 5). A maximum acceleration of 0.55g was recorded on the abutment instrument at Franklin Falls dam, 9.3 km from the epicenter. Other accelegraphs recording this event were 64-104 kilometers away. Tha records from most of these sites are unusable for source studies due to a poor signal-to-noise ratio and contamination due to long-period noise (T=~2 s).

Franklin Falls Records

The accelegrams from the abutment and downstream instruments at Franklin Falls were examined at the USGS, Menlo Park, California. The digital data had been processed by the Seismic Engineering Branch of the USGS. The corrected accelerograms, velocities, displacements, and their response spectra were processed using their standard computer programs AGRAM (Converse, 1983).

The three components of the displacement record from the abutment site are given in Figure 6 . In Figure 7 , the velocity record and acceleration spectrum are given for the two horizontal records. In constrast to the horizontal displacement records from the downstream site (Figures 8 and 9), the abutment records (Figure 6) show a single 1.5 s pulse. Additionally at ~13 Hz a very large acceleration (Figure 7) occurs that is apparently amplified in the abutment records. The vertical component at the downstream site (Figure 10) appears to be contaminated by long-period noise. Thus, we concluded that these records should not be used for determination of source parameters.

Since there are only two horizontal records from one site, source orientation and depth determined from the P-wave first motion and teleseismic studies were used as starting parameters. We started our analysis of the strong-ground motion data by trying to recover first-order characteristics of the source; that is, scalar seismic moment and source duration. This was first done by examining the displacement amplitude spectrum using a far-field approximation to determine seismic moment and the theory first formulated by Brune (1970, 1971) to calculate source size from the spectral corner frequency. Next, synthetic seismograms were calculated using Bouchon's discrete wavenumber method (Bouchon, 1981). A simple point source in a homogeneous layered medium was assumed. From this approach the main phases were roughly matched and seismic moment was determined. From the pulse width of the direct S source duration was constrained. With the estimates of source radius and seismic moment from the two approaches, static stress drop is calculated.

Displacement Amplitude Spectrum

To calculate M_0 we assume that the pulse shape and spectral character are based on the simple representation for far-field ground motion. From the ray-theoretical representation for the displacement of a heterogeneous elastic medium the expression for M_0 can be derived (Aki and Richards, 1979, Chapter 4). If we assume the receiver properties of density and wave velocity are similar to the source properties, this relation for shear wave arrivals becomes

$$M_o = 4\pi\rho\beta^3 R\frac{\bar{u}}{F^s} \qquad (1)$$

For our case, we use the parameter values: $\rho = 2.8 g/cm^3$, $\beta = 3.6 km/s$, $R = 9.3 km$, $F^s = (1.85)(.5)$, $\bar{u}$ = the low-frequency asymptote of the displacement spectrum. From Figure 30 we can determine $\bar{u}$ from the displacement spectrum. u=.03 cm*s at site 1 (longitudinal) and u=.05 cm*s at site 3 (transverse). This gives a Mo of $6.2 \times 10^{22} dyne*cm$.

Brune (1970, 1971) derived a relationship between corner frequency, f_o and the radius of a circular fault from the spectrum of S-waves. This relationship is given by

$$r_o = \frac{2.34\beta}{2\pi f_o} \qquad (2)$$

where corner frequency = 2.1 at site 1 (Figure 11b), 2.2 at site 3 (Figure 11d), and $\beta = 3.6 g/cm^3$. A value of appoximately 0.6 km is found for r_o. In using corner frequency to estimate radius, it is assumed that there is an inverse relation between pulse width and spectrum width. The measurement of corner frequency or pulse width determines estimates of rupture duration, i.e., the source dimension divided by the rupture velocity. Only by estimating or assuming a value for the rupture velocity can the source dimension be obtained from rupture duration. Secondly, the spectral shape and the corner frequency are assumed to to be constant over the focal sphere. If a large number of stations were used the differences would be averaged. However, with a single station estimate this assumption may not be valid.

Time Domain Modeling

Bouchon's discrete wavenumber method (Bouchon,1981) was used to calculate synthetic displacement records. The source time function used is given by a unit ramp function such that the derivative (velocity) is a triangle. The crustal models used are given in Tables 2 and 3. To model the records we needed to assume source parameters such as source orientation and depth determined from earlier parts of the study. Due to the uncertainty in these parameters, however, a large number of trial solutions were tried. For example, setting the nodal plane (N19E) to be fixed, different slip directions were systematically examined. The orientation that most closely matched the displacement waveforms given in Figures 8 and 9 was the solution given by the slip vector determined from the P-wave first motion solution. See Figure 12 for a comparison of the observed and synthetic seismograms.

Next, the value for the rise time was varied from .20 to 1.0 s The rise time, t_o, or source duration represents the amount of time from the initiation of slip to the termination of slip. The pulse width of the direct S wave and the general character of the waveform were used to constrain the source duration. Source duration greater than .50 s did not fit either the pulse width or the general character of the waveform. The best fit to the pulse width was for a value .4 s.

The horizontal instruments are oriented relative to the Franklin Falls dam. Therefore, the synthetic seismograms were rotated to this orientation. The transverse record (135°) and the longitudinal (225°) are close (~ 20°) to be

rotated to represent transverse and radial directions of motion. The longitudinal record is particularly sensitive to the source mechanism and instrument orientation. The displacement amplitude of the transverse component, in contrast, changes very little with small changes in orientation. The seismic moment used to match the displacement amplitude of the transverse component was 5.6×10^{22} dyne*cm, for the longitudinal component 1.7×10^{23} dyne*cm.

For a circular rupture, the fault radius can be obtained from

$$r = \frac{V_r V_h}{V_r + V_h t_d} \tag{3}$$

where V_r is the velocity of the rupture front, V_h is the velocity of the healing front and t_d is the duration of the source time function (Nabelek, 1984). For $V_r = .75\beta$, $V_h = \beta$, $\beta = 3.6$ g / cm^3 and $t_d = .4$ a fault radius of $r_o = 0.6$ km is found.

Stress Drop

Brune (1970, 1971) constrained the relationship of corner frequency to fault radius by assuming that the effective stress was equal to the average static stress drop. The relationship he derived is given by:

$$\Delta\sigma = \frac{7}{16} \frac{M_o}{r_o^3} \tag{4}$$

The moment estimates from the strong ground motion records are $M_o = 6.2 \times 10^{22}$ (from low frequency asymptote of displacement spectrum), $M_o = 5.6 \times 10^{22}$ dyne*cm (transverse component) and $M_o = 17.7 \times 10^{22}$ dyne*cm (longitudinal). Corresponding stress drops are $\Delta\sigma$ = 124 bars, 103 bars, and 353 bars. The average stress drop is proportional to the average slip divided by the least fault dimension. This estimate of stress release only approaches the actual average of the static stress drop over the rupture area if the stress release varies gradually over the fault surface (Boatwright, 1984).

DISCUSSION

At this point, estimates for seismic moment, source radius, and stress drop have been determined. To calculate these values we intially relied on the source mechanism determined by the P-wave first motion study. The results from the time domain modeling of the strong-ground motion records from Franklin Falls, NH and the inversion results from teleseismic station ANMO are roughly consistent with this result. Additional constraint of the source mechanism will be (hopefully) obtained from the modeling of the regional stations. With greater certainty in the source orientation, we could possibly reduce some of the scatter in the seismic moment estimates. Additionally, alternative methods for calculation of stress drop could be computed. One such measure is given by the dynamic stress drop (Boatwright, 1980). This technique requires measuring the initial slope of far-field waveforms,

and returns an estimate which is effectively an average of the dynamic stress drop over the area of the rupture event which radiated the pulse.

As mentioned earlier, in our modeling of the strong ground motion records we assumed a simple point source representation for the source in an essentially homogeneous medium. A dynamic ,finite fault source model such as a plane circular shear crack (Campillo and Bouchon, 1983) could be used. This is, of course, only one of many possible source models. With only one station is would be difficult to uniquely determine source complexity. Additionally, for the higher frequencies modeled in this study, heterogeniety in the crust probably effects our results. Thus, even by using a more realistic source model, the full waveform probably could not be completely synthesized due to the complexity of fine crustal structure.

FURTHER WORK

Modeling of Regional Data for Determination of Source Mechanism

The regional stations given in Table 1 will be used to constrain the focal mechanism determined from the P-wave first motions. Synthetic seismograms will be computed using Bouchon's discrete wavenumber method (Bouchon, 1981). Bouchon (1983) used this method to compute synthetic seismograms at regional distances for a strike-slip earthquake (M=4.1) which occurred in central France. He was able to reproduce the major features of the records including complexity and duration. For a simple model of two layers over a half-space mantle, all of the regional stations used can be fairly well represented by the same structural model (Table 2). The data for this part of the study are currently on line and the various instrument responses are known. With additional constraint on the source mechanism we may be able to better model the strong ground motion records and obtain a more reliable value for seismic moment and stress drop.

Use of Lg for determination of seismic moment

For moderate sized earthquakes in eastern North America, regional surface waves, particularly Lg are frequently used for determination of seismic moment, source dimension, and stress drop. Lg waves, the most prominent phase on regional continental records, have been shown to be guided waves made up of SH and SV waves (Der et al, 1979 and Bouchon 1983). From modeling studies of regional phases, Lg propagation was shown to be sensitive to random inhomogenities in the crust and deviations of the free surface or the Moho from plane parallel surfaces. Observationally, attentuation of Lg was found to be dependent on propagation path (Rondout Associates, 1980 and Patton, 1983). In a structurally complex area such as New England, we might therefore expect the determination of seismic moment from Lg waves to be quite variable. The seismic moment determined from strong motion and teleseismic data will be compared to moment determined using Lg from short-period, vertical records from the ECTN digital network (Table 1).

CONCLUSIONS

From P-wave first motion data a strike-slip mechanism was determined. Results of using teleseismic P-waves to invert for scalar seismic moment and source depth give estimates of ~3 km for depth and 3. x 10^{22} for seismic moment (Pulli *et al*, 1983). Using strong ground motion records from Franklin Falls, NH, the seismic moment was estimated from displacement amplitude spectrum to be 6.2 x 10^{22} dyne*cm and from time domain modeling of the records to be 5.8-17.7 x 10^{22} dyne*cm. Using the spectral corner frequency and the source duration from modeling of the direct S wave, a circular source radius of .6 km was determined. Static stress drop estimates ranged from ~100-350 bars.

ACKNOWLEDGMENTS

This work was supported by U.S. Nuclear Regulatory Commission Contract NRC-04-76-209 and by U.S. Geological Survey Contract 14-08-0001-21284.

REFERENCES

Aki, K., and P. Richards (1980), Quantitative Seismology - Theory and Methods, W.H. Freeman and Co., San Francisco.

Boatwright, J. (1980), A spectral theory for circular seismic sources; simple estimates of source dimension, dynamic stress drop, and radiated seismic energy, Bull. Seism. Soc. Am., v.70, p. 1-27.

Boatwright, J. (1982), A dynamic model for far-field acceleration, Bull. Seism. Soc. Am., v.72, p. 1049-1067.

Boatwright, J. (1984a), The effect of rupture complexity on estimates of source size, J. Geophys. Res., v.89, p. 1132-1146.

Boatwright, J. (1984b), Seismic estimates of stress release, J. Geophys. Res., in press.

Bouchon, M. and K. Aki (1977), Discrete wavenumber representation of seismic source wave fields, Bull. Seism. Soc. Am., v.67, p. 259-277.

Bouchon, M. (1979), Discrete wavenumber representation of elastic wave fields in three space dimensions, J. Geophys. Res. v.84, p.3609-3614.

Bouchon, M. (1980), Calculation of complete seismograms for an explosive source in a layered medium, Geophysics, v.45, p.197-203.

Bouchon, M. and K. Aki (1980), Simulation of long-period, near-field motion for the great California earthquake of 1857, Bull. Seism. Soc. Am., v. 70, p. 1669-1682.

Bouchon, M. (1981), A simple method to calculate Green's functions for elastic layered media, Bull. Seism. Soc. Am., v.71, p.959-971.

Bouchon,M. (1983), The complete synthesis of seismic crustal phases at regional distances, preprint.

Brune, J.N. (1970), Tectonic stress and the spectra of seismic shear waves, J. Geophys. Res., v.75, p. 4997-5009.

Brune, J.N. (1971) Correction, J. Geophys. Res., v.76, p.5002.

Chang, F.K. (1983), Analysis of strong-motion data from the New Hampshire earthquake of 18 January 1982, Technical Report, Geotechnical Laboratory, U.S. Army Engineer Waterways Experiment Station.

Converse, A.M. (1983), User's Manual for the Computer Code AGRAM, U.S. Geological Survey Open File Report.

Curtin, P., J. Pulli, and C. Godkin (1983), A new crustal model for central New England-implications for hypocentral calculations and fault plane solutions, ABSTRACTS Eastern SSA p.8.

Der, Z., C. Mrazek, E. Smart, and B. Barker (1979), Some aspects of Lg and Pg progation, Seismic Data Anlysis Center, Teledyne Geotech, 314 Montgomery Street, Alexandria Virginia 22314.

Dietrich, M., M. Prange, and M. Bouchon (1983), Synthetic vertical seismic profiles using the discrete wavenumber method, preprint.

Harkrider, D.G. (1983), Synthetics and theoretical seismology, Reviews of Geophysics and Space Physics, v.21, p.1299-1308.

Hasegawa, H. S.(1983), Lg spectra of local earthquakes recorded by the Eastern Canada telemetered network and spectral scaling, Bull. Seism. Soc. Am., v.73, p.1041-1061.

Knopoff, L., F.Schwab, and E.Kausel (1973), Interpretation of Lg, Geophys. J. R. Astr. Soc., v.33, p.389-404.

Modiano, T. and D. Hatzfeld (1982), Experimental study of the spectral content for shallow earthquakes, Bull. Seism. Soc. Am., v.72, p.1739-1758.

Nabelek, J.L. (1984), Determination of earthquake source parameters from inversion of body waves, Ph.D. Thesis, MIT.

Panza, G. F., F.Schwab, and L.Knopoff (1975), Multimode surface waves for selected focal mechanisms-III. Strike-slip sources, Geophys. J. R. Astr. Soc., v.42, p. 945-955.

Patton, H.J. (1983), Lg excitation and propagation in the Western United States, preprint.

Pulli, J.J. (1983), Seismicity, earthquake mechanisms and seismic wave attenuation in the Northestern United States, Ph.D. Thesis, MIT.

Prange, M. (1983), P-SV seismogram synthesis in layered media using the discrete wavenumber method, unpublished paper.

Pulli, J.J. Nabelek, and J. Sauber (1983), Source parameters of the January 19, 1982 Gaza, NH earthquake, ABSTRACTS Eastern SSA.

Randall, M.J. (1973), The spectral theory of seismic sources, Bull. Seism. Soc. Am., v.63, p.1133-1144.

Roundout Associates, Inc. (1980), Regional Seismic Wave Progation, Semiannual Technical Report, No. 5, 1 January 1980 - 30 June 1980.

Street, R., R. Hermann and O. Nuttli (1975), Spectral characteristics of the Lg wave generated by Central United States Earthquakes, Geophys. J. R. Astr. Soc., v.41, p. 51-63.

Taylor, S. (1980), Crust and upper mantle structure of the Northeastern United States, Ph.D. thesis, MIT.

Taylor,S. and M.N. Toksöz (1982), Crust and upper-mantle velocity structure in the Appalachian orogenic belt: Implications for tectonic evolution, Geol. Soc. Amer. Bull., v.93, p.315-329.

Table 1

Regional Stations

Station	Distance (deg)	Azimuth (N)
RSNY	260	297
MNT	273	325
GNT	322	349
OTT	387	304
GAC	391	309
CKO	538	303
SCP	597	341

Table 2

Northern Appalachian Model of Taylor (1980)

Depth (km)	V_p	V_s
0-15	6.1	3.6
15-40	7.0	4.1
40	8.1	4.8

Table 3

Northern Appalachian Model of Taylor (1980) with a thin sedimentary layer

Depth (km)	V_p	V_s
0-.2	4.5	2.6
.2-15	6.1	3.6
15-40	7.0	4.1
40	8.1	4.8

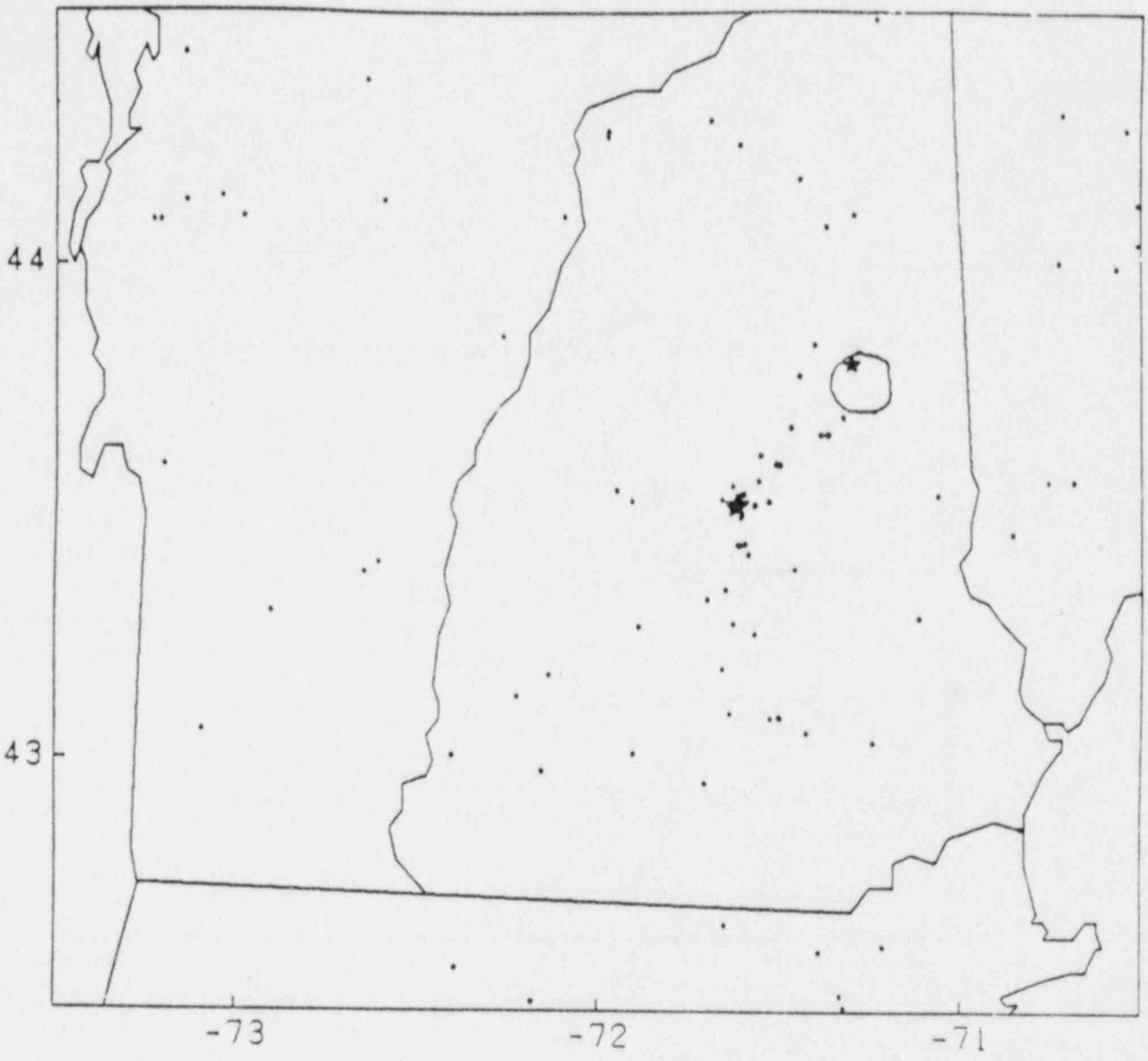

Figure 1. Location of the Gaza, NH earthquake (large star). The smaller star gives the location of the 1940 Ossipee earthquake, with the Ossipee pluton surrounding it. The small dots show the background seismicity for the time period of Oct 1975-June 1982.

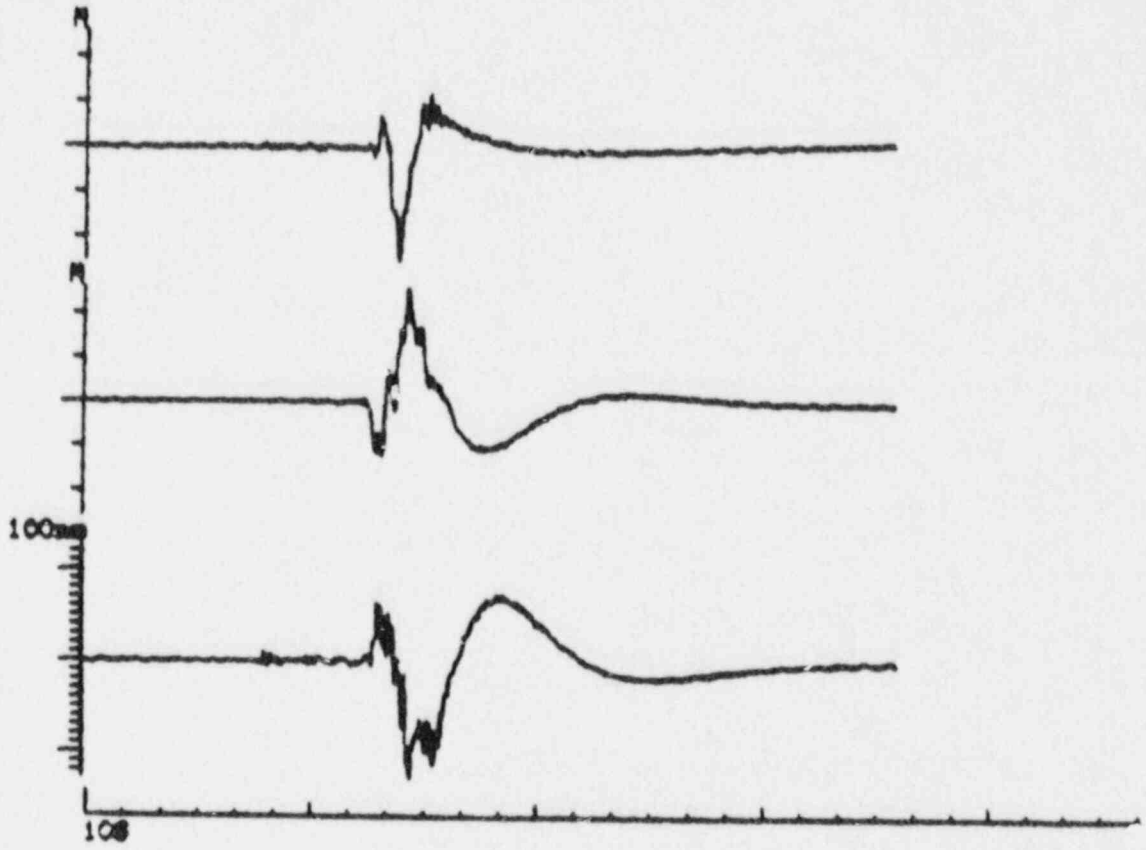

Figure 1 . Vertical, north, and east components of RSTN station RSNY.

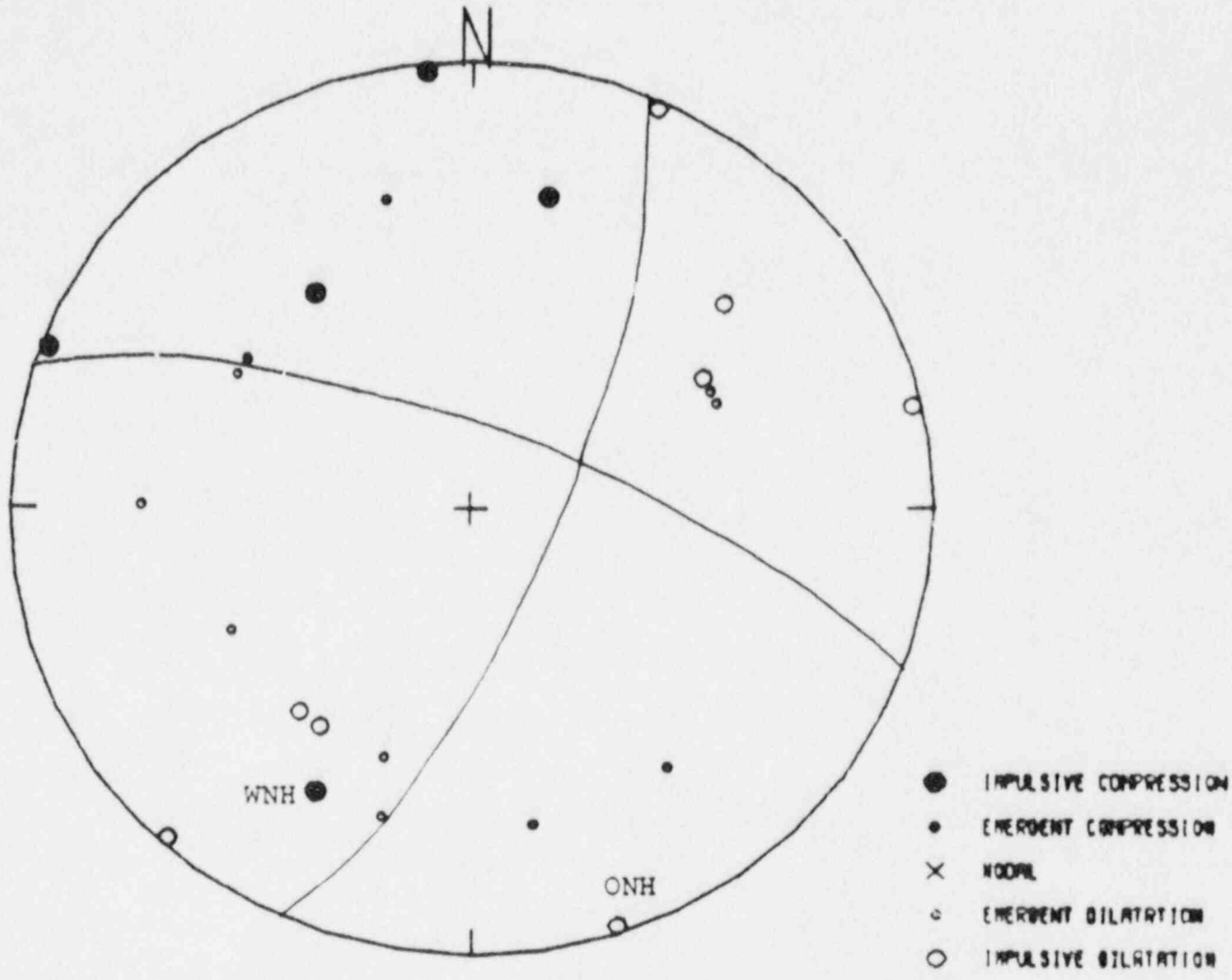

Figure 3. Lower focal hemisphere plot of P-wave first motion data.

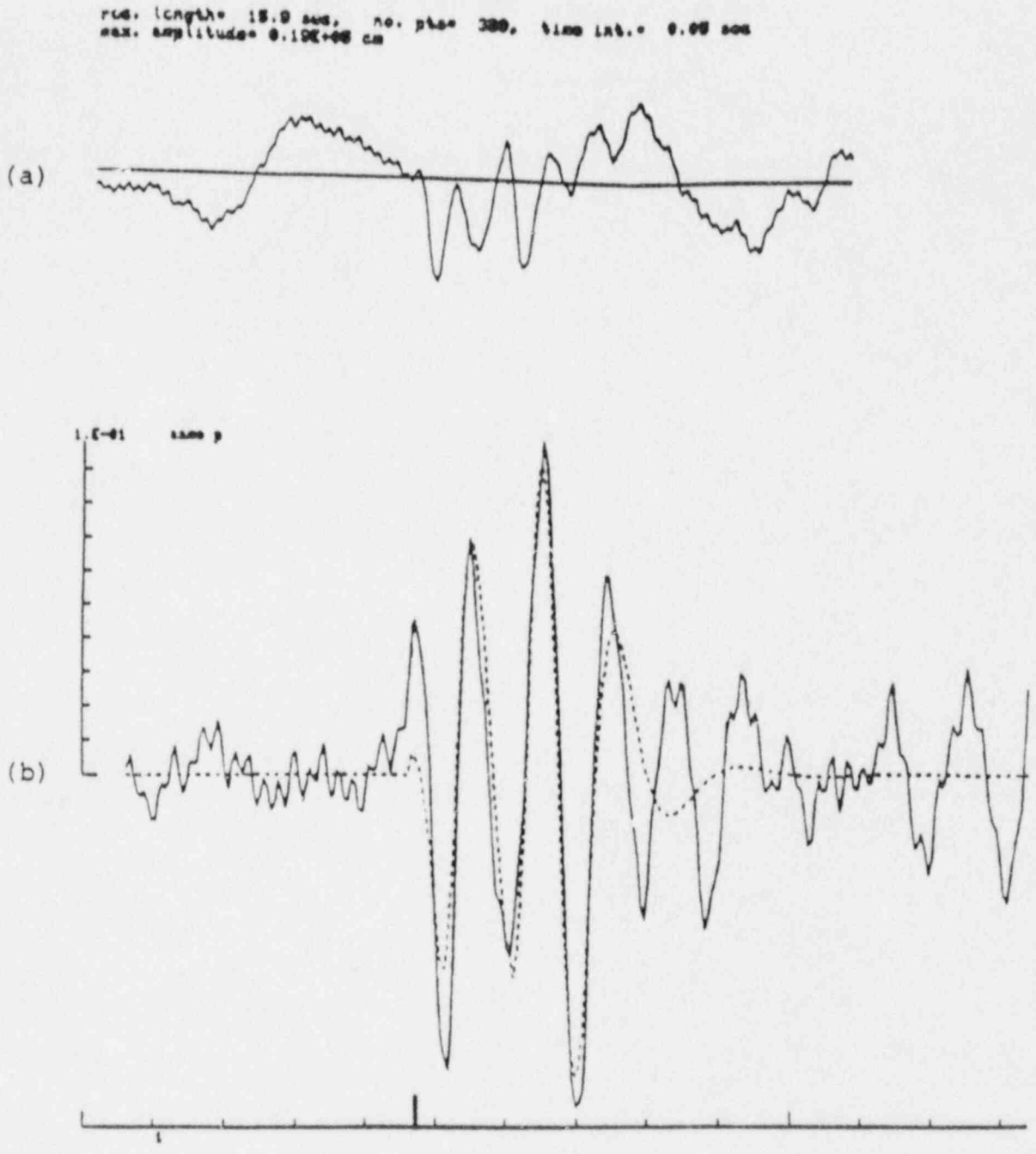

Figure 4 a. Original short-period, vertical seismogram from ANMO. Figure 4 b. Comparison of observed P-wave signal at station ANMO (solid line) with synthetic fit (dashed line).

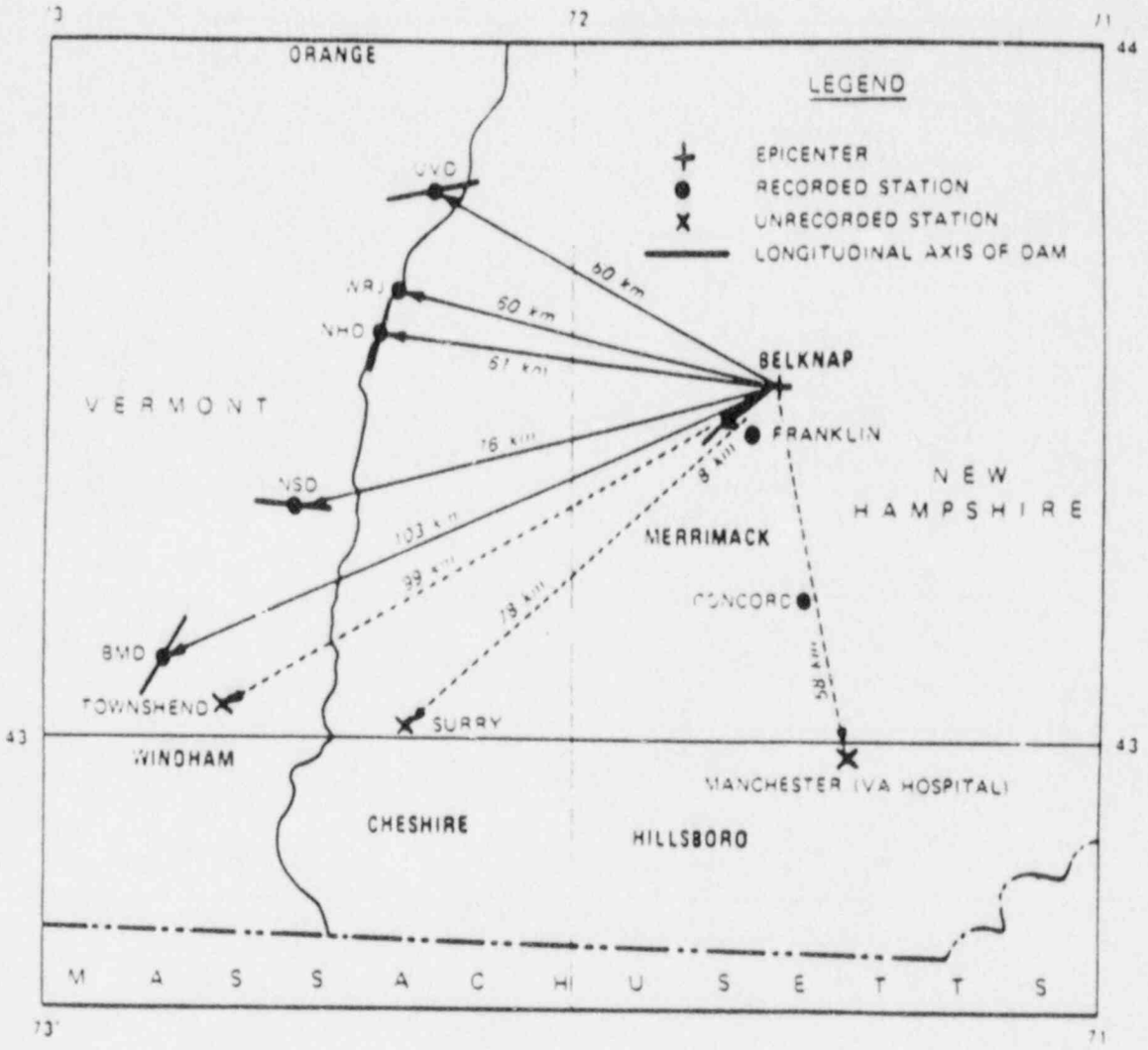

Figure 5 . Location of strong ground motion sites that were triggered during the Gaza, earthquake.

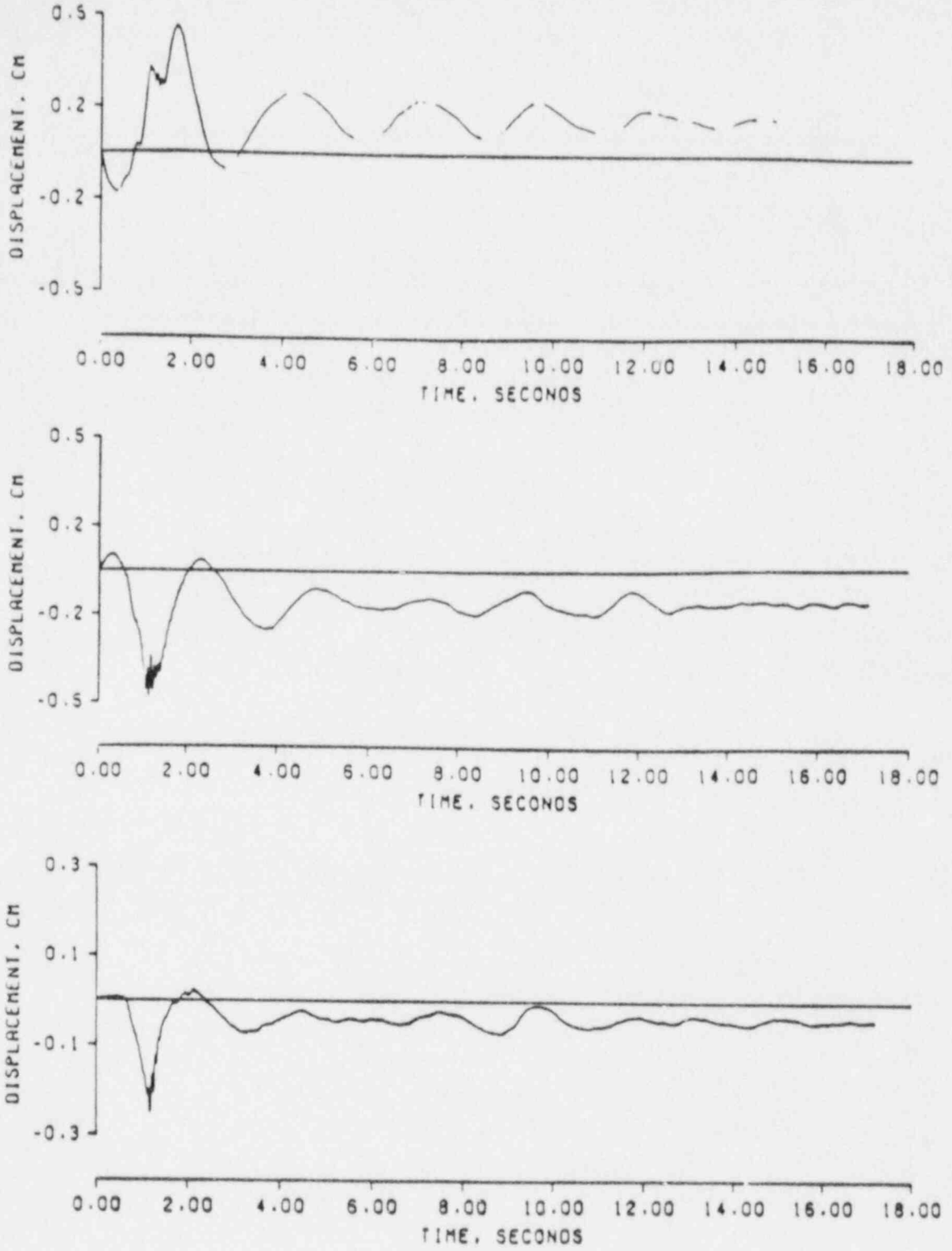

Figure 6. Displacement records from the abutment site at Franklin Falls Dam, NH for vertical, transverse, and longitudinal components.

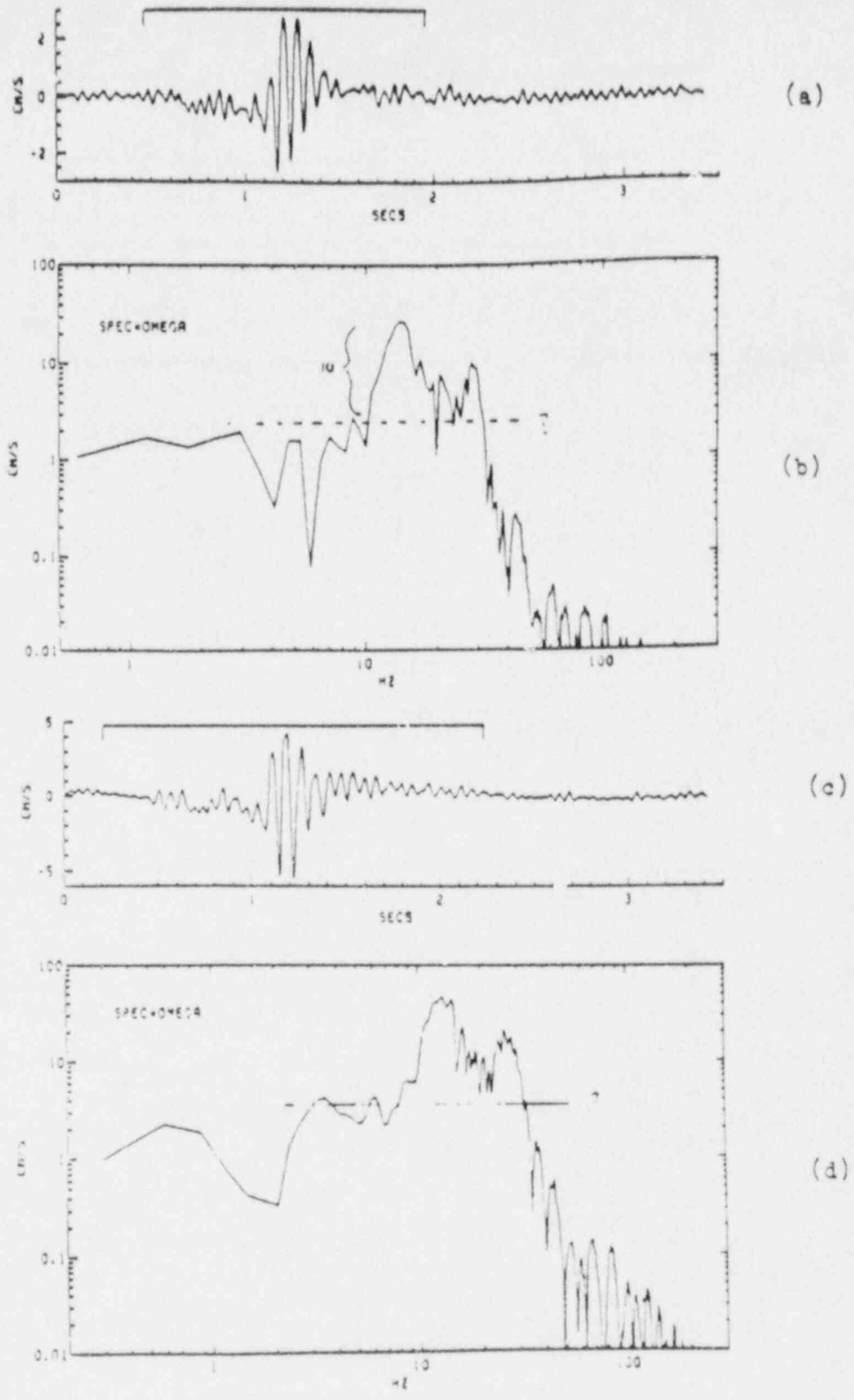

Figure 7a and 7b. Velocity record (7a) and acceleration spectrum (7b) from the abutment site no. 1. Figure 7c and 7d. Velocity record (7c) and acceleration spectrum (7d) from abutment site no. 3.

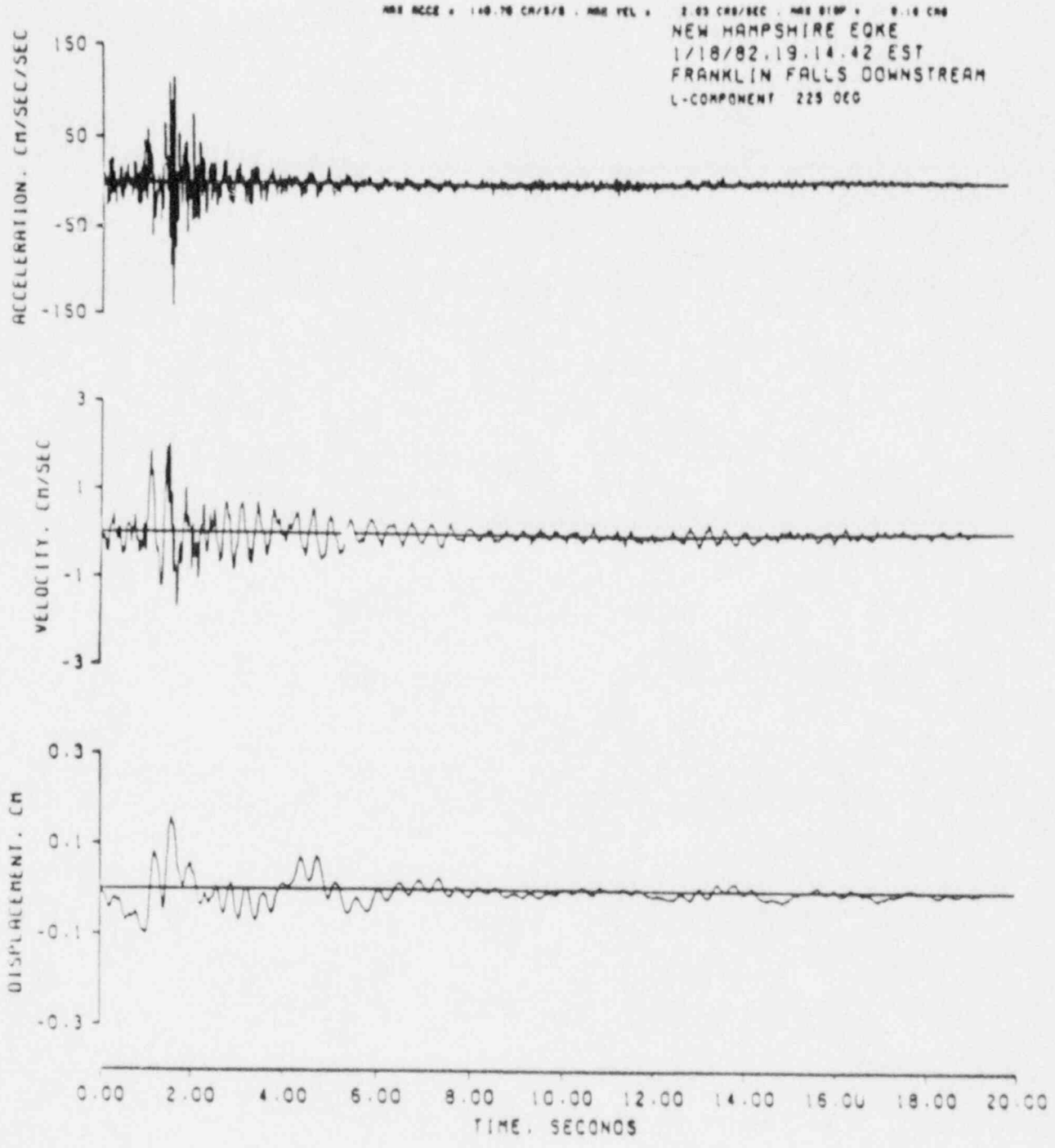

Figure 8 . Acceleration, velocity, and displacement records from the longitudinal component at the downstream site.

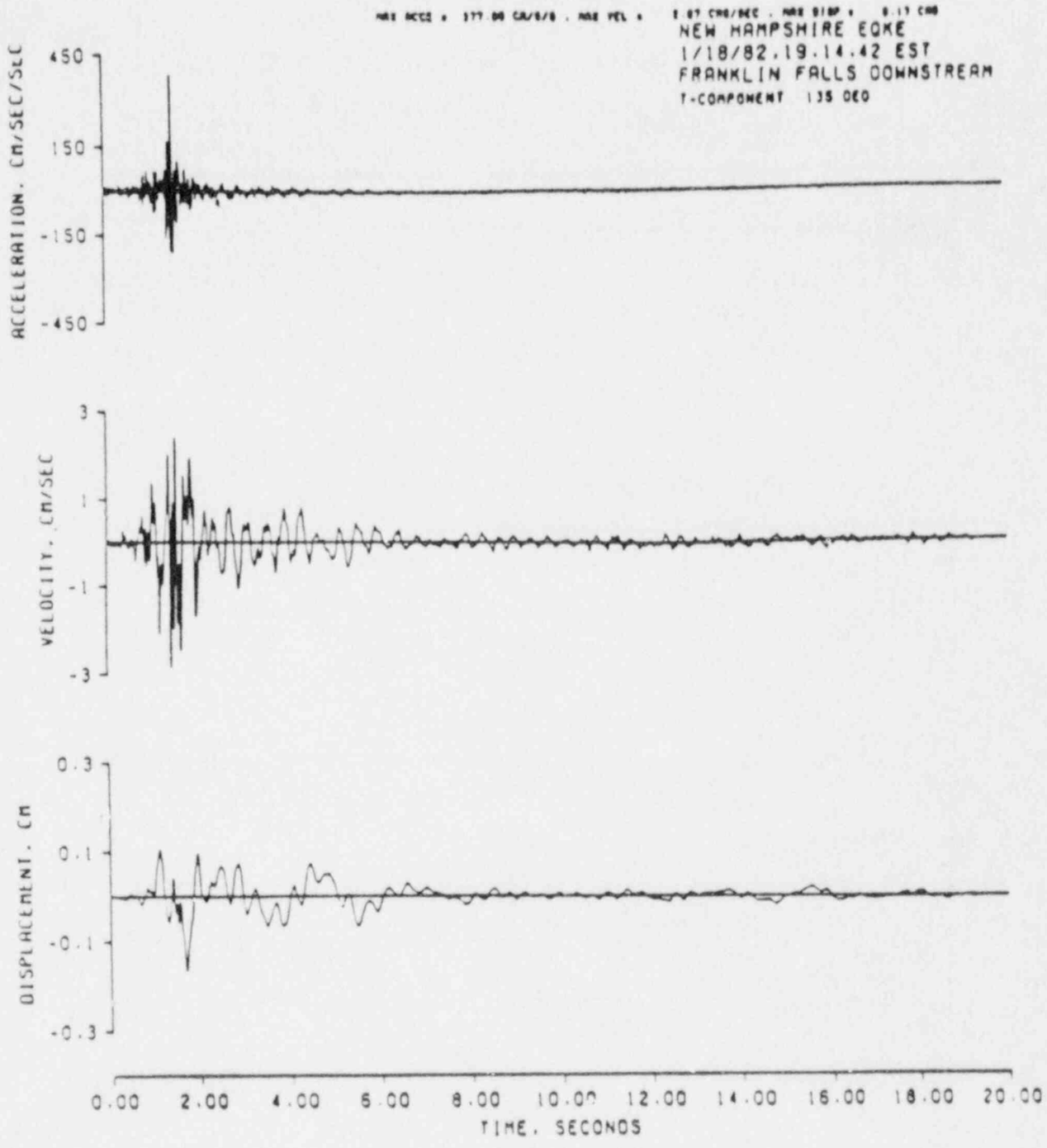

Figure 9. Acceleration, velocity, and displacement records from the transverse component at the downstream site.

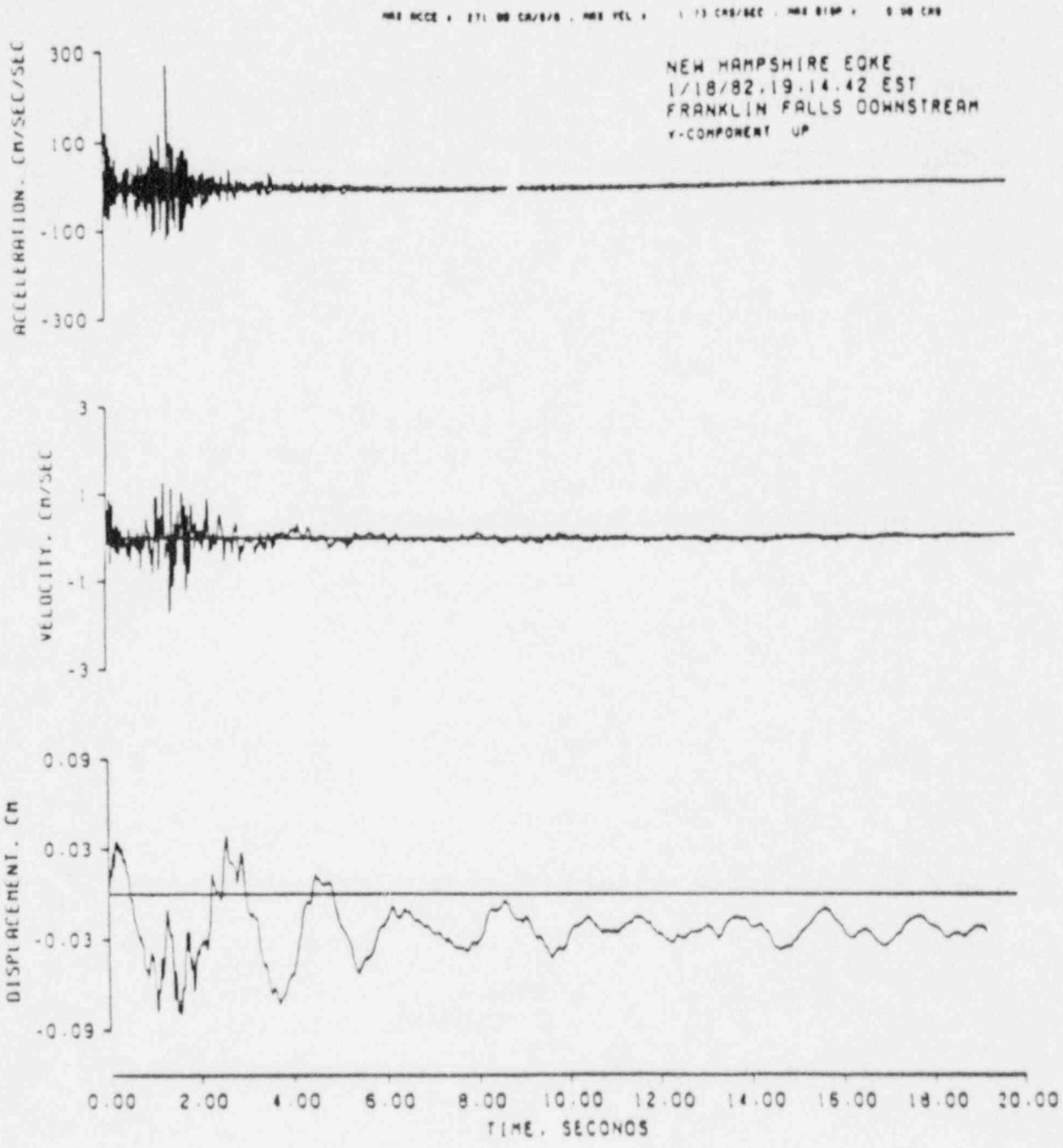

Figure 10. Acceleration, velocity, and displacement records from the vertical component at the downstream site.

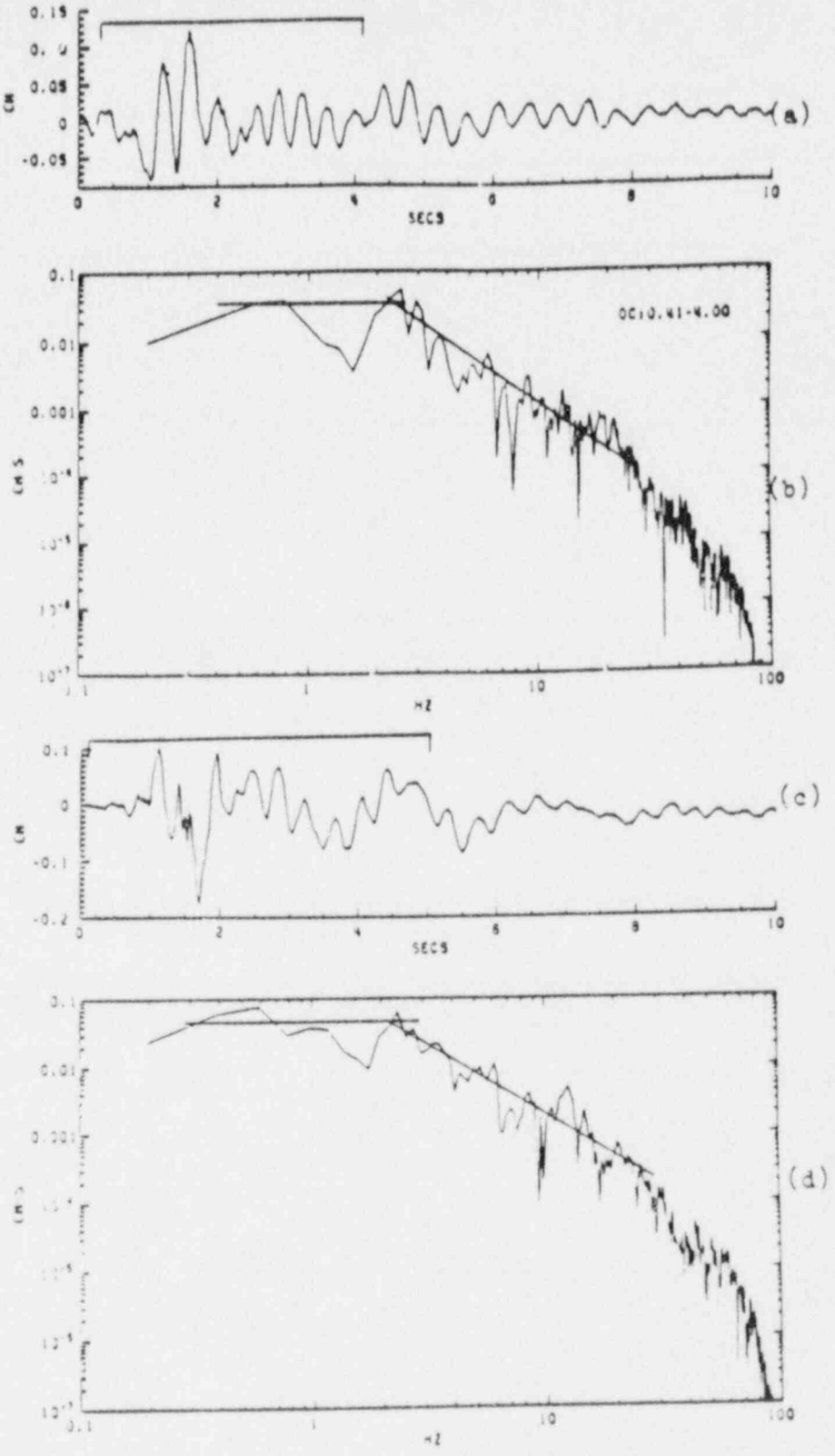

Figure 11a, 11b, 11c, and 11d. The displacement record (11a), displacement spectrum (11b), velocity record (11c) and acceleration spectrum (11d) from downstream site no. 1.

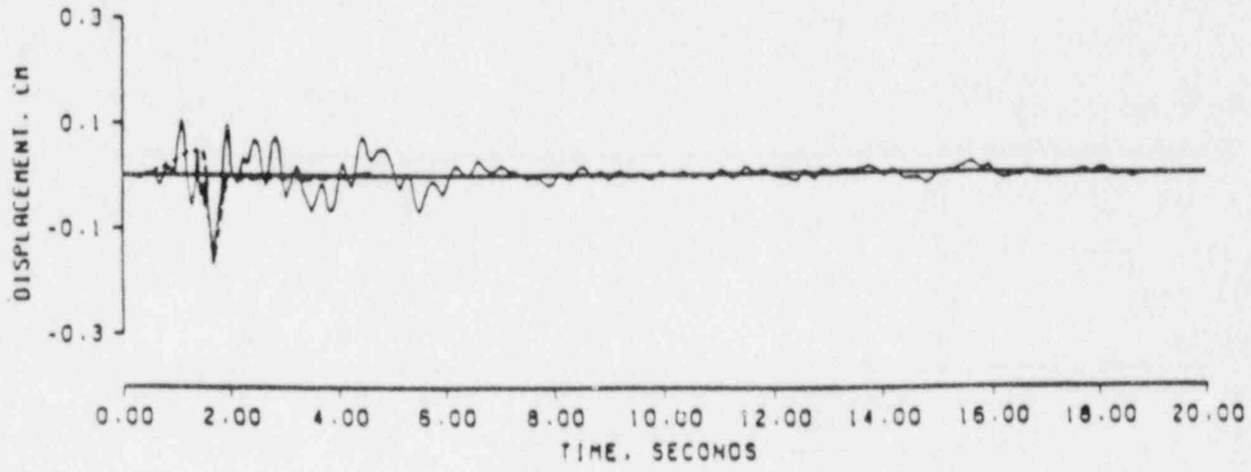

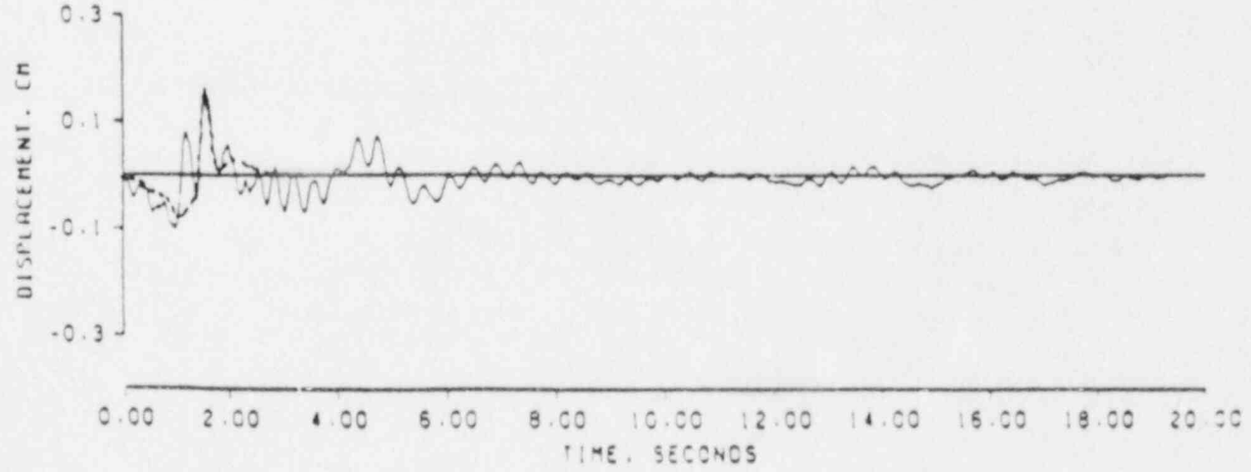

Figure 12. Comparison of observed and synthetic waveforms.

NRC FORM 335 (2.84) NRCM 1102, 3201, 3202

U.S. NUCLEAR REGULATORY COMMISSION

BIBLIOGRAPHIC DATA SHEET

SEE INSTRUCTIONS ON THE REVERSE

1. REPORT NUMBER (Assigned by TIDC, add Vol. No., if any)

NUREG/CR-5080

2. TITLE AND SUBTITLE

A Study of New England Seismicity with Emphasis on Massachusetts and New Hampshire

Final Report Covering the Period 1976-1985

3. LEAVE BLANK

4. DATE REPORT COMPLETED

MONTH: December YEAR: 1987

5. AUTHOR(S)

M.N. Toksoz, K. Kadinsky-Cade

6. DATE REPORT ISSUED

MONTH: January YEAR: 1988

7. PERFORMING ORGANIZATION NAME AND MAILING ADDRESS (Include Zip Code)

Earth Resources Laboratory
Dept. of Earth Atmospheric & Planetary Sciences
Massachusetts Institute of Technology
Cambridge, MA 02139

8. PROJECT/TASK/WORK UNIT NUMBER

9. FIN OR GRANT NUMBER

A4058

10. SPONSORING ORGANIZATION NAME AND MAILING ADDRESS (Include Zip Code)

Division of Engineering
Office of Nuclear Regulatory Research
U.S. Nuclear Regulatory Commission
Washington, DC 20555

11a. TYPE OF REPORT

Technical

b. PERIOD COVERED (Inclusive dates)

12. SUPPLEMENTARY NOTES

13. ABSTRACT (200 words or less)

This is the final report for U.S. Nuclear Regulatory Commission contract No. NRC-04-76-209 with the Massachusetts Institute of Technology (M.I.T.) entitled "A Study of New England Seismicity with Emphasis on Massachusetts and New Hampshire". The contract period was from 1976 to 1985. During that time network daily activities progressed from determining phase arrival times on analog records from a handful of field stations to operation of an efficient real-time data acquisition system with advanced seismic data analysis capabilities. Quarterly Progress Reports have provided continuous reporting of seismic activity in our area for monitoring purposes. Phase data from the M.I.T. network have regularly been included in the Northeastern U.S. Seismic Network (N.E.U.S.S.N) bulletins.

This report summarizes daily operations for the time period of the above contract, and then describes some of the scientific results obtained from data provided by this and surrounding regional seismic networks. The scientific results can be divided into several categories or topics: velocity structure models, earthquake hazard studies, and the determination of earthquake mechanisms and focal depths, crustal stresses and seismic wave attenuation. Key components in our ability to complete these studies have been the reasonably close station spacing (about 50 km) in the northeastern U.S. and the continuous operation of the networks over a period of several years.

14. DOCUMENT ANALYSIS – a. KEYWORDS/DESCRIPTORS

Earthquakes
Seismicity
New England
Velocity Structure
Focal Mechanism
Attenuation

b. IDENTIFIERS/OPEN ENDED TERMS

15. AVAILABILITY STATEMENT

Unlimited

16. SECURITY CLASSIFICATION

(This page) Unclassified

(This report) Unclassified

17. NUMBER OF PAGES

18. PRICE

UNITED STATES
NUCLEAR REGULATORY COMMISSION
WASHINGTON, D.C. 20555

OFFICIAL BUSINESS
PENALTY FOR PRIVATE USE, $300

SPECIAL FOURTH-CLASS RATE
POSTAGE & FEES PAID
USNRC
PERMIT No. G-67

120555078877 1 1AN1PA
US NRC-OARM-ADM
DIV OF PUB SVCS
POLICY & PUB MGT BR-POR NUREG
W-537
WASHINGTON DC 20555